INVESTIGATION OF SPATIO-SPECTRAL DYNAMICS OF LOCAL FIELD POTENTIALS IN PARKINSON'S DISEASE

A Dissertation

Presented to

the Faculty of the Department of Biomedical Engineering

University of Houston

In Partial Fulfillment

of the Requirements for the Degree

Doctor of Philosophy

in Biomedical Engineering

by

Ilknur Telkes

August 2017

INVESTIGATION OF SPATIO-SPECTRAL DYNAMICS OF LOCAL FIELD POTENTIALS IN PARKINSON'S DISEASE

Ilknur Telkes

Approved:

Chair of the Committee
Nuri Firat Ince, Assistant Professor,
Department of Biomedical Engineering

Committee Members:

Ahmet Omurtag, Associate Professor,
Department of Biomedical Engineering

Yingchun Zhang, Assistant Professor,
Department of Biomedical Engineering

Vallabh E. Das, Benedict-Pitts Professor,
College of Optometry

Ashwin Viswanathan, Assistant Professor,
Department of Neurosurgery

Joohi Jimenez-Shahed, Assistant Professor,
Department of Neurology

Suresh K. Khator, Associate Dean,
Cullen College of Engineering

Metin Akay, Professor and Founding Chair,
Department of Biomedical Engineering

ACKNOWLEDGEMENTS

Firstly, I would like to express my sincere gratitude to my advisor, Assistant Professor Dr. Nuri Firat Ince, for giving me this great opportunity to work with him in this great environment. Doing translational research is always hard and it requires interdisciplinary efforts and strong collaborations not only with medical field but also with industry. Dr. Ince with his extensive knowledge and experience guided me on this road like Gandalf the Grey guided Frodo in the mines of Moria. His continues support of my Ph.D. study and related research helped me to reach to my new journey. I could not have imaged having a better advisor and mentor for my Ph.D. study. As Gandalf said "now all we have to decide is what to do with the time that is given us".

Besides my advisor, I would like to thank the rest of my thesis committee: Associate Professor Ahmet Omurtag, Assistant Professor Yingchun Zhang, Professor Vallabh E. Das, Assistant Professor Ashwin Viswanathan, and Assistant Professor Joohi Jimenez-Shahed, for their insightful comments and encouragement, but also for the hard questions which helped me to widen my research from various perspectives.

My sincere thanks also goes to Dr. Ashwin Viswanathan and Dr. Joohi Jimenez-Shahed, who provided me an opportunity to join their team in the hospital and leading me working on diverse exciting projects. I have learned a lot from them.

I thank my friends for keeping me human in the tough years of the graduate school and for the stimulating discussions, sleepless nights we were working together before deadlines, and for all the fun we have had in the last four years.

Last but not the least, I would like to express my gratitude towards my mother, Ikbal Isikli. She is the Lady Galadriel of my life who has been always there to illuminate my life. Plus, I would like to thank my father, Suat Telkes, and my sister, Cansu Telkes, for supporting me spiritually throughout writing this thesis and my life in general. I always felt my family's motivation at every stage of my life.

This research was supported in part by National Science Foundation, award CBET-1343548.

INVESTIGATION OF SPATIO-SPECTRAL DYNAMICS OF LOCAL FIELD POTENTIALS IN PARKINSON'S DISEASE

An Abstract

of a Dissertation

Presented to

the Faculty of the Department of Biomedical Engineering

University of Houston

In Partial Fulfillment

of the Requirements for the Degree

Doctor of Philosophy

in Biomedical Engineering

by

Ilknur Telkes

August 2017

ABSTRACT

Parkinson's disease (PD) is characterized by the progressive loss of dopaminergic nigral neurons resulting in motor and non-motor deficits. Deep brain stimulation (DBS) of the subthalamic nucleus (STN) has emerged as an effective neurosurgical treatment for the patients with PD where their motor symptoms cannot be controlled with medications. Accurate localization of STN is an important factor defining the efficacy of DBS. The most common targeting method in DBS surgery is the microelectrode single unit activity recording, which is performed by listening to bursting firing patterns of individual neurons to identify the basal ganglia structures. However, it requires significant expertise and is fraught by potential technical difficulties. On the other hand, local field potentials (LFPs), owing to their oscillatory and robust nature, can overcome these technical issues. In this regard, we recorded LFPs from multitrack *microelectrodes* and *macroelectrode* in PD patients who underwent DBS surgery. We demonstrated for the first time that combination of different subband features derived from beta and high frequency oscillations of LFPs can be used to estimate the optimal track for DBS implantation and to identify the dorsal STN border with high accuracy. These results establish the initial evidence that LFPs can be strategically fused with computational intelligence in the operating room to increase the chance of optimal placement of the DBS electrode within the motor sub-territory of the STN, without an appreciable downside.

We also investigated the spatio-spectral patterns of LFPs in the most commonly accepted subtypes of PD, tremor dominant (TD) and postural instability and gait difficulty (PIGD). As of today, no underlying neural correlates have been identified. Here we show that activity in the subbands of LFPs recorded with *microelectrodes* from sub-

territories of the STN provide distinguishing neurophysiological information about these phenotypes. We found distinct patterns between TD and PIGD groups in HFOs and their interaction with the beta band in the dorsal and ventral regions of the STN. Our results indicate that the spatio-spectral dynamics of LFPs can be used as an objective method to distinguish the two major subtypes of PD. This observation provides support for distinct pathophysiologic mechanisms underlying these subtypes.

Table of Contents

LIST OF FIGURES

LIST OF TABLES

1. CHAPTER 1: General Introduction

The main focus of the present study is the functional utility of local field potentials (LFPs) intraoperatively recorded from multiple *microelectrodes* and a *macroelectrode* implanted into the subthalamic nucleus (STN) in Parkinson's disease (PD) for the improvement of deep brain stimulation (DBS). As of today, LFP techniques used for physiological confirmation of anatomical target in DBS surgery is the least common approach (1%) compared to the microelectode-single unit activity (MER-SUA) setup (83%) (Abosch et al., 2013). Considering the more robust nature of LFPs and sensitivity to oscillatory firing patterns of neural population, we believe that neural patterns embedded in LFPs can be extracted to further our understanding of the electrophysiological characteristics of PD. With the application of signal processing, intraoperative LFPs can serve as a strategic tool for localization of pathological territories and/or sub-territories in the STN that can improve the efficacy of DBS and facilitate the development of a personalized, closed-loop therapy.

The first chapter serves as a general introduction to literature overview of PD, the functional circuitry of basal ganglia in PD, and general information about the therapeutic strategies used in PD, followed by a background information on electrophysiological findings in PD. The general surgical methods and intraoperative recording techniques are provided in the next chapter. The following chapters consist of 3 major sections: (i) localization of STN in PD by using *microelectrode* LFPs, (ii) localization of STN in PD by using *macroelectrode* LFPs, and (iii) investigation of electrophysiological features of PD motor subtypes by using intraoperative LFPs. The specific aims of the studies

presented in the thesis will be described in each chapter in detail. A general summary and the significance of the study are given in the last chapter.

1.1. Parkinson's disease

Parkinson's disease is a complex neurodegenerative movement disorder with a progressive nature. PD was first described in 1817 by Dr. James Parkinson as a shaking palsy and then refined by Jean-Martin Charcot (Goetz, 2017). Today, PD is the second most common neurodegenerative disorder after Alzheimer's dementia and the incidence of the disease, according to the 2005 report of World Health Organization, has been arising day by day along with the increasing life expectancy (Bezard & Przedborski, 2011). Although PD can be observed at any age, it is most commonly seen in older adults. The mean age onset of the disease is estimated as 60 years, while age of 21-40 years is considered as young onset (Samii, Nutt, & Ransom, 2004). PD affects an estimated 1 million people in the U.S., with an annual incidence of 50,000 new cases per year (National Parkinson's Foundation. About Parkinson's disease. 2010 Jan).

PD includes broad spectrum of motor and non-motor features (Thenganatt & Jankovic, 2014). The main motor features include resting tremor, rigidity, bradykinesia (or akinesia), and postural instability with freezing while the non-motor symptoms include cognitive impairment, mood disorders and other psychiatric features, sleep disorders, and a variety of autonomic symptoms (Jankovic, 2008). The clinical criteria for PD determined by the United Kingdom Parkinson Disease Society Brain Bank are the presence of bradykinesia and at least one of the rest of the cardinal symptoms in addition to 3 supportive features (Jankovic, 2008; Thenganatt & Jankovic, 2014).

Bradykinesia is the most characteristic clinical feature of PD and it refers to slowness of planning, initiating, and executing of movement (Jankovic, 2008; Rodriguez-Oroz et al., 2009). The long reaction time, slower and smaller handwriting, or decreased arm swing when walking can be exemplified (Fahn, 2003). Akinesia refers to lack of movement. However, hypokinesia, one of the types of akinesia, corresponds to reduced frequency and amplitude of spontaneous movement (Rodriguez-Oroz et al., 2009). Bradykinesia/hypokinesia affects all voluntary and involuntary movements. Based on "kinesia paradoxia", it was proposed that PD patients with bradykinesia have intact motor programs but have difficulties accessing them without an external trigger such as a loud noise or visual cue (Jankovic, 2008).

Rigidity in PD refers to increased resistance to passive movement and it is constant throughout the range of movement (Klockgether, 2004). This so-called lead-pipe rigidity is observed in both flexor and extensor muscles. When patients have both resting tremor and muscular rigidity, "cogwheel" phenomenon which is a characteristic type of rigidity with a jerky, ratchet-like movements of joints can be observed (Jankovic, 2008; Klockgether, 2004).

The parkinsonian tremor is seen when the patient is at rest and it has typically 4-6 Hz frequency unlike the typical frequency seen in Essential tremor with 8-12 Hz (Schneider & Deuschl, 2015). Resting tremor typically starts in one finger and it stops with the voluntary movement. At the beginning of the disease, it can be seen only with stress, however its amplitude might get enhanced with stress or excitement in time (Fahn, 2003). PD patients might have additional tremor on posture or action tremor occurring

with movement (Schneider & Deuschl, 2015). Patients can have resting and action tremor together or postural and kinetic tremor with no resting tremor at all (Camara et al., 2015).

Postural instability is characterized by a stooped posture, decreased arm swing, and shuffling gait. Postural instability along with freezing of gait is a severe problem in PD patients since they are the main cause of falls and injuries (Maurer et al., 2003). Manifestation of postural instability and gait difficulty (PIGD) by reason of loss of postural reflexes occurs with the progression of the disease (Jankovic, 2008). For example, Hoehn et al. reported that only 37% (n = 70) of PD patients with a disease duration of 5 years or less had reached to stage III of Hoehn and Yahr scale meaning that severity of the disease is mild to moderate with some postural instability (Hoehn, Yahr, Hoehn, & Yahr, 1967). It is important to note that diagnostic specificity of postural instability is limited due to various problems in afferent pathways, efferent pathways, central processing, and even musculoskeletal mechanical function (Gelb et al., 1999).

1.2. Functional circuitry of basal ganglia in Parkinson's disease

The basal ganglia (BG) are a group of sub-cortical nuclei and linked to various functions like voluntary motor control and cognitive functions. Figure 1.1 shows the major anatomical components of BG which are the striatum, pallidum, subthalamic nucleus (STN), and substantia nigra (SN) (Nambu, 2011). The striatum is divided into caudate and putamen while the pallidum is divided into external (GPe) and internal (GPi) segments of the globus pallidus and ventral pallidum (VP). Additionally, SN is composed of substantia nigra pars reticulata (SNr) and substantia nigra pars compacta (SNc) (DeLong & Wichmann, 2007; Nambu, 2011). The striatum which is the major input structure of BG receives inputs from the entire cerebral cortex except the primary visual

cortex (Gerfen & Bolam, 2010). The STN forms the other input structure of BG which receives inputs mainly from the frontal cortex. On the other hand, GPi and SNr serve as the output structures from BG to thalamus and brainstem (DeLong & Wichmann, 2007). Even though BG innervate only the thalamus, the superior colliculus, and the pedunculopontine nucleus (PPN) in brainstem, BG has more functional roles in brain (Utter & Basso, 2008). BG is functionally sub-divided into three circuits: (i) motor circuit, (ii) associative circuit, and (iii) limbic circuit (Obeso et al., 2008). Each of these circuit originates from a specific area of the cerebral cortex and processed along the different components of BG through thalamus (Fig.1.2). The most commonly studied cortico-basal ganglia circuit is the motor circuit due to its important role in movement disorders (DeLong & Wichmann, 2007).

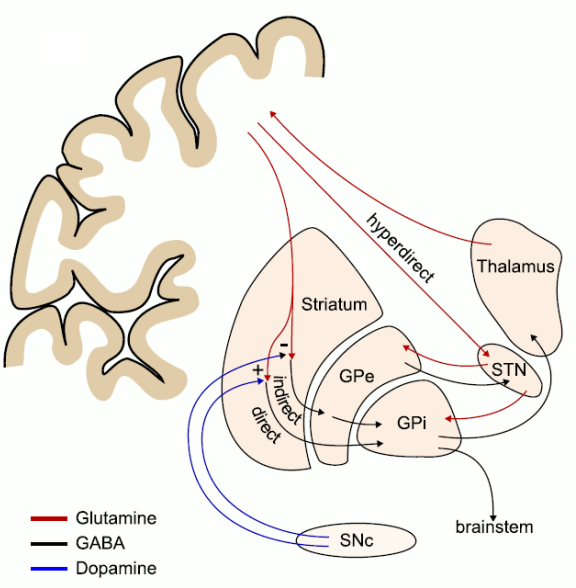

Fig.1.1. Anatomical components of basal ganglia from cross-sectional view with its connections (Adopted from J. S. Brittain & Brown, 2014).

STN is a crucial structure in these circuits and has a critical role of controlling motor functions, cognition, emotion, and thalamocortical excitability (Benarroch, 2008). That is one of the reasons why STN is selected target for stimulation not only in PD but also disorders like epilepsy or psychiatric disorders (Benarroch, 2008) (stimulation of STN will be discussed in the following chapters in detail). The STN is a small and ovoid-shaped structure surrounded by various structures such that fibers of internal capsule on

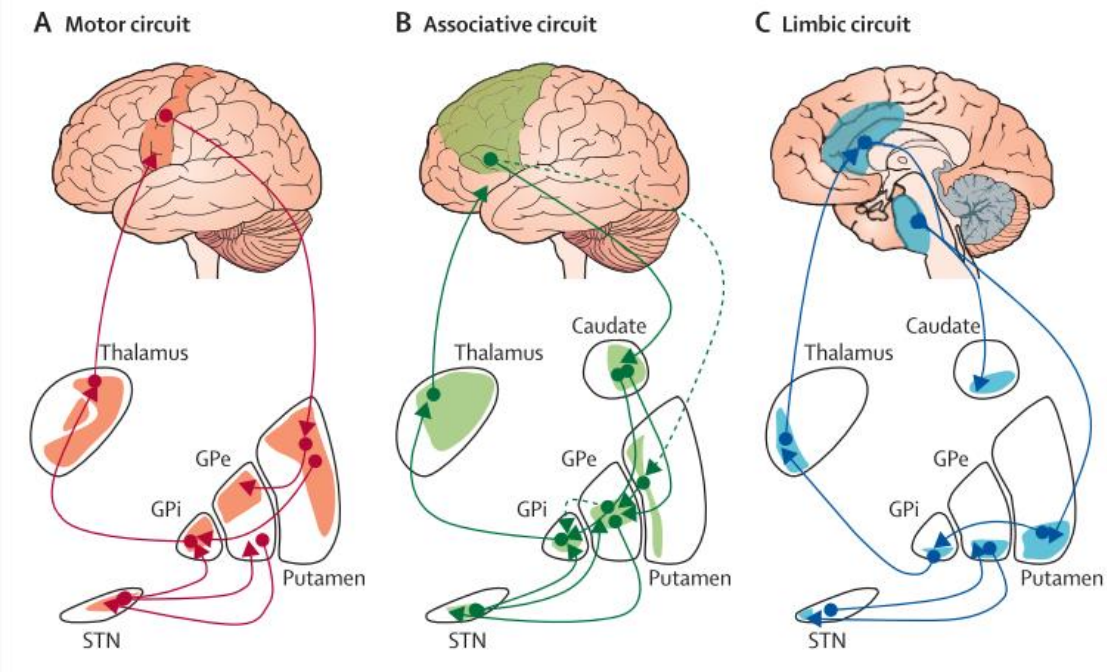

Fig.1.2. Functional organization of basal ganglia. (Adopted from Obeso et al., 2008).

anterior and lateral sides, anteromedially Fields of Forel (FF), posteromedially red nucleus (RN). Zona incerta (ZI) stands as a barrier in between STN and ventral thalamus while the SN situated in just below the ventral border of the STN (Hamani, 2004; Patel et al., 2008) (Fig.1.3.A). As in BG circuits, STN is also sub-divided into 3 different territories: (i) motor, (ii) associative, and (iii) limbic territory (Hamani, 2004; Parent & Hazrati, 1995). The large portion of the STN at dorsolateral direction corresponds to motor territory and it is further divided into somatosensory sub-territory on the medial side. Dorsolateral motor region of STN receives inputs from primary motor cortex (M1) while sensorimotor region from supplementary motor area (SMA), premotor cortex (PM), pre-SMA, and cingulate motor areas (CMA) in the cingulate sulcus (Nambu, 2011). The motor territory projects to GPe and GPi and play the crucial role in motor control. Ventral

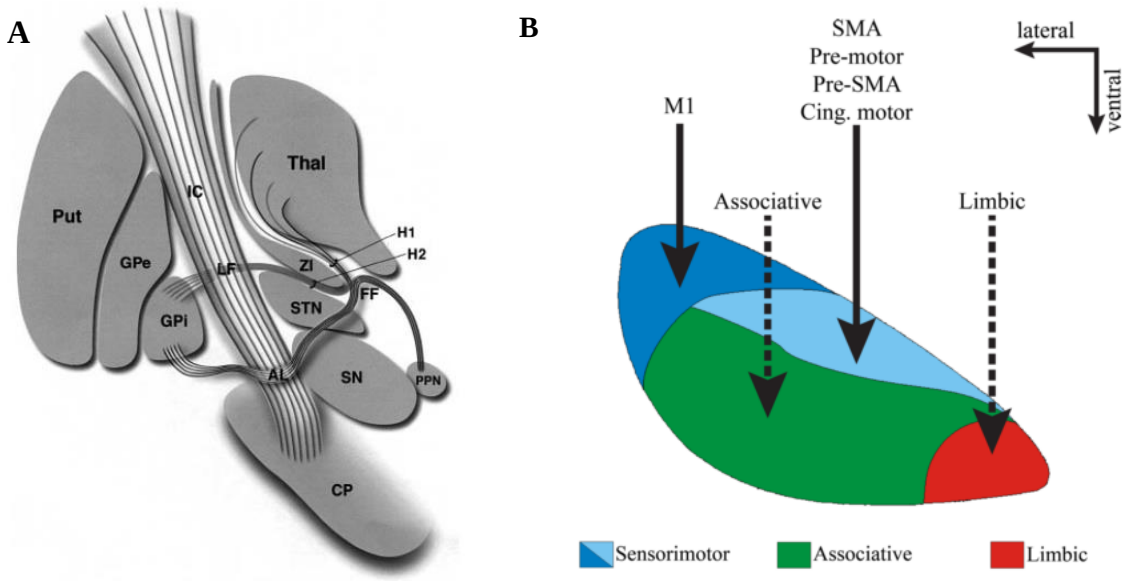

Fig.1.3. Representation of the anatomical structures associated with STN and functional territories of STN. **(**A) STN is in close proximity to BG structures and surrounded by dense bundles of myelinated fibers (Adopted from Hamani, 2004). (B) Functional subdivision of STN (Adopted from Mathai & Smith, 2011). CP = cerebral peduncle; IC = internal capsule; Put = putamen; Thal = thalamus.

to motor territory, there exits the oculomotor and prefrontal territories along with the associative territory. These regions received inputs from dorsolateral prefrontal cortex and frontal eye fields. By projecting to SNr, associative territory involves in oculomotor control and cognitive aspects of motor behavior. The limbic territory which is located at the most medial part of the STN controls the motivational and emotional aspects of motor behavior by receiving inputs from the medial prefrontal and anterior cingulate cortices and projecting to the ventral and medial pallidum (Benarroch, 2008).

Specifically, the basal ganglia motor circuit with the excitatory and inhibitory inputs and outputs functions through 3 pathways: (i) direct pathway, (ii) indirect pathway, and (iii) hyperdirect pathway (Fig.1.4) (Nambu, 2011). In the direct pathway, striatum receives excitatory inputs (glutamate) from cortex and secretes inhibitory

neurotransmitter gamma-amino butyric acid (GABA) into GPi/SNr. Since GPi/SNr gets inhibited, their inhibitory effect on thalamus is canceled out (dis-inhibition) resulting increase in firing rate of motor thalamus and brainstem. On the other hand, in the indirect pathway, striatal neurons project to GPi/SNr then to thalamus and PPN through GPe and STN. Indirect pathway results in increased inhibition on thalamus following a decreased motor activity. Hyperdirect pathway, as the name implies, contain a direct cortical input to STN which projects to the GPi/SNr. By this way, cortical excitation on GPi/SNr occurs faster than the direct and indirect pathways (DeLong & Wichmann, 2007; Nambu, 2011; Mathai & Smith, 2011).

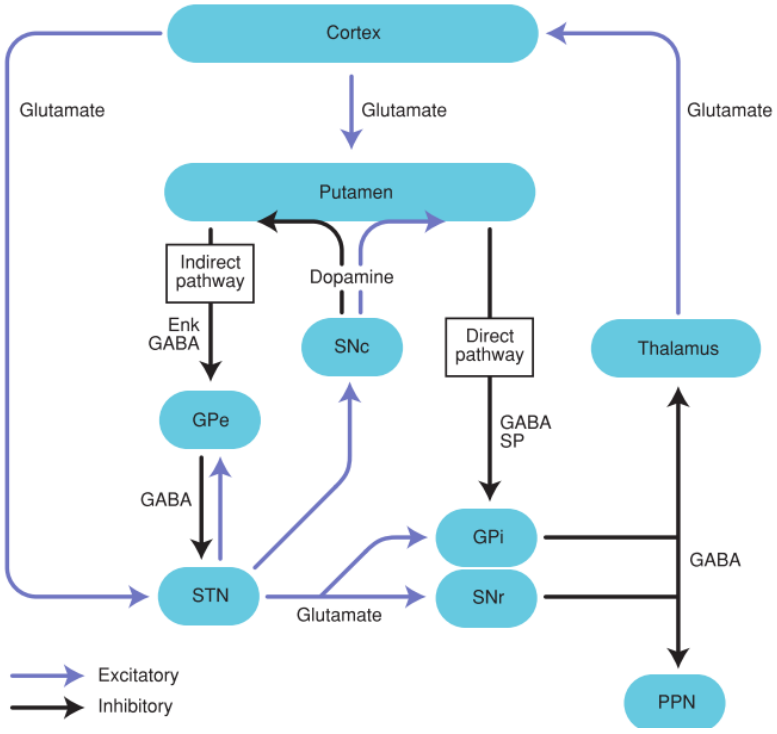

Fig.1.4. Basal ganglia motor circuitry in normal conditions. GABA = gamma-amino butyric acid; Enk = enkephalin; SP = substance P (Adopted from Cambridge University Press, 2003).

In PD, the BG motor pathways does not function properly due to dopaminergic neuron loss in the SNc (Lewis et al., 2011). The degeneration of these neurons results decrease of dopamine secretion into striatum which leads to decreased activity of the direct pathway and inhibition of the indirect pathway (Przedborski, 2017). The dopamine

depletion consequently increases the STN-mediated activation and decreases GPe-mediated inhibition. This alteration increases the inhibitory effect of thalamus on motor cortex resulting a decrease in motor activity (Przedborski, 2017; Meredith & Kang, 2006).

Three cardinal features of PD - bradykinesia/akinesia, rigidity, and resting tremor- are considered to be correlated to dopaminergic cell death in nigrostriatal region (Jellinger, 1999). However, in akinetic-rigid group, it was proposed that cell loss occurs in a more pronounced way and in the ventrolateral part of SNc while it is mild and more medial in tremor dominant (TD) group (Eggers et al., 2011). It was suggested that tremor might be also related to dopaminergic cell loss in retrorubral area (Jellinger, 1999). Unlikely, postural instability and gait disability (PIGD) in addition to non-motor features of the disease are associated to non-dopaminergic denervation (Fasano et al., 2012). It was found that combination of nigrostriatal and basal forebrain cortical cholinergic cell loss is related to slow gait speed in PD subjects (Bohnen et al., 2013). Lewis et al. by using functional magnetic resonance imaging also showed that cerebellothalamocortical (CTC) circuits are more active in TD patients compared to striatalthalmocortical circuits (STC) (Lewis et al., 2011). Helmich et al., by showing the active involvement of CTC circuit in PD tremor, supported that there is a differential involvement of CTC and STC circuits in PD subtypes (Helmich et al., 2013).

1.3. Therapeutic strategies in Parkinson's disease

The pathological hallmark of PD is the dopaminergic neuron loss resulting in dopamine depletion in the BG (Lewis et al., 2011). Therefore, current medical therapies for PD involves manipulation of striatal dopamine levels through medication such as

levodopa (L-DOPA), which is a precursor to the dopamine, norepinephrine, and epinephrine, in order to improve the cardinal motor symptoms of the disease (Strauss et al., 2014). However, in the long term, this treatment is complicated by the development of motor complications, including wearing off effects (fluctuations in efficacy) and dyskinesia (involuntary movements) (Jenner, 2013).

In addition to medical treatment, PD includes surgical and supportive treatment as well (Desouza et al., 2013). Surgical treatments for PD started to be used before levodopa treatment and, as of today, they evolved to deep brain stimulation (DBS) to overcome the medication induced complications in advance PD subjects (Fasano et al., 2012; Hariz et al., 2010). The first surgical applications starting in 1950s were including stereotaxic lesioning of BG structures or using stimulation to determine the lesioning area (Benabid et al., 1991; Albe-Fessard, 1973). The structures used for ablation for treatment of PD were the ventralis intermedius nucleus (Vim) of thalamus (thalamotomy), the globus pallidus (pallidotomy), ansa lenticularis (ansotomy), Forel's fields (campotomy), and the STN (subthalamotomy) (Spiegel et al., 1947, 1954, 1963; Meyers et al., 1951; Murata et al., 2003).

In 1987, Benabid et al. reported a reversible and adjustable approach for tremor, high frequency stimulation of Vim, in contrary to the ablative techniques (Benabid et al., 1987). It was followed by the high frequency stimulation of GPi (Spiegel et al., 1963) and then STN (Benabid et al., 1994). By this way, a new era for the treatment of advance PD has started. Over the past decade, electrical stimulation of deep brain structures has largely replaced ablative techniques in the surgical treatment of PD and ET. STN and GPi, which were approved by FDA in 2002, are frequently used as potential targets for

DBS in PD. For the PD phenotypes, it is not known whether stimulation of STN or GPi will lead to more optimal outcomes. STN DBS is effective in improving both resting tremor and action tremors (Diamond et al., 2007), and many groups favor targeting this nucleus over GPi when tremor is a prominent feature (Williams et al., 2014). Later, Vim stimulation is also reserved for tremor predominant PD. The primary limitation of this target is that it has little effect on other symptoms such as bradykinesia and rigidity. The STN as the most commonly used target will be the scope of the current studies mentioned throughout the thesis.

1.3.1. Patient selection for DBS

DBS has recently been proven to be an effective therapy for PD (Benabid, 2003) and it is offered to patients who have medication-refractory symptoms of PD, dyskinesia, or tremor (Okun & Foote, 2010). Patient selection for DBS is the first and a crucial step for optimal benefits. There are several factors to be considered for candidate selection:

- Diagnosis of PD should be re-confirmed due to the chances of misdiagnosis with other neurological disorders having the similar symptoms with PD.
- The symptoms with the best response to levodopa should be determined by checking the percentage of improvement in the Unified Parkinson's Disease Rating Scale (UPDRS) part-III (motor section). It should be noted that tremor may not be responsive to dopaminergic therapy, yet it may improve with STN DBS (Charles et al., 2002; Lang et al., 2002).
- Cognitive/psychiatric profile should be evaluated. Because, patients with cognitive decline might get worse after surgery (Morrison et al., 2004). As an

important factor related to cognitive decline, age should be considered as well (Saint-Cyr et al., 2000).

- Comorbidities without any risk or limit to DBS should be taken into account (Okun et al., 2007).

1.3.2. Targeting modalities in DBS

Accurate localization of DBS electrode is another crucial step for an optimal therapy in PD. There are several anatomical and physiological targeting methods used in DBS surgery for localization of STN. Anatomical targeting approach consists of direct and indirect methods. Direct method is defined as using radiological images of the target under stereotaxic conditions to determine the x-y-z coordinates of the target (Machado et al., 2006; Patel et al., 2008). Basically, direct targeting is based on magnetic resonance imaging (MRI) visualization of the structures. Today, advanced MRI technology allows us to directly visualize the structures (Strauss et al., 2014). Even though MRI-based approach provides advantages like less complex procedure, use of general anesthesia which is providing more comfort to patient, and less amount of risk for intracranial hemorrhage, it is not possible to clinically test the patient for therapeutic effect-side effect profile or electrophysiologically determine the borders of target nucleus (Groiss et al., 2009; Starr et al., 2014; Strauss et al., 2014). Plus, MRI distortion is not yet perfectly corrected (Benabid, 2003). Despite the visibility of STN or GPi in T2 images, any problem occurring at fusing MRI and computed tomography might lead to misinterpretation of the anatomy (Machado et al., 2006).

In the indirect targeting method, as the name implying, location of the target is determined by using stereotactic brain atlases and the coordinates of visible landmarks

such as anterior (AC) and posterior (PC) commissures to estimate the actual target coordinates (Machado et al., 2006; Patel et al., 2008). However, the biggest limitation of the method is the anatomical variations among individuals. Plus, interpretation of the coordinates by clinical team and the use of average values of the coordinates for targeting might be suboptimal due to brain shift (Machado et al., 2006; Patel et al., 2008).

Physiological targeting includes intraoperative microelectrode recordings (MER) and clinical testing with MER system or DBS lead for physiological verification of the target structure and therapeutic window (Abosch et al., 2013; Strauss et al., 2014). Today, the majority of centers with 83% use MER from individual neurons (single unit activity = SUA) to identify the characteristic neuronal firing patterns and to obtain physiological confirmation (Abosch et al., 2013; Foltynie et al., 2011). MER-SUA is performed in awake patients for the necessity of clinical testing. Multiple microelectrodes (typically up to five) are inserted in brain and cell firing patterns of structures are identified for selection of optimal trajectory to implant DBS electrode (Fig.1.5).

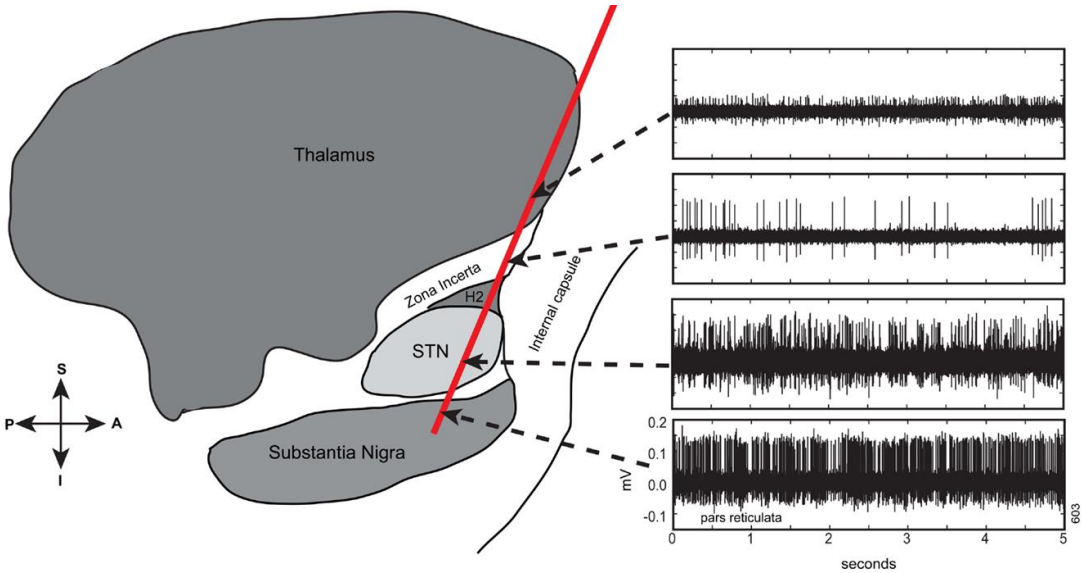

Fig.1.5. Functional localization of the STN showing the distinct neurophysiological spiking and spike background patterns (Adopted from Camalier et al., 2014)

However, the MER-SUA method has several limitations in practice such as subjective interpretation of complex signal patterns to localize the anatomical borders of the STN, being less stable and more "susceptible to technical (e.g., impedance) and physiological (e.g., cerebrospinal fluid and blood) fluctuations" (Thompson et al., 2014). Localization of STN via macroelectrode/DBS without MER is only used by 8% among centers (Abosch et al., 2013). Despite the advantages of using this technique alone in STN targeting (Xiaowu et al., 2010), microlesion effect, which might limit the clinician's ability to test and the therapeutic effectiveness in the operating room, and poor spatial resolution of the macroelectrode should be taken into consideration (Gross et al., 2006; Wang et al., 2014).

In addition to delivering stimulation, DBS electrode can also be used to record local filed potentials (LFPs) (Ince et al., 2008). LFPs represent the electrical activity of a neuronal population surrounding the electrode tip and carry synchronous and oscillatory firing patterns (Priori et al., 2004). They can be recorded from DBS electrodes and larger contacts of microelectrodes used for MER-SUA. LFP signals are more robust than SUA and found to be correlated with motor and non-motor symptoms of PD (Priori et al., 2013; Thompson et al., 2014). Along with the recent studies showing that LFPs recorded from STN in PD can provide differential electrophysiological information about subcortical structures, it is gaining interest to use LFPs in operating room for target localization (Chen et al., 2006; Holdefer et al., 2010; Ince et al., 2010; Kolb et al., 2017; Michmizos et al., 2008; Telkes et al., 2016; Wang et al., 2014). Functional characteristics of LFP will be discussed in the next chapter.

1.4. Electrophysiological findings in Parkinson's disease

LFPs represent the sum of extracellular potentials of numerous neurons in a region (Fig.1.6). The volume of this region contributing to the LFP signals may vary according to the size of electrode and where it is implanted. For example, with a very fine electrode, LFP is likely to reflect sum of synaptic activity of tens or thousands of neurons (Buzsaki, 2006). This aggregated extracellular activity generates an oscillating field due to synchronization mechanisms (Buzsáki et al., 2012).

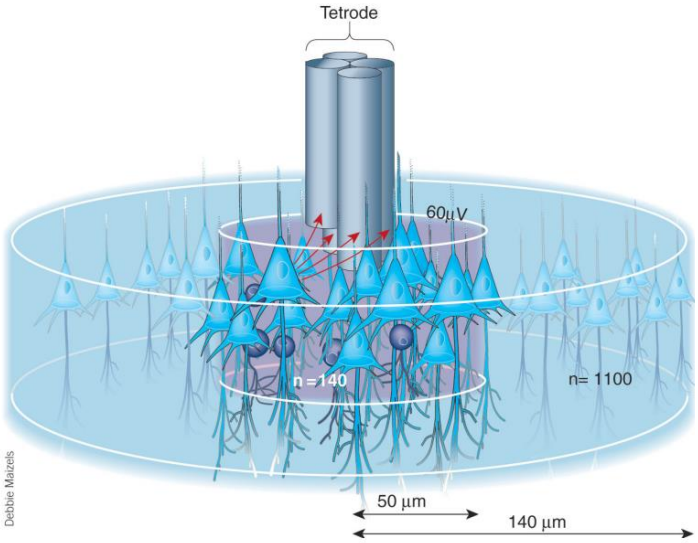

Fig.1.6. LFP recorded from a neuron population (Adopted from Buzsaki, 2004).

LFPs can be divided into a number of frequency bands, as follows: 0–3 Hz (delta), 4–7 Hz (theta), 8–12 Hz (alpha), 13–30 Hz (beta), 31–200 Hz (gamma), 200-300 Hz (slow high frequency oscillations, sHFO), and >300 Hz (fast high frequency oscillations, fHFO). Earlier investigations have documented that excessive beta oscillations in certain basal ganglia structures, especially in the STN, represent a pathophysiological feature of PD (Oswal et al., 2013; Weinberger et al., 2006). Excessive beta band activity is detected when the electrodes enter into the STN (Blomstedt et al., 2011; Brittain & Brown, 2014; Kane et al., 2009; Weinberger et al., 2006). Studies commonly reported that DBS attenuates the pathological beta oscillations in the STN possibly resulting in improvement in motor symptoms (Bronte-Stewart et al.,

2009; Eusebio et al., 2011,2012; Kühn et al., 2008) which indicates a similar modulatory effect of levodopa medication on beta oscillations (Kühn et al., 2006). On the other hand, the excessive HFO ranging from 200-400 Hz are considered to represent a pro-kinetic state, and appear with dopaminergic medication and/or induced movement (Foffani et al., 2003; Foffani & Priori, 2006; Özkurt et al., 2011; Trottenberg et al., 2006). More recently, studies showed that sHFOs are observed during resting/medication OFF state and they shift up to faster range (300-400Hz) by medication.

Recently, Lopez-Azcarate et al. proposed that phase-amplitude coupling (PAC) in STN might be part of mechanism for motor impairment in PD. The coupling is observed between the phase of beta band oscillations and the amplitude of HFOs in the medication OFF state and is reduced by levodopa administration and movement (Lopez-Azcarate et al., 2010). Since the frequencies (8-35 Hz) modulated by HFO amplitude are shown to be related to akinesia and rigidity in PD, HFOs and their modulatory role on STN beta oscillations might have a crucial pathophysiologic role in aberrant basal ganglia motor circuits such as in PD (Kühn et al., 2009).

1.5. Aim of the present studies

The overall aim of the present study is to provide a better understanding of the functional utility of LFPs recorded from STN in PD subjects during DBS surgery. The exact mechanism of DBS is still unknown, but its therapeutic effect on the cardinal symptoms of PD by stimulating STN is well studied. Accurate localization of DBS electrode in STN to maximize the symptom suppression and minimize the side effects by preventing the current spread to surrounding structures is a crucial step. We first recorded LFPs from acutely implanted microelectrodes, with higher resolution compared to DBS

lead, in multiple trajectories. By examining spatially localized subthalamic oscillations in STN and their spectral dynamics during resting state, we aimed to predict the optimal trajectory and the dorsal border of the STN for DBS lead implantation (Chapter 3). In the second study, we recorded LFPs from various depths and multiple contacts of the chronic DBS electrode which was implanted in the STN and investigated their spatio-spectral characteristics. Here, we aimed to predict the superior border of STN by eliminating the limitations of microelectrode use and the effect of subjective interpretation of MER-SUA (Chapter 4). We elucidated whether the LFP activity can be used functionally in the operating room for the localization of abnormal neural dynamics with more detailed electrophysiological correlates of disease manifestations and with a certain spatial specificity that can guide the placement of chronic electrode into the right target or territory. By exploring, for the first time, the spatially localized subthalamic activities along with their spectral characteristics in PD subtypes, we tested the hypothesis that the spatio-spectral patterns of LFPs recorded with microelectrodes from STN sub-territories can be used to distinguish PD patients with PIGD or TD motor subtypes (Chapter 5).

1.6. Scientific contribution

In the first part of the thesis, for the purpose of assisting with clinical decision making, we aimed to develop an automated approach by processing LFPs from multiple tracks to localize the dorsal border of STN and predict the macroelectrode implantation track identified by the neurosurgeon based on SUA interpretation. This work is novel, in that it is the first publication that explores different sub-bands of microelectrode LFPs in beta (8-30Hz) and high frequency range (200-450Hz) to identify the optimal track for chronic DBS electrode placement into STN. This work also contributes to knowledge

about the neurophysiology of PD by describing and visualizing the spatio-spectral patterns of LFPs. Because recording LFPs *simultaneous* with single neurons does not prolong the total duration of surgery, using this technique online in the operating room would increase the chance of optimal placement of the DBS macroelectrode within the motor sub-territory of the STN, without an appreciable downside. The study was published in *Frontiers in neuroscience* in 2016 (Telkes et al., 2016).

With the previous study we showed that LFPs along with their spectral features obtained from beta and HFO bands can be used to target the STN with high accuracy and optimize the DBS surgery. However, using of multiple electrodes and their sharp tips may cause intracranial hemorrhage. In this regard, with the increasing interest in using macroelectrode/DBS technique alone in STN targeting, we investigated functional use of LFPs recorded from DBS lead at various depths. By showing that the localization error of superior STN border between LFPs from DBS lead and microelectrode neuronal firing was around 1 mm with the beta and gamma band spectral features, we supported the use of intraoperative macroelectrode recordings, in conjunction with preoperative and/or intraoperative stereotactic imaging for target localization in PD. The study was published in *36th Annual International Conference of the IEEE Engineering in Medicine and Biology Society* in 2014 (Telkes et al., 2014).

In the last part of the thesis, we investigated the functional utility of LFPs in clinically defined PD subtypes. To best of our knowledge, for the first time we report that, activity in the subbands of LFPs recorded with microelectrodes from the sub-territories of STN provides distinguishing neurophysiological information about the most commonly accepted phenotypes of PD. In particular, high frequency oscillations and their

nonlinear interactions with beta band in dorsal and ventral sub-regions of the STN exclusively contain distinct patterns between TD and PIGD groups. We anticipate our findings will provide new possibilities for the interpretation of oscillatory dynamics of STN and that these well localized patterns can be used as objective neurobiomarkers to distinguish PD phenotypes and might lead future electrode technology and targeted stimulation strategies in the territories of STN for the personalization of DBS.

2. CHAPTER 2: General Methods

This chapter provides detailed description of the methods used in the studies presented in the thesis. Details of the patient demographics and the analysis specific to a study will be mentioned in the sub-sections of the relevant chapters.

2.1. Patients

This was a two-center study in which patients were recruited either at Baylor College of Medicine or Fairview Hospital of the University of Minnesota. The experimental protocol was approved by the Institutional Review Boards of the University of Minnesota, University of Houston, and Baylor College of Medicine. All patients provided written informed consent for study participation. All patients were diagnosed with idiopathic PD, and exhibited typical motor symptoms which were tremor, rigidity, and bradykinesia in addition to postural instability and gait difficulty. Patients were clinically evaluated by a movement disorder specialist and either Unified Parkinson's Disease Rating Scale (UPDRS) or Movement Disorder Society-Unified Parkinson's Disease Rating Scale (MDS-UPDRS) scores obtained in the off- and on-medication states were used to assess the severity of motor symptoms and signs.

2.2. Surgical procedure

All patients underwent functional stereotactic neurosurgery for the implantation of DBS electrode into the STN. Surgeries were performed in awake patients under the benefits of local anesthesia. Patients were asked to discontinue Parkinson’s medications 24 hours prior to DBS surgery. As per standard clinical protocol (see Fig.2.1), target coordinates and trajectory to the STN, were identified by fusing preoperative stereotactic

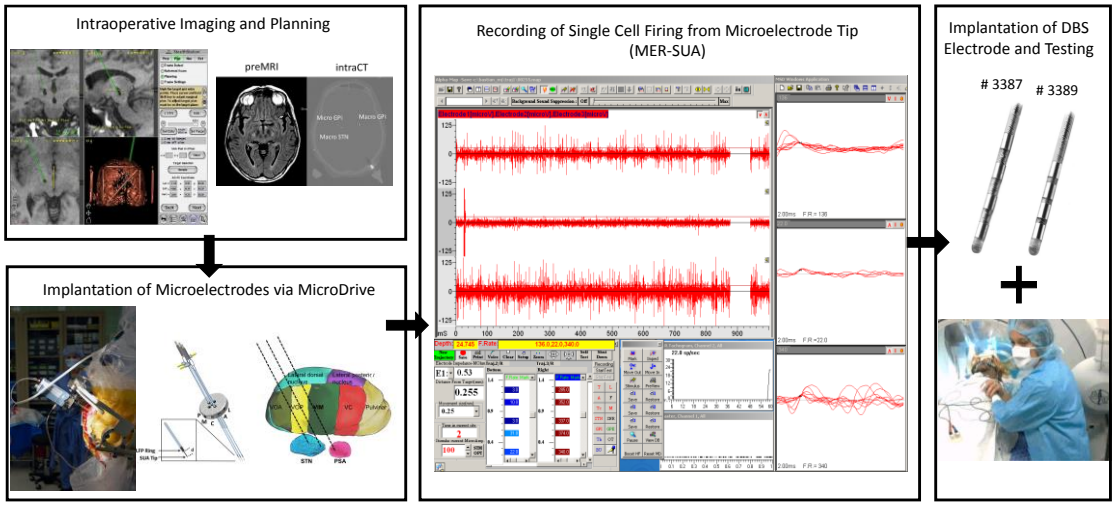

Fig.2.1. Standard clinical protocol of DBS surgery. (i) Intraoperative imaging and planning. (ii) Implantation of microelectrodes by using Microdrive. (iii) Recording of single unit activity from microelectrode tip. (iv) Implantation of DBS electrode into the selected track and verification of the target by stimulation and testing.

MRI to a preoperative or an intraoperative stereotactic CT scan on a neuro-navigational platform (StealthStation, Medtronic Corp, MN). Then, again based on standard clinical protocol, 2 or 3 simultaneous tracks were performed in each subject. The multiple microelectrodes were advanced through brain cannulas penetrating a multi-port BenGun. The superior and inferior borders of STN, along with the optimal depth for positioning the DBS electrode, were determined by the clinical team via electrophysiological mapping using MER-SUA, and the DBS electrode was implanted by the neurosurgeon based on these spatial data, followed by macro stimulation to confirm electrode location based on benefit and side effect profile—i.e., location within motor territory of STN, but not so close to border with adjacent internal capsule or medial lemniscus, that low-threshold stimulation- induced side effects were detected—followed by confirmatory intra-operative imaging modalities.

2.3. Intraoperative recordings

2.3.1. Microelectrode recordings

Following standard stereotactic techniques, and insertion of three brain cannulas and microelectrodes (Abosch et al., 2013), MER-SUA recording was carried out using a Microguide system (AlphaOmega Inc., USA) at 12 kHz. Simultaneous LFPs were recorded using an XLTEK-EMU128FS system (Natus, San Carlos, California) at 2 kHz with 16 bit A/D resolution or gHIAmp (gTec Inc, Graz, Austria) biosignal amplifier at 1.2 kHz or 2.4 kHz with 24 bit A/D resolution or 64-channel bioamplifier (Grapevine Neural Interface and Processor, Ripple, LLC, Salt Lake City USA) recording system at 2 kHz with 16 bit A/D resolution (see Fig.2.2).

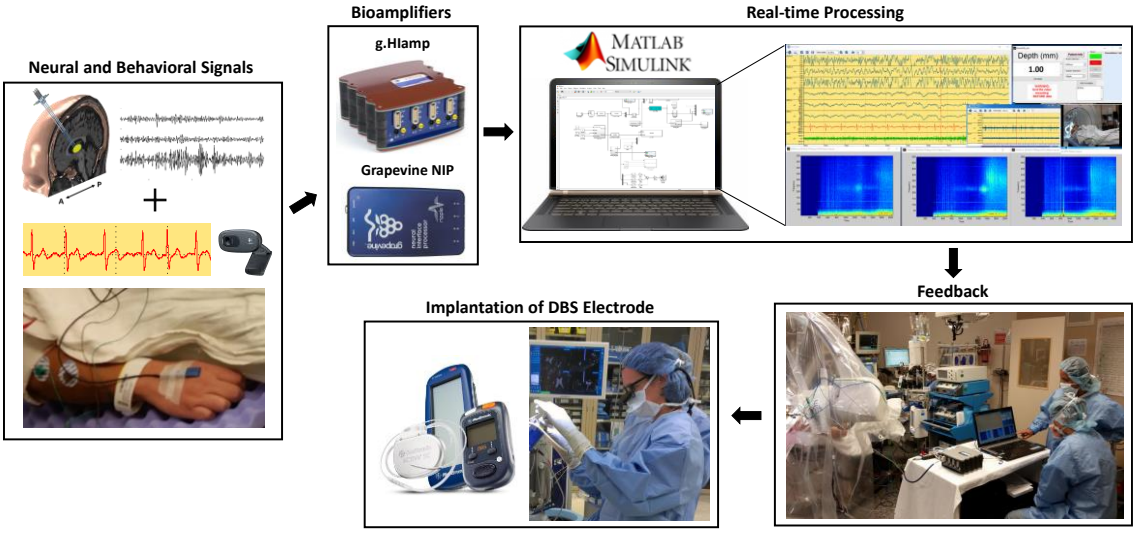

Fig.2.2. Intraoperative recording setup. (i) Recording of LFPs and SUA together with ECG, EMG, accelerometer signals, and video. (ii) Real-time processing of signals through a custom design Simulink model. (iii) Giving feedback about the optimal trajectory and the depth for implantation of DBS electrode. (iv) Implantation of DBS electrode.

The LFP recordings were obtained from a 1 mm wide stainless steel (SS) contact which is 3 mm (NeuroProbe, AlphaOmega Inc., USA) or 1 mm (MicroTargeting^{TM}, FHC Inc., USA) above the SUA recording tip and referenced to the cannula (Fig.2.3). All microelectrodes were advanced towards the estimated target using a NeuroDrive (AlphaOmega Inc., USA) with micrometer resolution. In order to synchronize the SUA and LFP recordings, the digital depth information of the NeuroDrive is transmitted from the MicroGuide system to LFP recording system using a TCP/IP connection. Initial recordings began maximum 25 mm above the intended final location of the electrode tip ("target") as determined by direct targeting methods and proceeded until the electrode reached maximum 5 mm below the MER-determined target. Electrodes were lowered in 1 mm steps until 10 mm above "target". Within 5 mm of the radiographic target, the step size was reduced to 0.5 or 0.25 mm to allow more precise identification of the borders. Duration of recordings at each depth was 15-30 seconds. At each depth, the subjects sequentially rested and after a certain depth (<10 mm) executed limb movements for 10-15 second period. The neurosurgeon used standard clinical techniques for localizing the STN, via real-time auditory and visual analysis of the recorded SUA. The dorsal, ventral,

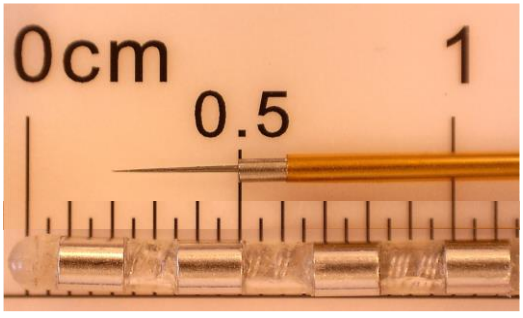

Fig.2.3. Representation of a microelectrode with a 1-mm SS contact (top) and a DBS electrode with 4 platinum–iridium cylindrical surfaces (bottom; model 3389).

and posterior borders of the targets were identified by noting increased background noise and cell firing rate. The STN neurons were examined for movement-responsive receptive fields (Molnar et al., 2005). In particular, the superior border of the targets was determined when the background activity increased and border cells were first observed among one of the tracks in MER-SUA. This position was used as the target value in the border identification. Among three tracks, the track with the longest span of bursting cell firing and movement responsive fields was selected for the chronic DBS electrode implantation.

During microelectrode trajectory to the specified targets, LFPs, high-definition video, upper and lower extremity electromyography (EMG), accelerometer signals, and electrocardiography (ECG) were recorded in order to capture and categorize patient movement, and to identify and remove any artifacts from recordings. The neurosurgeons were blinded to the LFP recordings in the operating room and the identification of the borders or the trajectories of the STN were not influenced by the LFP recordings.

2.3.2. Macroelectrode recordings

When the optimal trajectory and the optimal depth were identified for the estimated target based on electrophysiological methods as describes above, patients underwent bilateral/unilateral implantation of DBS electrode (model 3389 or 3387, Medtronic Corp, Fridley, MN) into STN in PD. These DBS electrodes contain four platinum–iridium cylindrical surfaces from deepest contact 0 to most superficial contact 3 (1.27 mm diameter and 1.5 mm length) and a spacing of 0.5 mm (see Fig.2.3) and 1.5 mm, respectively.

Similar to microelectrode recordings, DBS electrode was advanced towards the determined target using a NeuroDrive (AlphaOmega Inc., USA) starting from 20 mm above this target and continued until the electrode reached 3 mm below it. DBS electrode was moved down with 1 mm steps until 10 mm above estimated target and then the step size was reduced to 0.5 mm. LFPs were recorded from 4 contacts of the DBS electrode along with the sensor signals mentioned previously. Recordings were obtained for at least 30 seconds at each depth. When the electrode was determined at the optimal depth inside the target, an additional 2-minutes recording was obtained during resting period before target validation by stimulating DBS electrode. Signals were sampled at 2 kHz with 16 bit A/D resolution. Signals were transferred into a PC for off-line analysis.

2.4. Analysis

2.4.1. Preprocessing

All data were visualized and analyzed offline with custom in-house developed software in MATLAB 2014a (Mathworks, Natick, Massachusetts). Based on video, EMG and accelerometer signals, the data were annotated and resting state segments were extracted at each depth for further analysis.

2.4.2. Spectral analysis

In order to explore the frequency content of the LFP data at each depth, we generated a depth-frequency analysis similar to a time-frequency analysis. We observed that the LFP data were corrupted by many factors including tremor and/or environmental factors in the operating room setting. Therefore, we computed the LFP spectrum with a modified Welch periodogram method, including robust statistics. A fast Fourier

transform (FFT) was computed with a 1-second Hanning window and the window was shifted with 50% overlap. Simply, rather than using a mean operator, the median of the spectra of all sliding windows was calculated to eliminate localized artifacts in the spectrum. The method was repeated for each depth and individual spectra across depths were combined to generate a 2-D depth-frequency map (DFM) showing the depth-varying power spectrum of the LFPs. Each map was resampled with a 0.25 mm depth resolution and cubic interpolation to obtain equidistant depth values. A Gaussian kernel filter was used to smooth the maps in order to suppress noise and to reveal oscillations at bands of interest.

2.4.3. Phase-amplitude coupling

Phase-amplitude coupling for non-linear interactions between the phase of beta and amplitude of HFO bands was investigated by using a phase locking value (PLV) approach (Lachaux et al., 1999). We investigated the 150-450 Hz range as amplitude frequencies. The frequency band ranging from 4 Hz to 40 Hz was investigated as phase frequencies. LFP data were bandpass filtered with a 3rd-order Butterworth filter from 4 to 40 Hz with a 2-Hz bandwidth and 1-Hz shift. The same LFPs were filtered between 150 and 450 Hz in the HFO range with a 50-Hz bandwidth and 12.5-Hz shift using a 3rd-order Butterworth filter. The envelope of HFOs was computed by using the Hilbert transform and PLV was calculated for all combinations for each depth in the STN (Fig.2.4). Comodulograms were computed and the maximum PAC strength (values between 0 and 1) was extracted in each subject.

An analysis for statistical significance was performed over every single CFC calculated in order to check if the observed value differed from what would be expected

due to chance alone. To achieve this, a surrogate analysis was performed by calculating the coupling between randomly selected blocks of both amplitude and phase envelopes. The chance occurrence of coupling between phase and amplitude was estimated by using 200 surrogates, and a z-score was computed for each individual PAC. In order to account for multiple comparisons, Bonferroni's correction was applied (the significance level of the test a = 0.05/925, where the number of tests = 37 × 25, or 925).

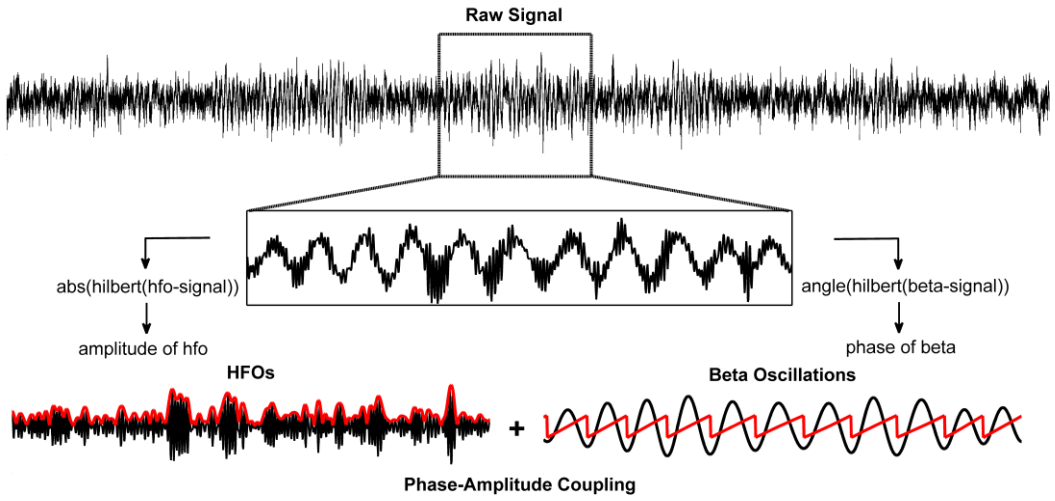

Fig.2.4. Simplified representation of phase-amplitude coupling.

3. CHAPTER 3: Prediction of the Dorsal Border of Subthalamic Nucleus and the Optimal Trajectory by Using *Microelectrode* Local Field Potentials

The work described in this chapter was published by Telkes et al. in *Frontiers in Neuroscience* in 2016 and used with permission from the journal.

3.1. Introduction

DBS of the STN is an effective therapy for the treatment of the motor symptoms of PD (Hariz, 2012; Herzog et al., 2004). However, STN stimulation can result in side effects arising from the spread of stimulation to structures surrounding the STN (Richardson et al., 2009). Moreover, sub-optimal positioning of DBS electrodes accounts for up to 40% of cases of inadequate efficacy of stimulation postoperatively (Okun et al., 2005). Thus, developing quantitative electrophysiological methods to define the optimal site of stimulation may help optimize DBS outcomes.

The task of the neurosurgeon is to place the DBS electrode within the motor territory of the STN, and well within the STN borders such that current does not spread to the surrounding structures, thereby resulting in stimulation-limiting side effects (Richardson et al., 2009). Although the surgical procedure varies somewhat between medical centers, targeting of the STN during DBS surgery generally includes preoperative stereotactic imaging (MRI), used in conjunction with stereotactic atlases. This step is followed by intraoperative electrophysiological techniques consisting of the conversion of neural activity, in the form of SUA recorded at the microelectrode tip, into audio and visual signals. This procedure is experience-based and depends critically on the neurosurgeon's and neurophysiologist's ability to recognize entry into the STN, based on a variety of cues.

In order to obtain a three-dimensional map of the STN and surrounding structures, multiple microelectrode recording tracks (typically up to five) (Benabid et al., 2009) are carried out, either sequentially or simultaneously. Determination of the optimal track for DBS implantation is a key component to successful therapeutic outcome. Optimal track selection is primarily based on MER-SUA, which is used to identify cells with firing characteristics consistent with STN neurons and response characteristics confirming the motor sub-territory of the STN (Falkenberg et al., 2006). Despite the common usage of MER-SUA during stereotactic surgery for PD, limitations of this technique include difficulties interpreting complex signal patterns to localize the anatomical borders of the STN, highly overlapping spiking characteristics of single neurons around the target structure, recording SUA from a very small region, sensitivity of SUA to noise, susceptibility of SUA to small amounts of blood or edema within the microelectrode track, and the binary nature of SUA (unlike LFP), all of which may affect the accuracy of STN localization in PD (Chen et al., 2006; Gross et al., 2006; Novak et al., 2011). The caliber of single-unit recordings can be easily diminished due to drift of the recorded unit away from the electrode tip, as a consequence of transmitted pulsations of the brain and other environmental conditions.

Interpretation of SUA recordings with computational intelligence was proposed as a new approach to help clinical decision making in the operating room (Wong et al., 2009). However, such approaches are still susceptible to the challenges of isolating single neurons in the operating room. LFPs represent the aggregate activity of neuronal populations, and are particularly sensitive to synchronous and oscillatory firing patterns (Gross et al., 2006; Priori et al., 2013). Recent studies indicate that LFPs in PD correlate

with both motor and non-motor symptoms of the disease, and their signals are more robust than SUA (Priori et al., 2013; Thompson et al., 2014). Importantly, LFPs are an objective and quantitative metric while MER-SUA is more qualitative and subject to inter-practitioner variability.

Although, the functional role of LFPs during DBS surgery is not fully established, we propose that they can be used to contribute to target localization in PD. In the present study, for the purpose of assisting with clinical decision making, we aimed to develop an automated approach by processing LFPs from multiple tracks to localize the dorsal border of STN and predict the macroelectrode implantation track identified by the neurosurgeon based on SUA interpretation.

3.2. Methods

3.2.1. Patients

Intraoperative LFPs were recorded from 22 patients (14 men, 8 women), who were diagnosed with idiopathic PD. Disease duration ranged between 1 to 20 years, with a mean of 10.55 years (standard deviation of 4.7 years). Clinical characteristics of the patients are given in Table 3.1. Details of the surgical procedure and electrophysiological recordings were mentioned in Chapters 2.2 and 2.3.1. In 3 of 22 patients, microelectrode mapping of right and left STN occurred on different surgical dates, as the surgical procedures were staged for clinical reasons. Therefore, these recordings were counted as separate, enabling 25 individual STN microelectrode recordings for LFP-based optimal track prediction.

Table 3.1. Clinical characteristics of the PD patients included in this study

Number of patients	22
Gender (women/men)	8/14
Age (mean ± std in years)	57 ± 11
Disease duration (mean ± std in years)	10.5 ± 4.7
Phenotypes:	
Typical	12
Tremor Dominant	5
Bradykinetic/Rigid	5
OFF/ON UPDRS† Scores (mean)ǂ	45.6 %
Number of microelectrodes recording (total)	75 in total

† UPDRS = Unified Parkinson's Disease Rating Scale
ǂ Pre-Operative Medication OFF-to-ON UPDRS Scores: Total Improvement

3.2.2. Data analysis

A schematic diagram of our signal processing pipeline is given in Fig.3.1. As an initial step the raw signals were visualized and it was observed that tracks were difficult to distinguish, due to a high amount of common activity masking spatially localized activity and/or artifacts resulting from abrupt movements of the patient and other environmental factors. In order to eliminate the common activity among tracks, but still preserve the track-specific neural activity, the LFP data on each track were de-correlated using a least mean square (LMS) algorithm with a steepest descent update. The general formula for the de-correlation method is as follows:

$$y(n) = w^T(n)x(n), \tag{3.1}$$

$$e(n) = d(n) - y(n), \tag{3.2}$$

$$\hat{e}(n) = \begin{cases} sign\big(e(n)\big) * 20 & if\ |e(n)| > 20 \\ e(n) & otherwise \end{cases}, \text{and} \qquad (3.3)$$

$$w(n+1) = w(n) + \mu \hat{e}(n) x(n), \qquad (3.4)$$

where $y(n)$ is the filter output, $\hat{e}(n)$ is the residual which is the de-correlated signal, $d(n)$ is the desired signal, μ is the step size, and $w(n)$ is time varying filter coefficient (M. Hayes, 1996). In the current method, each channel, $d(n)$, was predicted by using a linear weighted combination of other two channels, $x(n)$. LFP activity from 3 tracks were recorded continuously during the entire surgery while the microelectrodes were traveling to the estimated target. Consequently, the signal characteristic varied over depths. Since in each depth the signal was recorded for 15-30s, temporal variability exists in the signal. Therefore, the filter coefficients, $w^T(n)$, were updated on a sample by sample basis recursively to make the system to adapt to depth and time varying signal properties. At each iteration, the error, *e*(n), was calculated and this residual was used as the de-correlated LFP data in future steps for feature extraction and visualization. At 20 mm above the estimated target, all three tracks showed very similar signal characteristics indicating that they were in the white matter. Therefore, the initial filter coefficients were selected as the average of two channels with equal weights with the initialization of the filter coefficients $w(n) = 0.5$. By using this adaptive approach, we aimed to eliminate the common activity across tracks and suppress localized artifacts caused by patient movements and environmental factors. In order to prevent the system from being affected by high amplitude artifacts and to preserve the robustness, the error was saturated by using a 20 μV threshold (Eq.3.3). This threshold was determined experimentally and we

observed that the system recovered from localized artifacts pretty fast even if the artifact amplitude was too large.

Due to differences in spatial correlation of low and high frequency bands, the monopolar data were, first, decomposed into two frequency bands which were 8-200 Hz and 200-450 Hz by using a 2nd-order Butterworth IIR filter (Fig.3.1). The LMS algorithm was individually applied to these subbands with step size of $\mu = 0.0002$. Each track was de-correlated by using LFPs on the other two tracks. The algorithm was applied to each depth by transferring filter coefficients to the next depth. In this way, filter coefficients were not required to start from 0.5 at each new depth so that the algorithm would adapt faster and can use both temporal and spatial information of the past. Decomposed and de-correlated data were re-merged and spectral analysis was performed. In this regard, DFMs were generated as previously described in Chapter 2.4.2. Then, DFMs were normalized with the average baseline of three

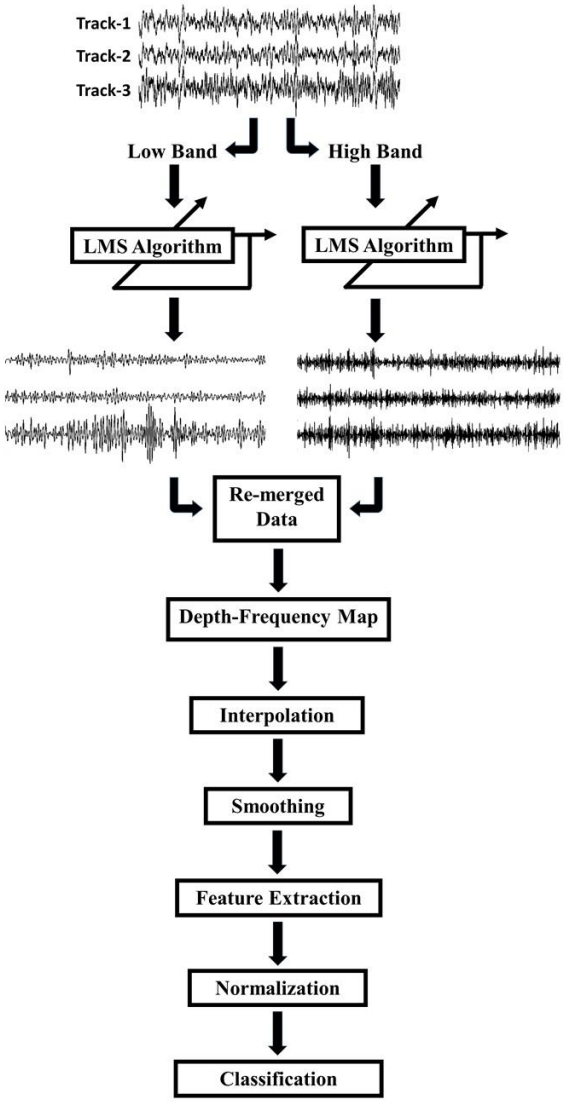

Fig.3.1. Schematic of the work flow.

tracks and transformed into log scale using the Eq.3.5 and Eq.3.6. The tracks were not normalized by their own baseline but by the mean of all three tracks in order to compare the signal power between them. The baseline used for normalization was selected as the highest depths which assumed to be in the white matter. Therefore the baseline was determined as top 5 depths (20 mm to 15 mm above the estimated target) in 22 recordings. However, in rest of the three recordings, since the analysis started from lower than 20 mm (such that 18 mm) due to artifacts, the baseline segment was kept shorter and selected as top 3 depths. The purpose of using higher depths was to avoid from including any thalamic activity in normalization segment. The baseline normalization formula is noted below:

$$\overline{b}_{avg} = \frac{\left(\bar{b}_1 + \bar{b}_2 + \bar{b}_3\right)}{3} \quad \text{and} \tag{3.5}$$

$$\overline{n}_{dfm} = 20 \times \log_{10}\left(\frac{\overline{r}_{dfm}}{\overline{b}_{avg} + \Phi(f)}\right), \tag{3.6}$$

where $\bar{b}_1,\ \bar{b}_2,\ \bar{b}_3$ are the baseline spectrum of each 3 tracks, $\overline{b}_{avg}$ is the average baseline power, $\overline{r}_{dfm}$ indicates the depth-frequency map, $\Phi(f)$ is a small regularization parameter which is applied for each frequency $f$and $\overline{n}_{dfm}$ is the normalized depth-frequency map.

In order to observe the depth-varying frequency content of LFPs, DFMs of the patients were visualized. We noted that when the electrodes reached the STN border identified by the neurosurgeon, generally there was also an excessive activity in the beta and HFO range. In order to identify the most beneficial track along with the dorsal border of the STN, the sub-band power was extracted from all tracks and normalized by using a subject-specific average baseline. Based on the distribution of neural activity on the

tracks, the sub-band frequencies were designated 11-32 Hz for beta band and 200-450 Hz for HFOs. The distribution of power in the STN among all tracks and the distribution of power only on the selected track inside and outside of STN (above the dorsal border of STN) were investigated by box and whisker plots. Student's t-test with two-sample was used to check if the distributions were significantly different or not.

3.2.3. Classification

After sub-band power features were normalized between zero and one with a Max-Min normalization method for inter-subject comparison, a linear discriminant analysis (LDA) was used for classification. The principle of LDA is to maximize the separation of classes while keeping the within class densities small by using linear combination of features, $\vec{v} \cdot \vec{z}$ (Alpaydin, 2010). The linear discriminant function:

$$g_i(z|v_i, v_{i0}) = v_i^T z + v_{i0} \text{ and}$$

$$= \sum_{j=1}^{d} v_{ij} z_j + v_{i0} \quad , \tag{3.7}$$

where $g_i(z)$ is the discriminant function for the input features z_j with sum of the weights v_j and threshold values v_{i0}.

3.2.3.1. Localization of the dorsal border of STN

In the present study, the dorsal border of STN identified by clinical team is predicted from the depth varying LFP data by using the decision distance of a linear classifier as shown in Fig.3.2.A. First an LDA classifier was trained by contrasting the LFP sub-band features coming from inside and outside of STN (above the dorsal border of STN). This classifier was evaluated at each depth and the returned decision distance

was used as a measure of confidence. The depth with the highest confidence for IN-STN decisions was marked. Then we traced the decision distances above this depth and found the location where the LDA classifier voted for OUT-STN. This point where the classifier made IN vs. OUT decision transition was finally chosen as the predicted dorsal border of STN. The difference between prediction and the STN border identified by MER-SUA was calculated in each patient and the root mean square (RMS) of the prediction errors was used to quantify the performance of the classifier. Further, statistical analysis by using Student's t-test and *F test* was conducted in order to compare the mean and the variance of predictions obtained by different subband features, respectively.

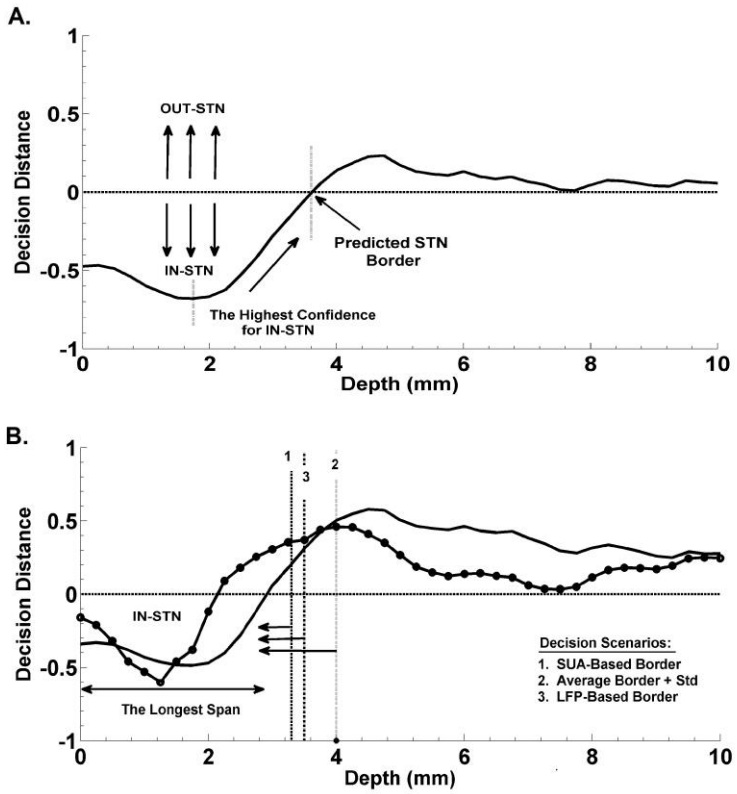

Fig.3.2. Prediction of the dorsal border of STN and prediction of optimal track. (A) Decision strategy in the prediction of dorsal border of STN. (B) Decision strategy in the optimal track prediction.

3.2.3.2. Prediction of the optimal track

The optimal track selection among three tracks is done by the neurosurgeons through interpreting the excessive single cell firings within the STN. Consequently, for the prediction of the optimal track using LFP data, an LDA classifier was trained by contrasting the LFP subband features of selected track vs. un-selected tracks below the dorsal border of STN. This classifier was evaluated at all depths as in the STN border prediction and the returned decision distance was used as a measure of confidence. The distance returned by the linear classifier was used in three different scenarios for final decision making (Fig.3.2.B). In the first scenario, the optimal track was predicted below the STN border provided by the neurosurgeon for that specific test subject based on the SUA interpretation. This represents the setup in which we fuse SUA- and LFP-based information. In the second scenario, no SUA information about the STN border of the test subject was used, and the decisions were given below the one standard deviation from the average of STN border estimated from all training subjects. In the third scenario, the optimal track decisions were made below the STN border which was derived solely from the LFP data. Specifically, here we explored whether or not the LFP could predict the optimal track without any SUA-based interpretation. We studied the classification performance below and above the STN border in these three different scenarios. A schematic diagram related to this process is given in Fig.3.2.B. Depth-varying LFP subband features of each track were classified using the trained LDA and a label and related decision distance were generated by the classifier for each depth. We classified one the tracks as the optimal one based on the longest span of decision distances voting for optimal track within the STN. Note that the longest span is a common approach used intraoperatively by neurosurgeons for MER-SUA-based optimal track selection. Note

that, if the track selected by neurosurgeon in the operating room did not match with the decision of the algorithm, the decision was counted as a misclassification.

The prediction of optimal trajectory was investigated using individual sub-band powers, beta and HFO, and their combination. To explore the benefit of the LMS algorithm over monopolar raw signals (raw signals), the same classification procedure was carried out with the raw data.

Finally, in order to assess the efficiency and reproducibility of the classification, a leave-one-subject-out method was used. In each step, one subject was used for testing, whereas the other subjects were used training the LDA classifiers for STN dorsal border and optimal track prediction. The procedure was repeated until the whole sample was classified. In addition, this procedure was performed separately for individual beta and HFO sub-bands of LFP and their combinations to examine their efficacy in classification performance.

In order to explore a relationship between classification results and post-operative simulation parameters used for the initial programming 6 months after the surgery were compared in correctly classified and misclassified groups. The distribution of stimulation amplitude, was investigated by box and whisker plots. Student's t-test with two-sample was used to check if the distribution of simulation amplitude, frequency, and, pulse width were significantly different or not.

3.3. Results

3.3.1. De-correlation of LFP data from multiple tracks

We analyzed LFP data derived from 75 MER tracks in patients with PD who were undergoing STN DBS electrode placement. Typical raw SUA and LFP data coming from

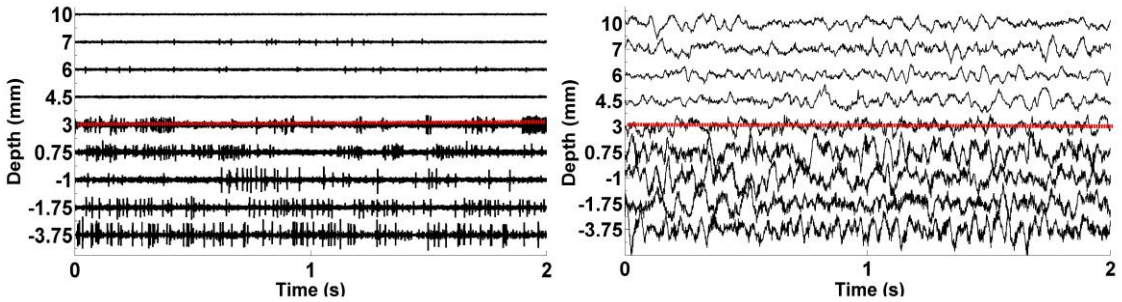

Fig. 3.3. The plots of raw SUA and LFP signals. The graphic on the left shows the single neuron activity lasting 2 seconds while the graphic on the right indicates the aggregate activity of neuron populations at the same depths with the same duration. The dorsal border of STN shown as red dashed lines is 3 mm for this representative subject.

various depths were shown in Fig.3.3. The red dashed line indicates the dorsal border of STN. The correlation between the two modalities is clearly seen. When the electrode enters the STN, both single cell firing and oscillatory activity increase.

In Fig.3.4.A-B, the mean correlation matrices of raw LFP data filtered in beta band (11-32 Hz) and HFO band (200-450 Hz) were shown. The correlation matrix in the beta band (Fig.3.4.A) explicitly shows that the spatial correlation between tracks is high whereas the correlation between tracks in HFO range is small (Fig.3.4.B). The small amount of correlation at HFO band in raw data also shows that oscillations at higher frequencies are more localized than the oscillations at lower frequencies. For these

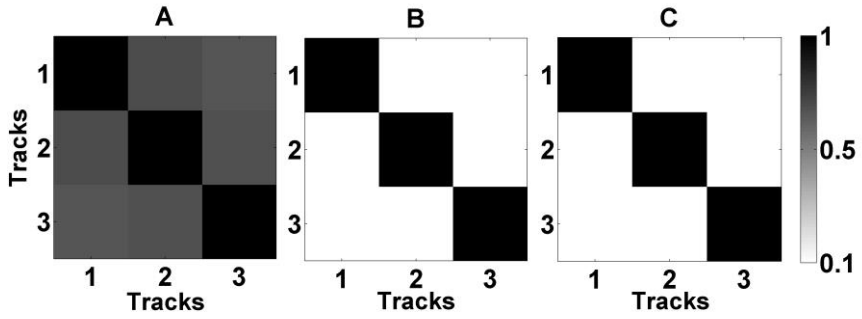

Fig. 3.4. Correlation matrices of raw and de-correlated data. (A)The correlation matrix of raw data in beta band (11-32 Hz). (B)The correlation matrix of raw data in HFO band (200-450 Hz). (C)The correlation matrix of subband-decorrelated data.

reasons, the LFP data were de-correlated with LMS separately in these frequency bands. It was found that the correlation between tracks is reduced after the LMS-based preprocessing step (Fig.3.4.C) which helped more to distinguish the tracks.

Fig. 3.5 demonstrates the effect of LMS algorithm by comparing it to the raw LFP signals. As it can be seen in Fig. 3.5.A-B-C, the raw LFP data have a high amount of common activity across all tracks at various depths which masks the spatially and temporally distinguishing patterns during targeting. In Fig.3.5.B, DFMs indicate that the high-energy low band activity among tracks masks other oscillations. The common

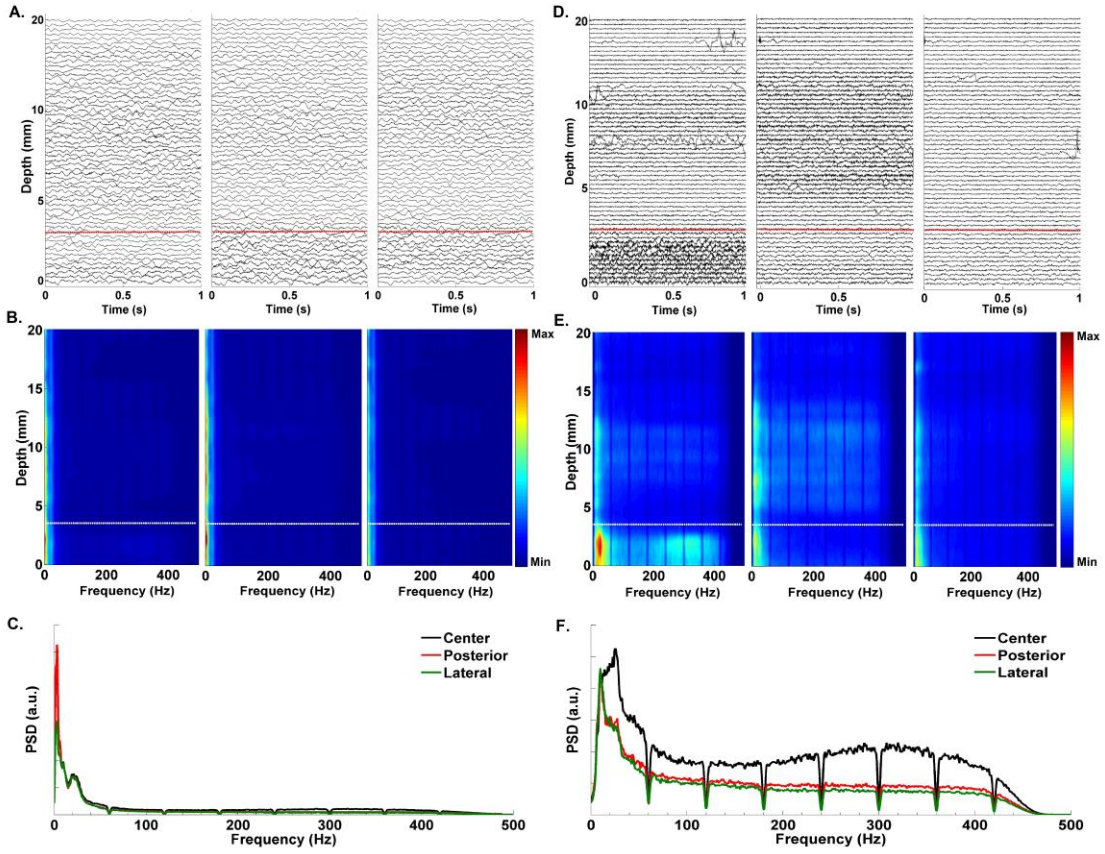

Fig.3.5. Effect of LMS algorithm. (A) Raw LFP distribution. (B) DFM generated from raw LFPs. (C) Power spectrum of raw LFPs. (D) De-correlated LFP distribution. (E) DFM of de-correlated LFPs. (F) Power spectrum of de-correlated LFPs. Red and white dashed line indicate the dorsal border of STN.

activity across three tracks and the high energy low band oscillations can be also seen in the power spectrum shown in Fig.3.5.C which was generated from the LFP data below the dorsal border of STN. On the other hand, target specific oscillations are clearly seen on de-correlated LFP data (Fig.3.5.D). In particular, the energy in the first track is much higher than the other two tracks and it is easier to observe the track differences and the estimated STN border depth for the target localization. The DFMs of these tracks shown in Fig.3.5.E demonstrate that the first track contains LFPs with higher energy in and high frequency bands below the dorsal border of the STN which is marked with a white dashed line. Furthermore, the power spectrum shown in Fig.3.5.F demonstrates that not all three tracks show excessive beta activity. There is an increase in the gamma band (35-55 Hz) and great enhancement in HFO range (200-400 Hz) in the first track compared to other tracks. The LMS algorithm not only reveals the pathological beta oscillations but also the HFOs having lower energy.

3.3.2. Spatio-spectral patterns of multitrack LFP

In order to provide a sense of the depth-varying frequency content of multitrack LFPs, we demonstrated representative normalized DFMs of de-correlated LFP data of all 3 tracks from four patients in Fig.3.6. In each map, the dorsal STN border is marked with a white dashed line. The excessive beta oscillations can be clearly seen in the first subject dominantly in the center track and localized to certain depths (Fig.3.6.A). The power of beta oscillations in the posterior and medial track is weak, yet it can be still observed. Furthermore, there is a strong and track-specific HFO around 350 Hz which is well aligned with the low band activity. On the other hand, in the subject presented in Fig.3.6.B, beta oscillations are observed in all tracks along with HFOs. Although the

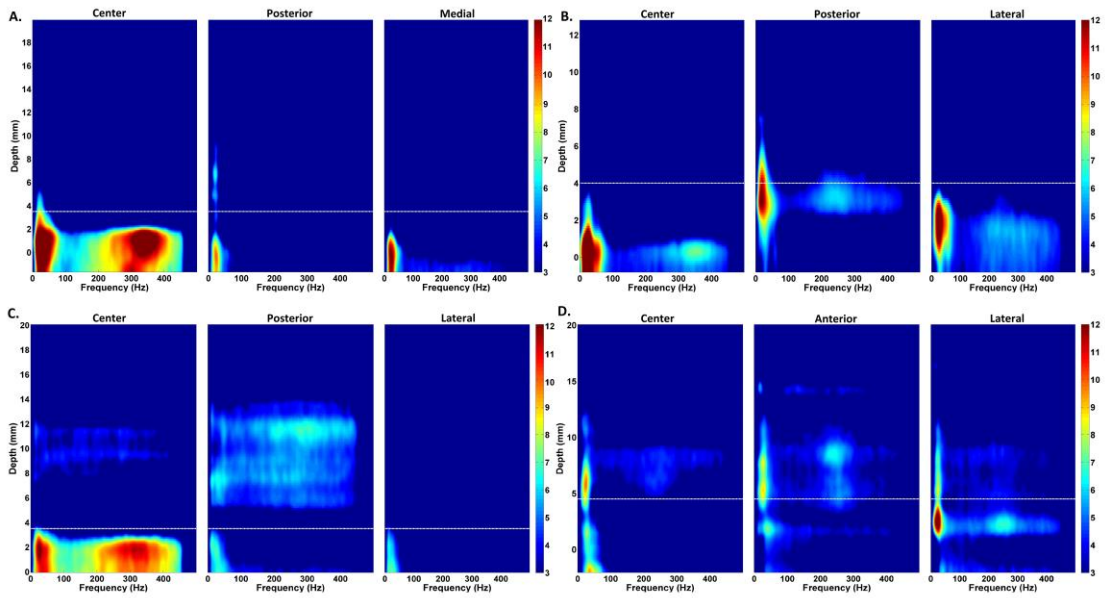

Fig.3.6. Normalized depth-frequency maps. Normalized DFMs of de-correlated LFP data of all three tracks from four representative patients are shown. The white dashed line indicates the dorsal STN border. In this subject, the selected track is anterior.

excessive LFP activity occurs below the STN dorsal border as for the patient presented in the Fig.3.6.A, the excessive depth varying spectral patterns are pretty track and region specific. The HFO on the center track sits at 350 Hz while it is located at 250 Hz on the posterior track. The lateral track shows wider but weaker oscillations. DFMs in Fig.3.6.C demonstrate a similar LFP characteristics to the first subject (Fig.3.6.A) with dominant beta oscillations and HFOs in the center track. Similarly, these oscillations are well aligned below the dorsal border and highly stronger than the beta oscillations in the other two tracks. Distinctly, strong oscillations at higher depths are observed above the dorsal border in the posterior track which might be related to thalamic activity. Note that we observed high frequency activity localized at higher depths above the dorsal border of STN in at least one of the un-selected tracks in 56% of recordings. The number of the un-selected tracks with the observed oscillations were: 8 posterior, 5 center, and 1 medial.

Similar to the HFO activity seen in Fig.3.6.C, these oscillations were noted from 11.5 mm ± 2.6 mm to 5.7 mm ± 2.4 mm (average values) above the estimated final location of the electrode tip. The tracks having higher-depth HFOs do not include strong beta activity. These oscillations have a longer spatial span with lower power. It is likely that these oscillations rise from thalamic structures (Falkenberg et al., 2006; Hutchison et al., 1998), and given their spatial distribution in relation to the beta band activity, they might be used as markers for STN localization. The fourth representative subject shown in Fig.3.6.D introduces a different LFP characteristic compared to others. None of the tracks are associated with strong, long span of beta oscillations. Specified border is not aligned with weak beta oscillations but the short lasting excessive one in the lateral track. All tracks demonstrate spatially different weak-to-minor HFOs. The overlap in the LFP activity between tracks, the weak activity across tracks and thalamic oscillations are some of the factors contributing to the challenges to the prediction of dorsal border of STN and selection of optimal track.

3.3.2.1. Intra-track and inter-track differences of LFP spectra

For the neurosurgeon selected track, the distribution of beta and HFO subband powers above and below the dorsal border of STN are given in Fig.3.7.A. The analysis shows that there is a significant difference between the power inside and outside the STN region (above the STN dorsal border) (t=44.72, p<0.001; t=34.89, p<0.001) in the selected track. As seen from the box-plot in Fig.3.7.A, the sub-band power is much higher inside the STN. When the subband power was compared between the optimal and other tracks (Fig.3.7.B), the distributions were found significant as well (t=16.47, p<0.001; t=15.17, p<0.001). The significance is consistent at the beta band and HFO

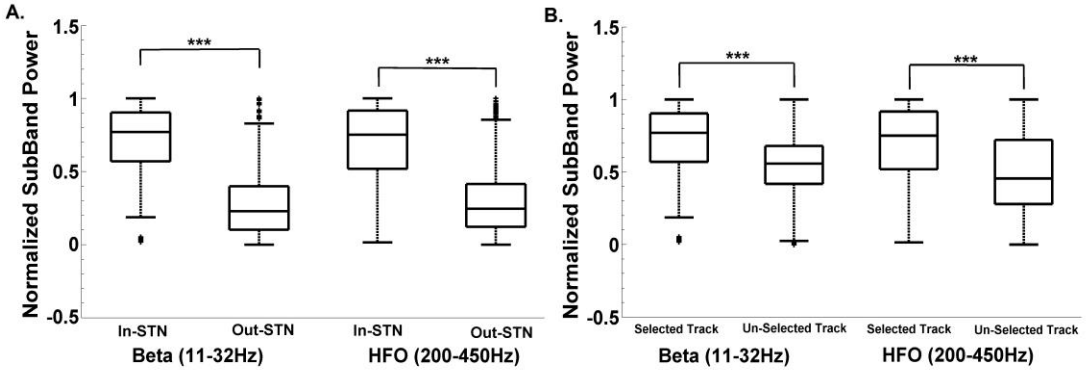

Fig.3.7. Intra-track and inter-track differences of LFP spectra. (A) IN and OUT of STN power distribution in the selected track in beta and HFO bands. (B) IN-STN power in the selected vs. un-selected tracks. ***statistically significant difference between distributions (α=0.01).

band in both distributions. The variance of HFO power in the un-selected tracks is higher than the variance in the selected track. Based on our previously mentioned findings, we postulate that thalamic activity in un-selected tracks might contribute to increased variance of HFO power when the distribution includes entire track.

3.3.3. Localization of the dorsal border of STN

The progression of prediction of STN dorsal border for representative subjects and the average results estimated from the entire patient population is shown in Fig.3.8. In Fig.3.8.A-B, decision distances returned by the classifier voting either for IN-STN or OUT-STN are shown for two representative subjects. The decision distance curves were obtained from the fused beta and HFO features. Note that the predicted STN border is shown with an arrow corresponds to the position where we find the maximum confidence point associated with IN-STN and trace back to the depth crossing zero. The dorsal border of STN provided by the neurosurgeon based on SUA interpretation is shown with a dashed vertical line. Fig.3.8.A shows a late prediction of the dorsal border (e = -0.75 mm) while Fig.3.8.B indicates an early border prediction (e = +1 mm). Fig.3.8.C

demonstrates the average border decisions with the standard deviation coming from all test subjects by using individual sub-band powers, beta and HFO, and fused features. The overall localization error of the dorsal border of STN was quantified by calculating root mean square (RMS) of the error between target values and LFP predictions across all subjects. The red and blue lines show the decisions obtained with beta and HFO band features indicating an RMS error of 1.98 mm and 1.18 mm, respectively. The mean value of prediction error for beta band features was 0.83 mm ± 1.84 mm while the mean of error for HFO band features was -0.23 mm ± 1.18 mm. The decisions obtained through

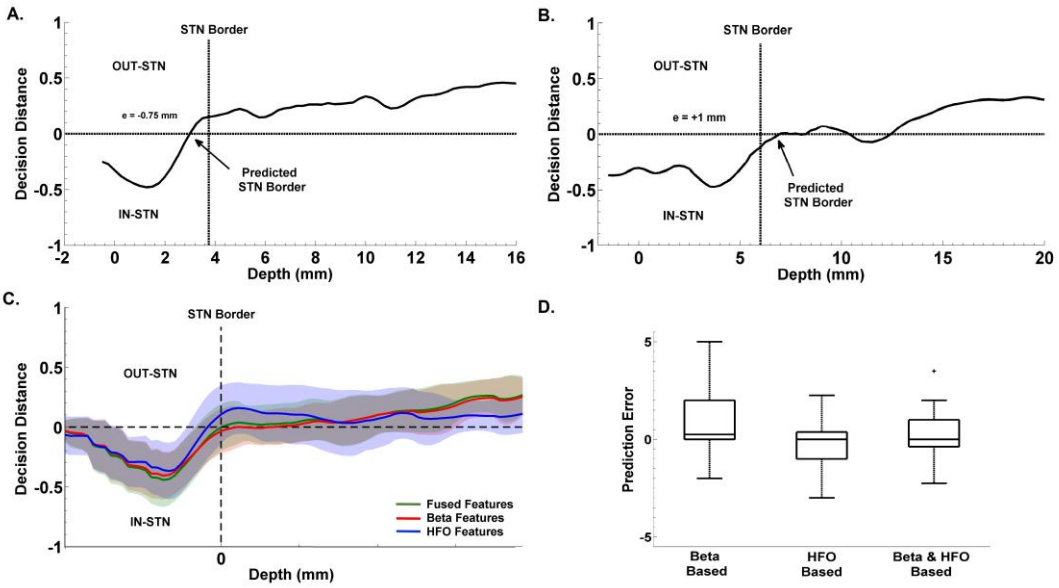

Fig.3.8. Localization of dorsal border of STN. (A-B) The decision distances returned by the classifier voting either for IN-STN or OUT-STN for two representative subjects. (C) The average border decisions with the standard deviation by using beta (red). HFO (blue), and fused features (green). (D) Comparison of prediction errors (RMS).

the fused beta band and HFO features had an RMS error of 1.22 mm with mean of 0.24 mm ± 1.22 mm. In Fig.3.8.D, the distribution of prediction errors are shown for each studied subband and their fusion. Student's two sample t-test analysis indicated that the difference between mean values of beta-based prediction error and HFO-based prediction

error was significantly different (t=2.22, p= 0.0322) while no statistically significant difference was found neither between beta-based prediction error and the error of fused features (t=1.23, p=0.2244) nor HFO-based prediction error and the error of fused features (t=-1.25, p=0.2185). When the variances of these distributions were compared by using an F test, the analysis showed that the difference between beta-based and HFO-based border prediction was only marginally significant ($F_{1,2}$=2.42, p=0.054) while there was no statistically significant difference between the variance of individual sub-band powers (beta and HFO) and fused power ($F_{1,3}$=2.26, p=0.075; $F_{2,3}$=0.94, p=0.88, respectively).

3.3.4. Prediction of the optimal track

We studied the optimal track classification in three different scenarios using the LFP data: i) below the SUA-based STN border, ii) below one standard deviation from the average STN border obtained from training data, and iii) the LFP-based STN border. We trained the LDA classifier using individual subband powers and their combination. Our results towards the prediction of optimal track from LFP data is given in Table 3.2. We note that the best results were obtained from the combined subband power features and consistently in all these scenarios, the optimal track prediction accuracy was 80% (shown in bold type) indicating that the classifier can predict the track targeted to the STN in 20/25 recordings. These results show that prediction of optimal track can be performed independently from single unit

Table 3.2 Prediction rates of classifier

Power of IN STN in all tracks

	LMS Data	Raw Data
Beta	0.72	0.64
HFO	0.68	0.68
Beta & HFO	**0.80**	0.68

recordings. When the beta and HFO subband features were used individually, the classification accuracy dropped to 72% and 68% respectively. When the procedure was repeated with the raw data, the prediction rate was poor. In particular, the classification accuracy was 64% for beta band power and 68% for the HFO and fused features which supports the observation that HFOs obtained in monopolar configuration are already highly de-correlated among different tracks.

Despite the spatially localized thalamic oscillations, the classification results obtained above the STN border were quite poor. The prediction accuracy was found to be 40% when the classification was computed above SUA-based or LFP-based STN border. Decision accuracy with average STN border was even lower at 36% by using fused sub-band power. The results indicate that the LDA classifier trained with the LFP features above the STN cannot predict the optimal track with a reasonable accuracy and was close to chance level.

The progression of classification over depths for three representative subjects are shown in Fig.3.9.A-C. In each plot, the STN border location provided by the neurosurgeon based on the SUA interpretation is also represented with a vertical dashed line. The decision distances in both selected and un-selected tracks returned by the classifier are close to each other down to the dorsal border of STN. Since the spectral characteristics of LFPs change inside the STN compared to higher depths, we observe a sudden change between the decision distances as well. If only one of the tracks deviates from the others and reaching the highest confidence level, it is easily determined as the optimal track by classifier. If more than one track are voted for the optimal track (below the zero line in Fig.3.9) with high confidence levels, algorithm gives the optimal track

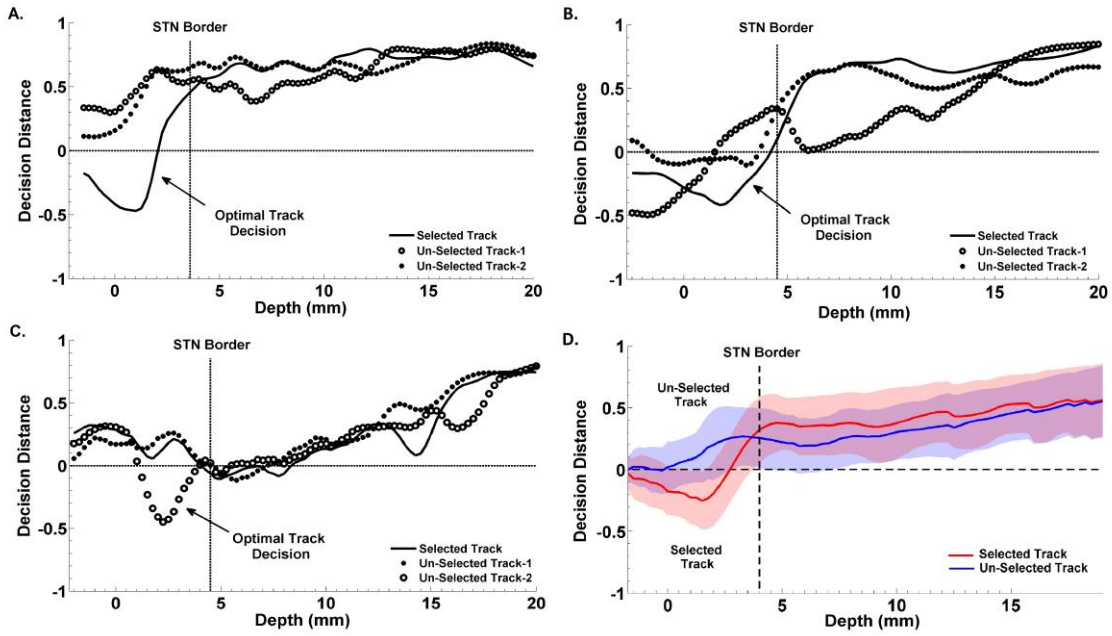

Fig.3.9. Progression of classification in optimal track prediction. (A-C) The progression of classification over depths for three representative subjects. The black dashed lines show the MER-SUA based STN border. (D) The average optimal track decisions with the standard deviation.

decision by computing the longest span of the selected track votes. The progression of the classification for a misclassified subject is given in Fig.3.9.C. The average decisions for the optimal track of all subjects with the associated standard deviation are given in Fig.3.9.D. A clear separation is observed in decision distances between selected and un-selected tracks indicating a high percentage of correct prediction among the subjects.

3.3.4.1. Distribution of selected tracks

Table 3.3 shows the frequency of selected tracks based on MER-SUA interpretation and LFP processing. As per standard clinical protocol, the initial trajectory to target STN is determined by preoperative stereotactic imaging. Three tracks are selected by the neurosurgeon based on the initial planning for microelectrode recordings.

The initial expectation is that the center track will hit the STN while other tracks account for possible targeting error. Then based on the MER-SUA recordings the optimal track is selected among these three trajectories. Although the image based planning aims to hit the STN with the center track, Table 3.3 demonstrates that intraoperative MER-SUA-based decisions among 25 recordings is not biased toward the center track. We note that the selection frequency is higher in anterior track based on MER-SUA mapping. In addition, the posterior track is not selected at all. When the selection frequency based on LFPs is studied, it can be seen that both MER-SUA and LFP decisions match with a high percentage but LFP based prediction was more in favor of the center track. Overall, our results indicate that stereotactic planning does not perfectly correlate with intraoperative electrophysiology based track selection and highlight the variance in track selection.

Table 3.3 Frequency of track selection in the present study

Comparison of SUA-based and LFP-based track selection		
	Anterior: 10/**9**	
Medial: 2/**1**	Center: 8/**10**	Lateral: 5/**4**
	Posterior: 0/**1**	

The selection frequency based on LFPs are shown in bold type.

3.3.4.2. Post-operative programming parameters

We explored whether there exist any difference in programming parameters between the correctly and misclassified patients. In particular we investigated the post-operative simulation parameters such as voltage, frequency and pulse width which were selected during the programming 6 months after the surgery. The distribution of selected stimulation voltages are presented in Fig.3.10. We note that the average stimulation

voltage used in correctly classified group is 1.72 ± 0.63 V while it is 2.12 ± 0.69 V in misclassified group. Student's two sample t-test analysis indicates that the difference in voltages between two groups is not statistically significant (t= -1.16, p= 0.2595). However, one of the misclassified subjects we observed has high level beta and HFO activity in both selected and un-selected track and this patient is stimulated with 1 V. This indicates that both tracks could be viable. When this subject is removed from the misclassified group, we note that the mean post-operative stimulation voltage increases to 2.4V ± -0.46 for the misclassified population. The difference in post-operative stimulation voltages between correctly classified and misclassified groups without this outlier becomes marginally significant (t= -1.92 p= 0.0685). No significant difference is found either in the frequency (183.1±5.8 Hz) or in the pulse width (90±26.5 μs) between groups (t= -0.74, p= 0.4692 and t= 0.96, p= 0.3477, respectively).

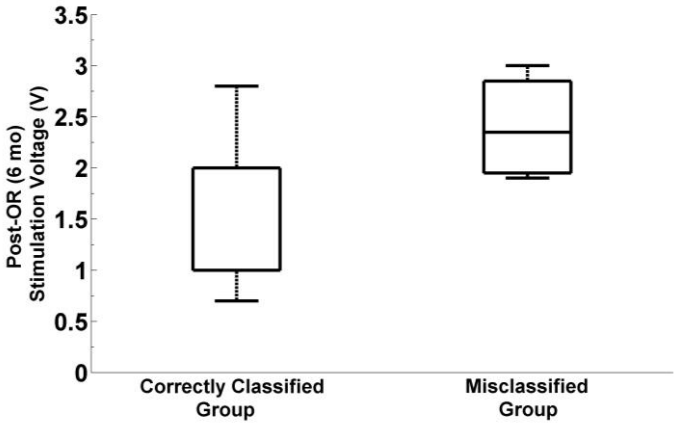

Fig.3.10. Distribution of post-operative stimulation voltages in correctly classified and misclassified groups.

3.4. Discussion

Significant variability exists in the axial and coronal orientation of the STN in humans (Patel et al., 2008), and the motor territory of the STN is small, measuring approximately 4-6 mm extent from dorsal to ventral. These factors combined with brain

shift between preoperative stereotactic imaging and intraoperative electrode brain penetration can lead to targeting errors in the operating room. Pre- and intra-operative clinical imaging methods alone are suboptimal for accurate placement of a DBS electrode; they are subject to distortion, and visualization of a clear differentiation between the STN and surrounding structures can be difficult. In this regard, our study also indicates a considerable amount of variance in track selection. Under the assumption of hitting the STN through center track by image based planning, track selection was not found to be biased toward the center track in the intraoperative MER-SUA-based decisions indicating that stereotactic planning does not perfectly correlate with intraoperative electrophysiology based track selection.

Accurate localization of STN motor territory through intraoperative electrophysiology is a crucial step for DBS electrode implantation (Gross et al., 2006; Zonenshayn et al., 2000). As recently as 2013, an international survey of high-volume DBS implanting sites revealed that 83% of centers use microelectrode recording indicating that the most commonly used electrophysiological mapping method remains MER-SUA recordings (Abosch et al., 2013). However, the method has several limitations in practice as subjective interpretation of complex signal patterns to localize the anatomical borders of the STN, being less stable and more "susceptible to technical (e.g. impedance) and physiological (e.g. cerebrospinal fluid and blood) fluctuations" (Thompson et al., 2014). As Gross et al. indicated, the number of groups using solely macroelectrode/DBS mapping to target the STN without any microelectrode recording is high (Chen et al., 2006; Gross et al., 2006; Telkes et al., 2014). Although there are advantages of using macroelectrode/DBS technique alone in STN targeting like carrying

less amount of risk for intracranial hemorrhage since there is no multiple trajectories and due to the blunt-tip of the macroelectrode (Xiaowu et al., 2010), the drawbacks like microlesion effect which might limit the clinician's ability to test or therapeutic effectiveness in the operating room and poor spatial resolution should be taken into consideration (Gross et al., 2006; Rezai et al., 2006; Wang et al., 2014). Although asleep, MRI-based non-MER-guided surgery is gaining sway (Starr et al., 2014), the possibility of clinically testing a DBS electrode prior to permanent implantation does not exist as yet in the context of such a procedure.

Earlier investigations have documented that excessive beta oscillations in certain basal ganglia structures, especially the STN, represent a pathophysiological feature of PD (Kane et al., 2009; Lopez-Azcarate et al., 2010; Oswal et al., 2013; Weinberger et al., 2006). Excessive beta band (8-30 Hz) activity is detected when the electrodes enter into the STN (Brittain & Brown, 2014; Kühn et al., 2008; Levy et al., 2002). Similarly, excessive oscillations at very high frequency ranging from 200-400 Hz are also observed (Lopez-Azcarate et al., 2010; Özkurt et al., 2011; Priori et al., 2004). Even though these high frequency oscillations are considered to represent a pro-kinetic state, and appear with dopaminergic medication and/or induced movement (Foffani et al., 2003, 2006; Trottenberg et al., 2006), others have demonstrated that HFOs (>200Hz) can still be observed in the STN during the medication OFF state or at rest (Lopez-Azcarate et al., 2010). In our study, all patients discontinued with their short and long acting medication before the surgery and were in OFF state. As others, we observed HFOs in the resting state and increased band power along with entry into the STN. Existence of excessive beta band and high frequency band oscillations within the STN in PD can be used in

target localization. However, the variability and patient-specific characteristics of spatial distribution of excessive beta and HFOs should be taken into consideration (Chen et al., 2006; Wang et al., 2014; Weinberger et al., 2006).

Despite a few publications using intraoperative microelectrode LFPs for STN localization (Holdefer et al., 2010; Michmizos et al., 2008; Wang et al., 2014), to our knowledge, no studies exist on the functional use of LFPs recorded from multiple microelectrodes for the selection of the optimal trajectory targeting the STN in PD. The present study demonstrates that using spectral features of LFP to identify the optimal track without any decorrelation technique provide sub-optimal results due to widely distributed neural signals and/or artifacts masking the spatially and temporally distinguishing patterns during targeting. Therefore, the LMS algorithm is used as an efficient technique to decorrelate the tracks by keeping localized activities in each. The adaptive LMS algorithm is widely used in the biosignal processing field since early 80s for signal enhancement due to its efficiency and low complexity (Chen et al., 1990; Ferrara & Widrow, 1982; Widrow et al., 1975). Since the decorrelation is being done recursively without violating the causality constraint, where each channel is predicted by the current samples of other data channels, the algorithm can be easily executed on standard PC architectures in real-time. Since it is an adaptive technique, the time and depth varying parameters allows tracking time and depth varying LFP activity and does not suffer from the cross talk as much as in the common average based derivation. It should be noted since it estimates current signal by using a linear combination of other signals the LMS algorithm cannot fully eliminate the high amplitude artifacts if they are not distributed among the tracks, which constitutes a major drawback of the algorithm.

One way of reducing the effect of large artifacts and keep the system stable is to use an error threshold with upper and lower boundaries. Another important factor influencing the benefit of the algorithm is the learning parameter, μ. It should be investigated by considering signal properties such that adaptation of the system should be neither very slow nor very fast.

Spectral analysis showed that beta oscillations are getting stronger as the electrodes approach the STN. Not only beta oscillations but also strong HFOs can be observed in the STN area well aligned with beta oscillations. This strong relation is noted in the tracks selected by neurosurgeons in 17 recordings out of 25. In rest of the 8 recordings, HFO was either weak or fully absent or they were noted only in one of the un-selected tracks. The energy changes above and in the STN were used to localize the dorsal border. The RMS error of prediction for the dorsal border of STN is obtained from 1.18 mm to 1.98 mm when the different features are used. The minimum prediction error is found with the power of HFOs (1.18 mm) indicating that, despite the unknown functional role of these high frequency components, they can still be eligible in STN targeting. The LFP is a continuous process and does not suffer from SUA isolation challenge while the target variable is a SUA driven information which is also prone to interpretation error and SUA isolation challenge. Considering the dorsa-ventral size of STN, 1.22 mm prediction error in depth with the fused features may represent 11% in DBS electrode 3387 or 16% in 3389 difference which can be easily compensated with the multiple contacts of the DBS electrode.

The features computed above the STN border provided poor results in prediction of optimal track. We note that the optimal track can be predicted with higher accuracy

with the features obtained below the dorsal border of STN. Analysis manifest that 14 recordings out of 25 (56% of entire dataset) indicate spatially distinct HFOs together with beta activity above the dorsal border of STN (see Fig.3.6.C-D) in at least one of the un-selected tracks. It can be assumed that these relatively weak oscillations located away from the dorsal border of STN are recorded from thalamic structures. To our knowledge, this considerable amount of thalamic oscillations in PD are not well studied phenomena. These findings presented here might be used as spatial markers in STN localization and might form the basis of further investigation into PD pathophysiology from a spatio-spectral perspective.

It should be noted that our classification technique could not predict the selected track in 20% of the subjects. We did not observe a gender difference between these five misclassified subjects. Specifically, three of them were men and two of them were women. None of the misclassified patients were tremor dominant. Three of these patients were typical PD and the other two were bradykinetic/rigid. The mean age and disease duration were 62.2 ± 13.6 and 12 ± 4.6, respectively and were not significantly different from other correctly classified patients (62.1 ± 8.3 and 10.1 ± 4.6, respectively). The misclassification in the 20% of the patients occurred due to many different factors in LFP signal including weak activity or similar activity between tracks. During these recordings, we did not use any sedation. Therefore, weak activity cannot be related to anesthesia. In one patient with typical PD phenotype, the LFP signal was weak across all tracks. We noted that the beta and HFO activity started to develop towards the bottom border of the planned target deeper than the other patients. We believe that in this particular patient the weak activity across all tracks can be described with the electrode positions. Our

observations indicate that the three tracks just started to enter the STN and did not fully went through it. In another misclassified case, the LFP activity was quite strong and similar in two out of three tracks. Therefore, the classifier output was very close for these two tracks. In the other three patients, the HFO activity in the SUA selected track was weak compared to LFP selected track. Studies hypothesize that maximum beta band (13-32 Hz) and gamma band (48-220 Hz) power is highly correlated with stimulation programming parameters in DBS chronic electrode (Ince et al., 2010). When a particular contact pair on the electrode shows strong beta and gamma oscillations, it's assumed that the electrode is closer to the source so that lower stimulation would provide better symptom improvement and less side effects. The present study supports these results. We observed higher stimulation voltages in those patients where the LFPs did not correlate with MER-SUA selected tracks. Despite the lack of statistical significance, the stimulation voltages in the 6-month-programming of implantable pulse generator (IPG) indicate lower values in the patient group having stronger LFPs in beta and/or HFO bands. A study with larger sample size would be needed to test the validity of this observation.

4. CHAPTER 4: Localization of Subthalamic Nucleus Borders by Using *Macroelectrode* Local Field Potentials

The work described in this chapter was published by Telkes et al. in *36th Annual International Conference of the IEEE Engineering in Medicine and Biology Society* in 2014, and used with permission from the IEEE Society.

4.1. Introduction

An important factor contributing to the efficacy of DBS is the accurate localization of STN in the brain. The small volume of STN motor territory, its depth from the cortical surface, and its proximity to other critical neural structures, make precise targeting crucial as well as challenging (Obeso et al., 2010). Together with stereotactic imaging, MER is the most commonly used physiological technique to determine STN location for chronic implantation of DBS macroelectrode (Zaidel et al., 2009). In MER-SUA, i.e., the electrical activity resulting from individual neurons, is recorded by microelectrodes characterized by small diameter and high impedance. The resulting signal patterns are interpreted in order to localize the anatomical borders of STN (Taghva, 2010). The number of MER trajectories being used in localization can vary based on technical factors and institutional preference from one to five or more (Cagnan et al., 2011). Following MER target localization, microelectrodes are withdrawn and replaced by the quadripolar DBS macroelectrode. Although MER provides useful information for guiding surgery, the procedure carries a risk of intracranial hemorrhage due to usage of multiple electrodes and sharp tip of these microelectrodes (Xiaowu et al., 2010). Moreover, the interpretation of signal characteristics by neurophysiologists or neurosurgeons makes the procedure more open to human error with the increased surgical

time, especially in the multi-target cases requiring MER interpretation that is more complex (Taghva, 2010).

Unlike MER-SUA, macro electrode recordings are based on LFPs which represent the aggregate activity of neuronal populations in the region of the electrode contact (Chen et al., 2006). In PD, LFP recordings from STN are an important indicator of neural rhythms (Ince et al., 2010). Studies have demonstrated an excessive synchrony in beta band (13-30 Hz) activity in STN (Jenkinson & Brown, 2011).

The aim of the present study was to explore the informational content of LFPs recorded from macro DBS electrodes, in order to identify the anatomical borders of STN. Since LFPs can easily be recorded from macro contacts, their use in the operating room can reduce surgery time and serve as a useful tool for target validation.

4.2. Methods

4.2.1. Patients

Intraoperative LFPs by DBS electrode were recorded from 6 patients (5 men, 1 women), who were diagnosed with idiopathic PD. Disease duration ranged between 3 to 11 years, with a mean of 8.5 years (standard deviation of 2.9 years). Details of the surgical procedure and electrophysiological recordings were mentioned in Chapters 2.2 and 2.3.2. All patients underwent unilateral implantation of a DBS electrode into STN (only used model # 3389: Medtronic Corp, Fridley, MN).

4.2.2. Data analysis

Recorded LFP data were annotated and visualized in the XLTEK system and then exported into MATLAB (Mathworks, Natick, Massachusetts) for processing. LFP data from all four contacts were low-pass filtered using an FIR filter with a 450-Hz cutoff

frequency, and then down-sampled to 1000 Hz for analysis (Ince et al., 2010). During preprocessing of LFP data, monopolar signals were converted into bipolar derivation (0-1, 1-2, 2-3). It should be noted that each bipolar contact represents the LFP activity at different depths with 2 mm spacing. Consequently, LFP data derived from all bipolar contacts (which sample different depths) were combined and processed together.

In order to explore the frequency content of the LFP data at each depth, we generated a depth-frequency analysis similar to a time-frequency analysis. Details of the approach was mentioned in Chapter 2.4.2.

We investigated the depth-frequency maps and extracted the energy of LFP sub-bands at each depth to identify the superior STN border. The sub-band energy values at each depth were first filtered by zero-phase filtering in both forward and reverse directions to smooth the data. Then, output was interpolated with 0.5 mm resolution. Instead of joining data points by straight line segments using a linear interpolation, a cubic interpolation method was chosen. Finally, the interpolated signal was normalized between zero and one with a Max-Min method.

In order to identify the superior STN border using normalized sub-band energy features, we first determined a 10% threshold to find noticeable energy increase with respect to higher depth values. Then, we computed the first derivative of the data to inspect the change in energy of consecutive data points. We identified the superior STN border using the following criteria:

- energy value exceeds the 10% threshold
- the slope of the signal is positive for the three consecutive points
- the slope was taken into account after 7 mm and below

In order to compare the borders identified by MER-SUA and LFP, a paired student t-test was conducted. Moreover, the root mean square (RMS) of these differences was calculated.

4.3. Results

The raw LFP data of a representative subject is shown in Fig. 4.1.A. Typical artifacts which resulted from abrupt movements of the patient and other environmental factors can be seen at the higher depths. After the electrode reached a certain depth, high amplitude LFP activity was observed. This amplitude change occurred consistently in all subjects between the superior and inferior border of STN as identified by MER-SUA. To give a flavor about the frequency content of LFP activity at various depths, the depth-frequency map of the same subject is shown in Fig. 4.1.B. We observed a clear increase in beta-band energy within the STN borders (as defined by MER-SUA).

Surprisingly, excessive LFP activity was not limited to the beta-band but was also observed at higher bands, ranging up to 450 Hz. Based on these observations, we decided to use beta (13-30 Hz) and gamma frequency bands (48-450 Hz) for localization of STN border. Similarly, filtered LFP signals indicate an increasing trend inside the STN in these bands (Fig.4.1.C-D) that may provide an alternative approach to localize the borders.

In Fig.4.2, the sub-band energy plots for all subjects in the beta (A) and gamma bands (B) are demonstrated. The sub-band data of all subjects were normalized to its maximum value and aligned with respect to the average superior border of the STN (red dashed line). Except one subject, (data in orange color) in all cases the beta band energy is well correlated with the STN superior border.

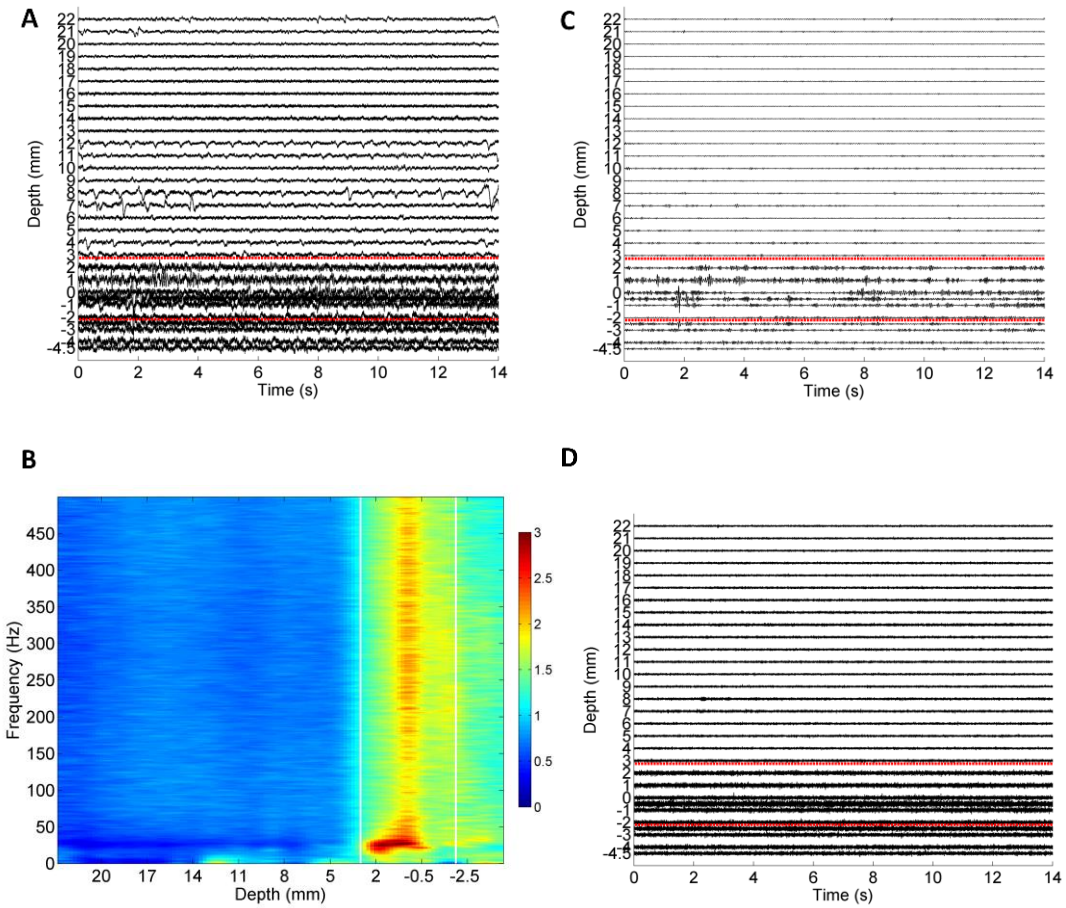

Fig.4.1. LFP dynamics for a representative subject. (A) The raw LFP data. (B) Spectral analysis. (C-D) Bipolar LFPs band passed filtered at 13-30 Hz and 48-500 Hz, respectively. White and red dashed lines show the upper and bottom borders of STN.

Figure 4.3 shows the variance values of representative subject with the differences of consecutive data points at each depth at beta band. In order to select the superior border of STN, a 10% threshold was applied and the first data point below 7 mm passing the threshold and having a positive slope (increasing energy trend) was selected as the superior border. Up to 7 mm, all subjects were having a consistent variance and 7 mm was the first point having an increased standard deviation (pink shaded area) from the average and the unlikely possibility of above depths being top border (10 mm is

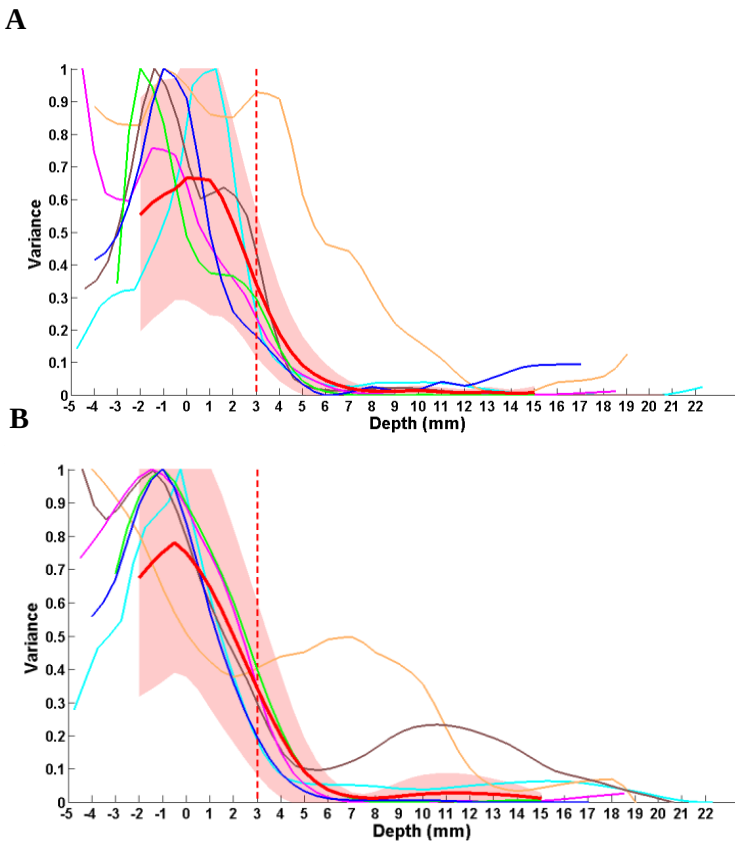

Fig.4.2. Variance-vs-depth plots. The red lines show the mean variance along the depths and the pink shaded areas show ± standard deviation around the mean.

corresponding 7 mm above the average superior border), 7 mm was chosen as threshold depth value.

The mean value of superior STN border estimated with MERs was 3.61 ± 0.92 mm while the mean value of superior border derived from macro electrode LFP recordings was 4.67 ± 1.03 mm and 4.08 ± 1.56 mm in beta and gamma bands, respectively. The root mean square (RMS) of the difference between MER and LFP was 1.26 mm in beta and 1.06 mm at gamma band. The mean ± standard deviation of distance was -1.00 ± 0.84 mm and -0.42 ± 1.07 mm in beta and gamma bands, respectively. Student t-test analysis pointed that the differences between macroelectrode recordings and MERs were statistically significant for beta band ($p=0.03$, $\alpha=0.05$), however non-significant for gamma band ($p=0.38$, $\alpha=0.05$).

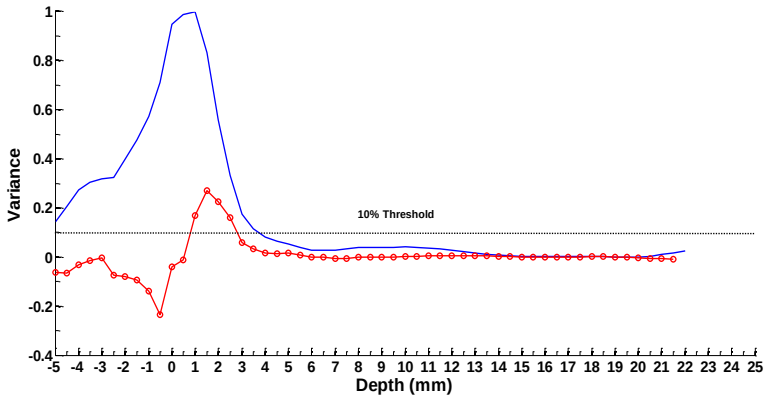

Fig.4.3. Variance vs depth plot with the differences between each consecutive data points for a representative patient.

4.4. Discussion

Previous studies suggested that the excessive beta-band activity of LFP can be used to localize STN. In the present study, during a DBS electrode implantation surgery, we recorded LFPs from four contacts of DBS macro electrodes in six patients. We observed increased LFP activity between the superior and inferior STN borders. After computing the LFP spectrum at each depth, we observed that excessive activity occurs not only in the beta-band, but also in the higher bands, ranging from 40 up to 450 Hz. Subsequent data analysis has shown that the localization error of superior STN border between macro electrode recordings and MER-SUA was around 1 mm in both beta and gamma band. These results support the use of intraoperative macro-electrode recordings, in conjunction with preoperative stereotactic imaging for target localization in PD. Due to the more robust nature of the LFP signal- derived from populations of neurons, instead of single neurons, LFP signal based confirmation of DBS location might be more advantageous than MER-SUA. LFP-based DBS surgery might also lend itself to a more automated approach to interpreting complex intraoperative neurophysiology rather than

the current scenario that requires significant expertise in auditory MER-SUA interpretation. It should be also noted that due its comparatively large contact size and between contact spacing, the DBS macro electrode has poor spatial resolution than the MER. For instance, for a bipolar contact derivation, at least a 3.5 mm displacement is required for both contacts to pass through a structure. In contrast, MER is characterized by superior spatial resolution as the SUA activity is recorded from the tip of the microelectrode, which has a length of several microns in length. Another drawback of the study is regarding only the superior border of the STN. In DBS surgery, the target depth is primarily the inferior border of STN rather than the superior border. However, because of the risk of serious side effects in case of further insertion of electrode, it is difficult to record data from lower depths.

5. CHAPTER 5: Electrophysiological Footprints of Motor Subtypes of Parkinson's Disease

5.1. Introduction

The great variability in clinical manifestations of Parkinson's disease such as motor and/or cognitive features or age at onset of the disease along with its prognosis allow different subtype classifications (Marras & Lang, 2013; Stebbins et al., 2013). Despite the various subgroups determined by data-driven approaches (Graham & Sagar, 1999; Lewis, 2005; Selikhova et al., 2009), the most commonly accepted and studied phenotypically defined subtypes of PD are: (i) tremor dominant (TD), (ii) postural instability and gait difficulty (PIGD), and (iii) a mixed type which includes balanced distribution of the symptoms of PIGD and TD (Jankovic, McDermott, et al., 1990; Nutt, 2016). This categorization is based on the clinical observations evaluated often by using the Unified Parkinson's Disease Rating Scale (UPDRS) or the revised version of it released by the Movement Disorder Society (MDS-UPDRS) (Stebbins et al., 2013). Studies have shown that patients with TD-PD have a relatively slow disease progression and the annual increase in symptom severity in PIGD is larger (Jankovic & Kapadia, 2001). In particular, severe cognitive dysfunction is consistently seen in PD patients with late-onset or in PIGD patients while TD-PD patients or those with young-onset show either no cognitive impairment or less (Marras et al., 2014; Halliday & McCann, 2010; Rajput et al., 2009). One study showed that the signs of dementia appeared in TD patients only after PIGD symptoms developed (Alves et al., 2006). Evaluation of motor subtypes over time indicated an instability such that most of the TD subtype at the onset of the disease switched to MIX subtype by emerging more akinetic/rigid symptoms with the

disease's progression and years of therapy (Schiess et al., 2000). The distinction between these subtypes are further shown with different modalities in which different morphology, neurochemistry and/or circuitry were demonstrated in parkinsonian basal ganglia (Eggers et al., 2011; Lewis et al., 2011; Rossi et al., 2010; Schiess et al., 2000).Yet, absence of a reliable diagnostic marker and changing nature of symptoms in time might lead to suboptimal treatment.

A meta-analysis study by reviewing literature from 1988 to 2014 for clinical diagnosis of PD via a Bayesian approach indicated that the pooled diagnostic accuracy, with respect to specificity, performed by movement disorder experts was initially 76.4% and increased to 84.9% after follow-ups (Rizzo et al., 2015). Several studies also reported that accuracy of clinical diagnosis of PD was not very high and even less than 80% (Gelb et al., 1999; Hughes et al., 1992; Rajput et al., 1991). Even if the accuracy of diagnosis was increased to 93% by using detailed diagnostic criteria, cases of atypical parkinsonism could be still missed by being misdiagnosed with the common atypical parkinsonian disorders like progressive supranuclear palsy, multiple system atrophy, dementia with Lewy bodies or vascular parkinsonism (Hughes et al., 1992; Lewis, 2005; Poewe & Wenning, 2002). Considering that PD is the most common misdiagnosis for ET (Jain et al., 2006), differentiation of PD from non-degenerative tremor disorder like ET, is also crucial to provide a beneficial therapy to the patient (Newman et al., 2009).

DBS of the STN is an effective therapy for the treatment of motor symptoms of PD. STN is a small and ovoid-shaped structure surrounded by various structures such that fibers of internal capsule on anterior and lateral sides, anteromedially Fields of Forel (FF), posteromedially red nucleus (RN). Zona incerta (ZI) stands as a barrier in between

STN and ventral thalamus while the substantia nigra (SN) situated in just below the ventral border of the STN (Hamani, 2004; Patel et al., 2008). It has been well accepted that sensorimotor region of STN which is located at the dorsolateral side is an effective target for alleviation of cardinal symptoms of PD (Herzog et al., 2004; Saint-Cyr et al., 2002). Further, it was found that stimulation of dorsal region of STN including FF and/or ZI might provide a better efficacy and symptom improvement (Voges et al., 2002; Yelnik et al., 2003). Plaha and his colleagues showed that the highest improvement in UPDRS scores was noted in the ZI-stimulation group (Plaha et al., 2006). More importantly, the most remarkable improvement in this group was seen in tremor scores compared to rigidity and bradykinesia.

It has been proposed that different morphology, neurochemistry and/or basal ganglia circuitry underlie the PD subtypes, especially between TD and PIGD. Yet, to our knowledge, no electrophysiological pattern linked to the two subtypes has been identified in the basal ganglia. Absence of a reliable biomarker might lead to suboptimal treatment using DBS. Here, we tested the hypothesis that the spatio-spectral patterns of LFPs recorded with microelectrodes from STN sub-territories can be used to distinguish PD patients with PIGD or TD motor subtypes.

5.2. Methods

5.2.1. Patients

Intraoperative LFPs were recorded from 27 patients (10 women, 17 men) who were diagnosed with idiopathic PD (see Chapter 2.2 for surgical details). Patients included in this study exhibited typical motor symptoms, including tremor, rigidity, bradykinesia, and postural instability and gait difficulty. Patients were clinically

evaluated by a movement disorder specialist and either UPDRS or MDS-UPDRS scores obtained in the off- and on-medication states were used to assess the severity of motor symptoms and signs. In order to designate the motor phenotypes of the patients, tremor scores and postural instability-gait scores of UPDRS or MDS-UPDRS were calculated using the formula suggested by Jankovic et al. (Jankovic, McDermott, et al., 1990; Stebbins et al., 2013). The tremor scores were calculated from UPDRS part-II question 16, part-III questions 20 and 21 or MDS-UPDRS part-II question 2.10 and part-III questions 3.15-3.18. In order to obtain PIGD scores, UPDRS part-II questions 13-15, part-III questions 29 and 30 or MDS-UPDRS part-II questions 2.12, 2.13 and part-III questions 3.10-3.12 were used7. If the ratio of average tremor score and average PIGD score was greater than or equal to 1.5, or the PIGD score was zero, patients were grouped as TD. If the ratio is less than or equal to 1, patients were categorized as PIGD. Patients with a ratio of TD to PIGD between 1 and 1.5 were excluded from the analysis. Clinical characteristics of included subjects are provided in Table 5.1. For 3 patients (1 TD and 2 PIGD) the phenotyping was documented but the UPDRS data was not available at the time of data analysis.

5.2.2. Data analysis

Spatial projection: When microelectrodes enter the STN, an excessive oscillatory activity is observed. In order to fuse information from multiple electrode tracks and increase the signal-to-noise ratio as compared to the original signals in each individual trajectory, a spatial projection based on the weighted linear combination of LFPs from 3 tracks was utilized (Fig.5.1.A). First, artifact-free LFP data in each trajectory were divided into two groups: (i) LFP data recorded from those depths at which the electrodes were determined

Table 5.1 Patient Demographics and Clinical Characteristics

Phenotype	Patient Index	Sex	Age	Disease duration	Age onset	Tremor/PIGD Ratio[a]	Side	Improvement (%)[b]
PIGD	1	F	71	12	59	NA	Left	32
	2	M	70	19	51	1.0	Left	20
	3	F	56	15	41	0.0	Left	66
	4	M	71	6	65	0.6	Left	18
	5	F	60	13	47	0.1	Left	14
	6	F	73	12	61	0.8	Left	24
	7	F	62	10	52	NA	Right	33
	8	F	77	11	66	0.1	Right	16
	9	M	58	11	47	0.4	Right	14
	10	M	61	1	60	0.0	Right	9
	11	M	69	8	61	0.1	Right	24
	12	M	69	19	50	0.0	Left	32
	13	M	67	10	57	0.0	Left	15
TD	14	M	59	3	56	1.7	Left	28
	15	M	61	5	56	3.1	Right	12
	16	M	68	13	55	2.2	Left	7
	17	M	47	13	34	6.9	Left	20
	18	M	64	5	59	1.8	Left	4
	19	F	67	6	61	NA	Left	NA
	20	F	66	7	59	∞*	Left	12
	21	M	50	15	35	2.1	Left	21
	22	M	54	9	45	2.3	Left	22
	23	M	64	12	52	1.7	Left	24
	24	F	80	25	55	4.1	Right	29
	25	F	49	6	43	3.6	Left	39
	26	M	61	9	52	3.0	Right	18
	27	M	55	4	51	∞*	Right	17

[a]Mean tremor scores divided by mean PIGD scores based on preoperative medication OFF UPDRS or MDS-UPDRS scores part II-III. *Ratio is infinite. [b]Percentage of improvement in UPDRS or MDS-UPDRS part III medication ON vs OFF. NA: not available.

to be in STN, and (ii) LFP data recorded between dorsal border of STN and 5 mm above it, which were used as baseline. LFP signals at these depths were filtered between 4 Hz and 450 Hz cutoff frequencies by using a 2nd-order Butterworth filter. Then, 3x3 spatial

covariance matrices, $\sum_{STN}$ and $\sum_{Base}$, were calculated using the LFP data from 3 tracks. Using objective function (5.1)

$$\lambda = \frac{\omega^T \sum_{STN} \omega}{\omega^T \sum_{Base} \omega} \quad (5.1)$$

we searched for a spatial projection vector, w, in order to maximize the variance ratio $\boldsymbol{\lambda}$. This is a generalized eigenvalue decomposition (GED) problem and the eigenvector corresponding to the largest eigenvalue was chosen to maximize $\boldsymbol{\lambda}$. Ultimately, 3-track LFP data at each depth were projected into a single virtual channel using this eigenvector w which combines the recordings in a linear weighted fashion (Fig.5.1.A). This projection simply fused information of multiple tracks and maximized the variance of LFP data recorded in STN while minimizing the variance of recordings obtained out of STN. The projected data were used in further analysis for feature extraction and to investigate the spatio-spectral dynamics of the LFPs.

Spectral analysis: A modified Welch periodogram method with robust statistics as described in Chapter 2.4.2 was used to investigate the LFP data in the frequency domain at each depth. DFMs generated for each patient were aligned according to the dorsal border of the STN, which was identified in each case based on MER-SUA. By this method, depth equals to 0 mm was used to signify the dorsal border of the STN in all subjects. In addition to individual maps, all DFMs were averaged independent of the patient's phenotypic designation, and a global baseline spectrum with minimum power was calculated above the dorsal border. Then, individual DFMs of TD and PIGD subjects were separated, and a single map was generated for each phenotype by intra-group averaging. These two maps were normalized according to equation (5.2) by previously extracted baseline spectrum and are shown in dB scale,

$$n_{dfm} = 20 \times log_{10}\left(\frac{r_{dfm}}{base}\right), \quad (5.2)$$

where n_{dfm} is the normalized DFM in dB scale, r_{dfm} is the raw DFM and the base is the baseline spectrum.

Visualization of DFMs revealed localized slow and fast high frequency oscillations (HFOs, 150-450 Hz) in the STN. In order to further characterize these focal activities, from the average DFM, the peak frequency between 150 and 450 Hz at each depth was obtained starting from the dorsal border until the final depth. Then, STN was divided into dorsal and ventral regions based on the shift in peak frequency of HFOs. This segmentation was applied to all subjects. The rest of the analyses were then individually computed in these defined segments to explore the spectral dynamics of LFPs in the dorsal and ventral regions of the STN (Fig.5.1.B).

Subband Features. An average LFP power spectrum was computed within the dorsal and ventral regions in each subject. Additionally, a baseline power spectrum was computed from the LFP data recorded between dorsal border of STN and 5 mm above it. In total, three spectra representing baseline (out of STN), dorsal STN, and ventral STN segments were derived per subject (Fig.5.1.C). The beta band range was used as 8-35 Hz. The lower and upper frequency limits for subband features in HFO range were determined according to visual inspection of the average spectra in groups without any normalization. Slow HFO (sHFO) range was defined from 200 to 260 Hz (due to a sharp peak in the dorsal STN region in the TD group), and a fast HFO (fHFO) range was defined from 260 to 400 Hz. Subband powers in the beta, slow and fast HFO frequency bands were computed in the dorsal and ventral STN regions and normalized to the

corresponding baseline power and converted to dB scale, representing the relative in-STN power change in different sub-territories.

Phase-amplitude coupling. Phase-amplitude coupling for non-linear interactions between the phase of beta and amplitude of HFO bands was investigated by using a phase locking value (PLV) approach which was described in Chapter 2.4.3. We investigated the 150-450 Hz range as amplitude frequencies. The frequency band ranging from 4 Hz to 40 Hz was investigated as phase frequencies. Comodulograms in the dorsal and ventral sub-territories were computed and the maximum PAC strength (values between 0 and 1) was extracted in each subject (Fig.5.1.D).

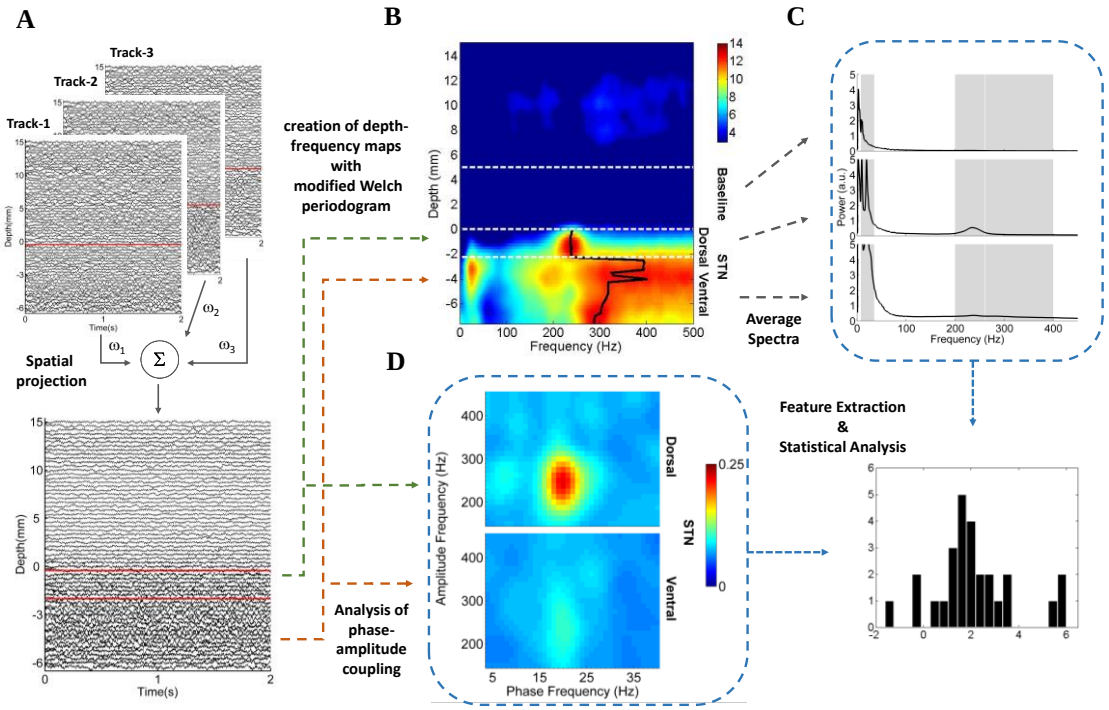

Fig.5.1. Schematic diagram representing the workflow. (A) Raw LFPs with calculated spatial projection vectors. The dorsal MER-SUA based STN border marked with red dashed line. (B) A typical example of DFM of a TD subject. (C) Average power spectrum obtained from each segment shown in B. (D) PAC of the same TD subject.

Statistical analysis. Statistical analyses were also performed in Matlab 2014a. In order to assess the normality and the homogeneity assumptions of the Student's t-test for the feature distribution, the Shapiro-Wilk test and Levene's test were used, respectively. However, assumptions were not held for most of the variables. Therefore, the non-parametric Mann-Whitney U-test for unpaired samples and the Wilcoxon signed-rank test for paired samples were used. The Mann-Whitney U-test was applied to compare the spectral features and the maximum PAC strength between phenotypes. For the intra-group comparisons of the spectral features obtained from the same region, the Wilcoxon signed-rank test was used. The significance threshold was set to 0.05 in all the statistical analyses.

Receiver operating characteristic (ROC) curves were generated for extracted features and the area under the ROC curve (AUC) was used to quantify the discrimination power of features between phenotypes. To quantify the correlation between LFP features and the tremor and PIGD scores, a Spearman's correlation analysis was used.

5.2.3. Results

LFPs from the STN obtained with 3 simultaneous microelectrodes were recorded in 27 PD patients (Fig.5.2.A). Based on UPDRS or MDS-UPDRS scores of these patients, 14 of them were identified as TD and 13 as PIGD. Visual inspection of the raw LFPs indicated an increased oscillatory activity in both PIGD and TD patient populations upon the electrode entry into the STN. The wideband LFP power difference between in and out STN was found statistically significant (in STN vs out STN, $p<0.001$, Wilcoxon's test) without any distinction between groups ($Z=0.024$, $p=0.981$, Mann-

Whitney U test) (Fig.5.2.B-D). However, depth frequency maps (DFMs) revealed distinct spatio-spectral patterns of LFPs between the TD and PIGD groups of PD patients.

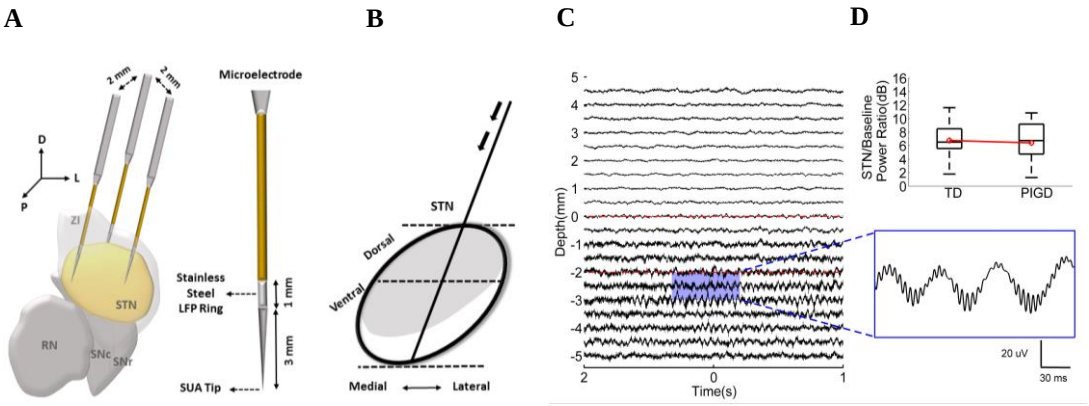

Fig.5.2. LFPs recorded from multiple microelectrodes. (A) 3-D representation of microelectrode implantation into STN. (B) The trajectory of an optimally placed microelectrode from coronal view. (C) Projected LFPs in each depth. (D) Power ratio of STN to baseline in TD and PIGD groups.

Fig. 5.3.A shows the average DFMs of TD and PIGD groups by being aligned to 0 mm. In the TD group, a strong and quite localized 200-to-260 Hz activity was observed beginning at the dorsal STN border (0 mm) and extending 2 mm below it. These sHFOs were well aligned both with beta oscillations (8-35 Hz) and with the dorsal STN border. No clear sHFO peak could be observed in the average DFM of PIGD subjects. The beta oscillations and HFOs in the PIGD group appeared slightly inferior to the dorsal border. Spatio-spectral patterns of LFP oscillations in STN were investigated in detail by dividing STN into (i) dorsal and (ii) ventral regions (Fig.5.3.A, panels with zoomed in view). The panels next to DFMs indicating the zoomed in view of the spatial distribution of peak frequencies between 150 and 450 Hz calculated from average DFMs in TD and PIGD groups. The left panel shows the 2mm-span of the shift from sHFO to fHFO in TD group (mean ± s.d. of depths of shift, 1.93 ± 1.46 mm). Since there is no clear shift in

PIGD group, DFMs in all subjects were divided into dorsal and ventral regions based on the observations in TD group. Once the electrodes advanced ventrally, it was noted that both groups demonstrated fHFO with wider bandwidth ranging from 260 to 400 Hz (mean ± s.d. of TD, 290 ± 26 Hz; PIGD, 322 ± 32 Hz) and with a significant difference between the peak frequencies of two groups (Z=-2.479, p=0.013, Mann–Whitney U test).

The averaged LFP spectra in dorsal and ventral subregions for each group are shown in Fig.5.3.B. Top row represents the dorsal average power spectra and bottom row represents the ventral average spectra in frequencies below 100 Hz and above 100 Hz. Gray shaded areas represent the beta band (8-35 Hz), sHFO (200-260 Hz), and fHFO bands (260-400 Hz), respectively. Statistical analysis showed that band power of beta, sHFO, and fHFO were all significantly larger in ventral region compared to values in dorsal region in both groups (Wilcoxon's test, TD-beta: Z=2.323, p=0.010; TD-sHFO: Z=2.260, p=0.012; TD-fHFO: Z=3.264, p<0.001; PIGD-beta: Z=3.075, p=0.001; PIGD-sHFO: Z=3.145, p=0.001; PIGD-fHFO: Z=3.075, p=0.001).

The sFHO power in the dorsal subregion of the STN was significantly higher in the TD group compared to the PIGD group (Z=2.402, p=0.016, Mann–Whitney U test). However, no significant difference in sHFO power was found in the ventral subregion (Ventral-sHFO: Z=0.849, p=0.396). Similarly, there was no significant difference noted in the beta or fHFO power in the dorsal or ventral subregions between groups (Fig.5.3.C) (Mann–Whitney U test, Dorsal-beta: Z=0.704, p=0.482; Dorsal-fHFO: Z=1.480, p=0.139; Ventral-beta: Z=0.024, p=0.981; Ventral-fHFO: Z=0.898, p=0.369.

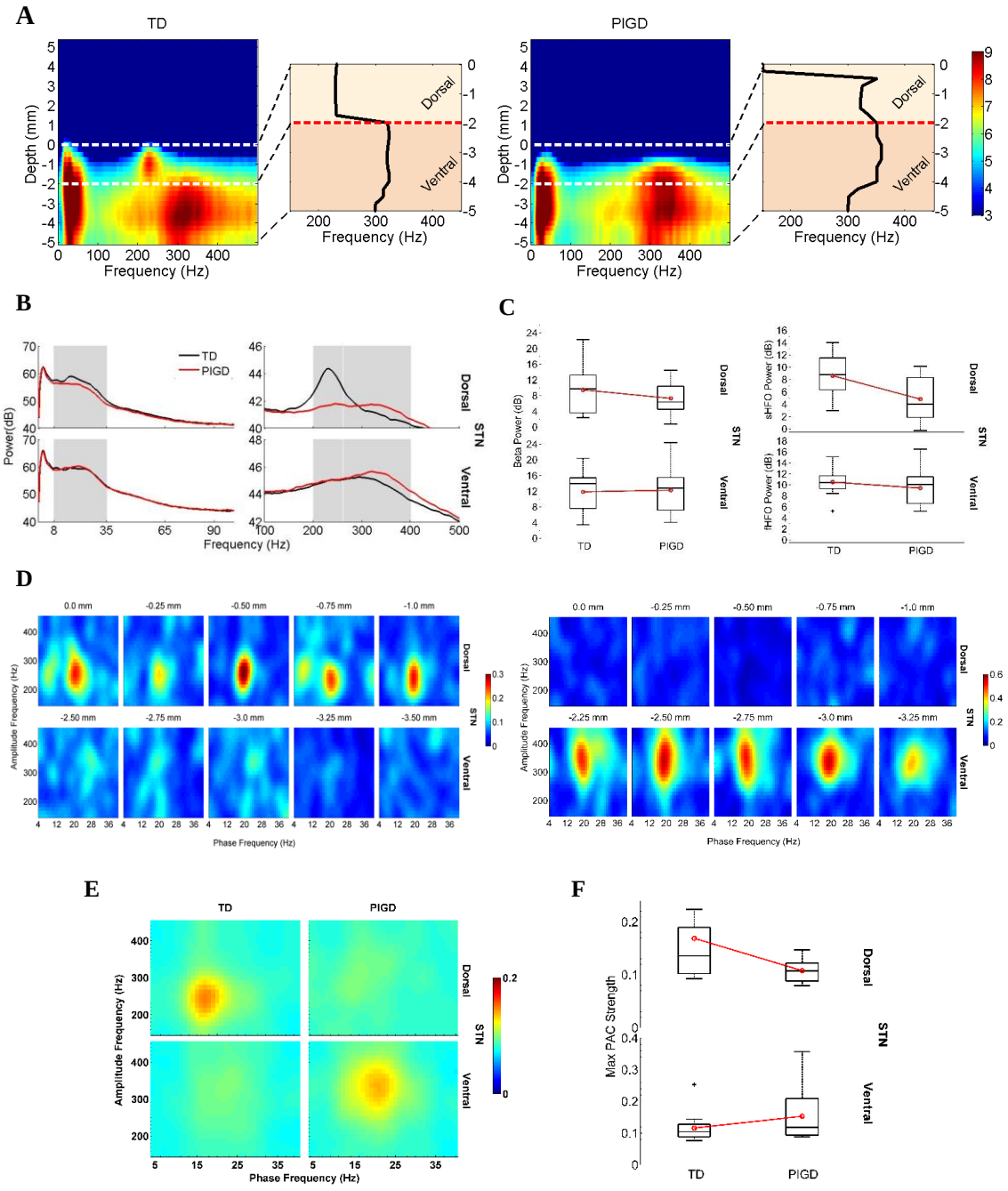

Fig.5.3. Spatio-spectral and PAC dynamics of LFPs in TD and PIGD groups. (A) Average DFMs of TD and PIGD groups. (B) Average power spectra generated from dorsal and ventral regions. (C) Subband power distributions. (D) PAC computed depth-by-depth for a representative TD (left) and a PIGD (right) subject. (E) Average PAC in each group. (F) Maximum PAC strength distribution across phenotypes.

Fig. 5.3.D shows the comodulograms representing the PAC estimated from individual depths in dorsal and ventral subregions for a representative TD and a PIGD subject. The PAC analysis executed in each depth indicated a strong interaction between the phase of beta oscillations and the amplitude of HFOs. However, the spatial localization of PAC was distinct. While PAC in TD subject was observed in the dorsal subregion, PIGD subject demonstrated a PAC in the ventral subregion. Moreover, while the amplitude frequency of the dorsal couplings was centered in the sHFO band, the ventral PAC occurred at fHFO range.

The average coupling in each group further supported our finding of spatially isolated PAC along with the distinct amplitude frequency components (Fig.5.3.E). The maximum PAC values obtained from the dorsal subregion were significantly higher in the TD group ($Z=2.000$, $p=0.023$, Mann–Whitney U test). Although both phenotypic groups exhibited fHFOs in the ventral subregion with significantly different peak frequencies, PAC analysis indicated a significantly higher coupling in the PIGD group ($Z=1.877$, $p=0.030$; Fig.5.3.F). In addition to the significantly higher PAC strength found in the dorsal subregion for TD and the ventral subregion for PIGD, the corresponding HFO (amplitude) frequencies were also significantly different ($Z=-2.857$, $p=0.004$) indicating that amplitude modulation occurs at distinct frequencies in the TD and PIGD patients.

The ROC curves obtained from the sHFO and fHFO powers together with power ratio of sHFO to fHFO computed in the dorsal and ventral subregions are shown in Fig.5.4.A. A statistically significant difference in sHFO to fHFO power ratio was observed between phenotypes only in the dorsal subregion (Dorsal, $Z=3.373$, $p=0.001$;

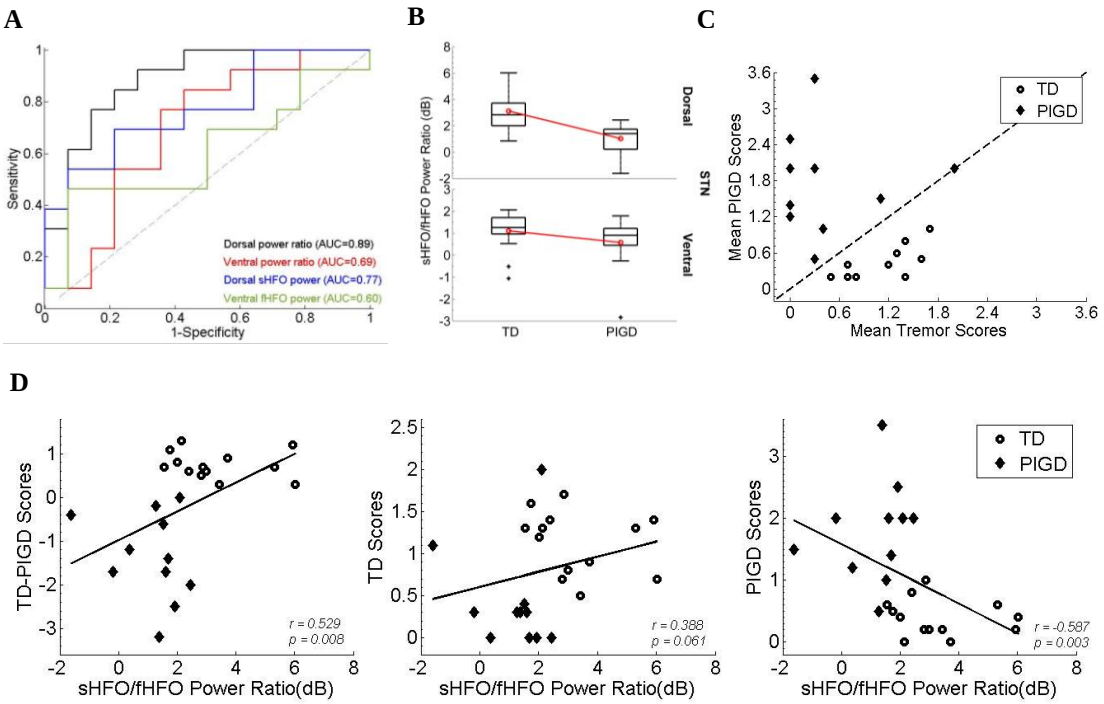

Fig.5.4. Discrimination and correlation. (A) ROC curves discriminating TD from PIGD by using spatio-spectral features (B) sHFO/fHFO power ratio distribution between TD and PIGD. (C) Distribution of mean tremor and mean gait scores across subjects. (D) Correlation between dorsal sHFO/fHFO power ratio and the tremor and gait scores.

Ventral, Z=1.674, p=0.094, Mann–Whitney U test; Fig.5.4.B). This feature also provided the highest discrimination between phenotypes (area under curve, AUC, ratio of sHFO power to fHFO power in dorsal sub-region, 0.89; ratio of sHFO power to fHFO power in ventral sub-region, 0.69; dorsal sHFO power, 0.77; ventral fHFO power, 0.60).

To assess whether the spatio-spectral features of LFPs were related to UPDRS and/or MDS-UPDRS scores for tremor or gait-related scores, a correlation analysis was performed. Figure 5.4.C shows the distribution of mean tremor scores vs mean gait-related (PIGD) scores across all subjects, highlighting the presence of PD subjects with considerable tremor and gait problems in the study. Correlation analysis showed that sHFO to fHFO power ratio was positively correlated with the difference of mean tremor

and mean PIGD scores (Spearman correlation, r=0.529, p=0.008; Fig.5.4.D-left panel) as well as with the mean tremor scores only (r=0.388, p=0.061; Fig.5.4.D-middle panel). Comparison to PIGD scores showed a negative but stronger correlation with the power ratio (r=-0.587, p=0.003; Fig.5.4.D-right panel). Even though the HFO power ratio worked well for distinguishing between phenotypes, the ratio did not reflect a direct correlation to the level of severity of tremor or gait within groups.

5.3. Discussion

Microelectrode LFPs recorded from the sub-territories of STN provided distinguishing information about the most commonly accepted TD and PIGD phenotypes of PD. We observed that both groups showed beta band activity with similar energy while the most striking difference was found at the higher frequencies. In particular, compared to PIGD group, the LFPs of TD group included significantly strong sHFO in the dorsal region of STN. Both groups exhibited fHFOs in the ventral region with slightly higher peak frequency in PIGD group but without any significant difference between their powers. Other studies have reported sHFO in OFF medication state (Lopez-Azcarate et al., 2010; Özkurt et al., 2011) and a shift from sHFO to fHFO range in those PD patients who were administered with L-DOPA (Foffani et al., 2003; Lopez-Azcarate et al., 2010; Özkurt et al., 2011). Here we show that even though recordings were obtained during medication OFF state, the fHFOs can also be observed in the STN. The peak frequency of HFOs were distinct in the sub-territories of STN and phenotype specific.

We also show a significantly stronger coupling between the phase of beta and amplitude of sHFO in the dorsal region of STN in TD group. Although similar signal power was observed in fHFO range in the ventral sub-territory of the STN in both groups,

PAC between beta band and fHFO were found significantly higher in PIGD group. The PAC patterns reported in STN and cortex were linked to the pathophysiology of PD (de Hemptinne et al., 2015; Özkurt et al., 2011) as L-DOPA administration resulted in symptom improvement and absence of PAC between beta band and HFOs range in STN-LFPs (de Hemptinne et al., 2015; Lopez-Azcarate et al., 2010; Özkurt et al., 2011). Given the known somatotopic organization of the STN, the existence of the PAC in the ventral region might explain the severe cognitive dysfunction in PIGD patients. Although previous electrophysiological studies have identified cells firing at tremor frequencies in the STN (Levy et al., 2002), yet still, it is not known whether or not there exists a particular cell firing specific to motor subtypes of PD in the STN. In patients with TD-PD, intraoperative recording of LFPs in the STN revealed clusters of tremor-associated coupling between STN and tremor EMG that were spatially distinct for different muscles (Reck et al., 2009). In our study, no concurrent single cell activity to LFP was recorded in the operating room. At this point it is not clear if the dorsal sHFO and its coupling with beta band are results of clusters of tremor cells. Never the less, our observations show that not only the peak frequencies of HFOs but also their nonlinear interaction with the phase of beta band seems to have an important role in distinguishing between phenotypes.

In the present study, patients were evaluated by a movement disorder specialist in the clinic and either UPDRS or MDS-UPDRS scores were obtained. Even though the number of items in the MDS-UPDRS were used as suggested by Stebbins (Stebbins et al., 2013), phenotype designation was performed for both tests by using formula suggested by Jankovic (Jankovic et al., 1990). Even if the threshold values suggested by Stebbins et

al. were used for categorization, phenotype designation would not be different except for one PIGD patient with considerable tremor. Therefore, to be consistent, we used the former formula. Although the LFP patterns could distinguish both groups, we were unable to find a relationship between them and the UPDRS scores within each group (only a weak correlation). The weak correlation between LFP patterns and UPDRS values could be due to the measurement of neural and behavioral data at distinct time points. Moreover, subjective assessment of UPDRS by human experts might be another co-founding factor.

In summary, we showed that activity in the subbands of LFPs recorded with microelectrodes from sub-territories of the STN provide distinguishing neurophysiological information about the most commonly accepted subtypes of PD. We studied 27 patients with PD and found distinct patterns between TD and PIGD groups in high frequency oscillations and their interaction with the beta band in the dorsal and ventral regions of the STN. Our results indicated that the spatio-spectral dynamics of LFPs can be used as an objective method to distinguish the two major subtypes of PD. These observations might lead the development of novel stimulation strategies and electrode technology targeting the territories of STN for the optimization and personalization of deep brain stimulation.

6. CHAPTER 6: General Summary and Significance

The first part of the present study describes an automated approach for electrophysiological localization of STN, using microelectrode-recorded LFPs acquired during DBS surgery simultaneous to MER. This work is novel, in that it is the first study to combine different sub-band features derived from beta (11– 32 Hz) and HFOs (150–450 Hz) of LFPs in order to (1) estimate the optimal track for DBS implantation, and (2) identify the dorsal STN border, with high accuracy. This work also contributes to knowledge about the neurophysiology of PD by describing the spatial localization of HFOs. Because recording LFPs simultaneous with MER-SUA does not prolong the total duration of surgery, using this technique online in the operating room would increase the chance of optimal placement of the DBS macroelectrode within the motor sub-territory of the STN, without an appreciable downside. Fused with existing mapping techniques, automated online LFP analysis may increase the accuracy of the DBS macroelectrode placement. This might contribute to the efficacy of DBS by reducing the stimulation voltage and associated side effects. Since the electrode placement is guided by LFP activity, the current technique could also be useful to monitor the LFP events which are capable to fine tune the future DBS settings in a closed loop paradigm (Ince et al., 2010; Priori & Foffani, et al., 2013; Rouse et al., 2011).

In addition to the use of LFPs recorded from microelectrodes in order to provide a supplementary tool for target localization in operating room, in the second part of the thesis, we have shown that LFPs recorded from chronic DBS electrode can also serve as a tool for STN localization in PD patients. Instead of implantation of DBS lead directly into the STN as in MRI-based targeting approach, insertion of the lead as in the

microelectrode implantation technique and recording signals depth-by-depth might provide electrophysiological mapping of the trajectory by using oscillatory nature of LFPs. By reducing the risk of intracranial hemorrhage which might be caused by using multiple trajectories or the sharp tips of the microelectrodes and by predicting the STN superior border with a small localization error (approximately 1 mm) which can be compensated with the large contacts of DBS electrode (> 1.5 mm), this study supports the use of spatio-spectral features of LFPs, which were intraoperatively recorded from chronic DBS electrodes, in conjunction with preoperative and/or intraoperative stereotactic imaging for target localization in PD.

In the last part, we have shown that spatio-spectral patterns and cross frequency interactions of LFPs carry substantial information that can distinguish between PD subtypes. Considering the more rapid progression, poorer prognosis, and the faster rate of cognitive decline in the PIGD subtype in addition to the major clinical and pathological differences compared to the TD subtype, the identified localized patterns further support the differentiation of these two subtypes from neural perspective and may provide insight into their pathophysiologic mechanisms. As recently as 2013, an international survey of high volume DBS implanting sites revealed that 83% of centers use microelectrode recording indicating that the most commonly used electrophysiological mapping method remains MER-SUA recordings (Abosch et al., 2013). LFPs are more robust signals than single cell activity recorded from high impedance microelectrode tip and particularly sensitive to synchronous and oscillatory firing patterns (Priori et al., 2004; Gross et al., 2006). It was also shown that LFPs are better correlated to motor and non-motor symptoms of PD (Priori et al., 2004; Thompson et al., 2014). In our recent study we have

shown that microelectrode LFPs can also be used for the localization of STN for DBS electrode implantation (Telkes et al., 2016). In this regards, our findings also demonstrate the feasibility of using LFPs for identification of physiological signatures of PD subtypes, and can provide a rationale for individualized DBS targeting within the sub-territories of STN using novel lead designs and/or stimulation strategies.

REFERENCES

Abosch, A., Timmermann, L., Bartley, S., Rietkerk, H. G., Whiting, D., Connolly, P. J., Lanctin, D., Hariz, M. I. (2013). An International Survey of Deep Brain Stimulation Procedural Steps. *Stereotactic and Functional Neurosurgery*, *91* (1), 1–11. http://doi.org/10.1159/000343207

Albe-Fessard, D. (1973). Electrophysiological Methods for the Identification of Thalamic Nuclei. *Journal of Neurology*, *205*(1), 15-28.

Alpaydin, E. (2010). *Introduction to Machine Learning* (2nd ed.). Cambridge, Massachusetts: The MIT Press.

Alves, G., Larsen, J. P., Emre, M., Wentzel-Larsen, T., & Aarsland, D. (2006). Changes in Motor Subtype and Risk for Incident Dementia in Parkinson's Disease. *Movement Disorders*, *21* (8), 1123–1130. http://doi.org/10.1002/mds.20897

Benabid, A. L. (2003). Deep Brain Stimulation for Parkinson's Disease. *Current Opinion in Neurobiology*, *13*(6), 696–706. http://doi.org/10.1016/j.conb.2003.11.001

Benabid, A. L., Chabardes, S., Mitrofanis, J., & Pollak, P. (2009). Deep Brain Stimulation of the Subthalamic Nucleus for the Treatment of Parkinson's Disease. *Lancet Neurol*, *8* (1), 67–81. http://doi.org/S1474-4422(08)70291-6 [pii]\r10.1016/S1474-4422(08)70291-6 [doi]

Benabid, A. L., Pollak, P., Gross, C., Hoffmann, D., Benazzouz, A., Gao, D. M., Laurent, A., Gentil, M., and Perret, J. (1994). Acute and Long-Term Effects of Subthalamic Nucleus Stimulation in Parkinson's Disease. *Stereotactic and functional neurosurgery*, *62* (1-4), 76-84.

Benabid, A. L., Pollak, P., Hoffmann, D., Gervason, C., Hommel, M., Perret, J. E., De

Rougemont, J., and Gao, D. M. (1991). Long-Term Suppression of Tremor by Chronic Stimulation of the Ventral Intermediate Thalamic Nucleus. *The Lancet*, *337* (8738), 403–406. http://doi.org/10.1016/0140-6736(91)91175-T

Benabid, A. L., Pollak, P., Louveau, A., Henry, S., & De Rougemont, J. (1987). Combined (Thalamotomy and Stimulation) Stereotactic Surgery of the VIM Thalamic Nucleus for Bilateral Parkinson Disease. *Stereotactic and functional neurosurgery*, *50* (1-6), 344-346.

Benarroch, E. E. (2008). Subthalamic Nucleus and Its Connections Stimulation. *Clinical Implications of Neuroscience Research*, 1991–1995. http://doi.org/10.1212/01.wnl.0000313022.39329.65

Bezard, E., and Przedborski, S. (2011). A Tale on Animal Models of Parkinson's Disease. *Movement Disorders : Official Journal of the Movement Disorder Society*, *26* (6), 993–1002. http://doi.org/10.1002/mds.23696

Blomstedt, P., Sandvik, U., Linder, J., Fredricks, A., Forsgren, L., & Hariz, M. I. (2011). Deep Brain Stimulation of the Subthalamic Nucleus Versus the Zona Incerta in the Treatment of Essential Tremor. *Acta Neurochirurgica*, *153* (12), 2329–2335. http://doi.org/10.1007/s00701-011-1157-4

Bohnen, N. I., Frey, K. A., Studenski, S., Kotagal, V., Koeppe, R. A., Scott, P. J., Albin, R.L.,and Muller, M. L. (2013). Gait Speed in Parkinson Disease Correlates with Cholinergic Degeneration. *Neurology*, *81*(18), 1611–1616. http://doi.org/10.1212/WNL.0b013e3182a9f558

Brittain, J. S., and Brown, P. (2014). Oscillations and the Basal Ganglia: Motor Control and Beyond. *NeuroImage*, *85*, 637–647.

http://doi.org/10.1016/j.neuroimage.2013.05.084

Bronte-Stewart, H., Barberini, C., Koop, M. M., Hill, B. C., Henderson, J. M., and Wingeier, B. (2009). The STN Beta-Band Profile in Parkinson's Disease Is Stationary and Shows Prolonged Attenuation After Deep Brain Stimulation. *Experimental Neurology*, *215* (1), 20–28. http://doi.org/10.1016/j.expneurol.2008.09.008

Buzsaki, G. (2006). *Rhythms of the Brain*. Oxford University Press.

Buzsáki, G., Anastassiou, C. A, and Koch, C. (2012). The Origin of Extracellular Fields and Currents--EEG, ECOG, LFP and Spikes. *Nature Reviews. Neuroscience*, *13* (6), 407–20. http://doi.org/10.1038/nrn3241

Cagnan, H., Dolan, K., He, X., Contarino, M. F., Schuurman, R., van den Munckhof, P., Wadman, W.J., Bour, L., and Martens, H. C. (2011). Automatic Subthalamic Nucleus Detection From Microelectrode Recordings Based on Noise Level and Neuronal Activity. *Journal of Neural Engineering*, *8* (4), 46006. http://doi.org/10.1088/1741-2560/8/4/046006

Camara, C., Isasi, P., Warwick, K., Ruiz, V., Aziz, T., Stein, J., & Bakštein, E. (2015). Resting Tremor Classification and Detection in Parkinson's Disease Patients. *Biomedical Signal Processing and Control*, *16*, 88–97. http://doi.org/10.1016/j.bspc.2014.09.006

Charles, P. D., Van Blercom, N., Krack, P., Lee, S. L., Xie, J., Besson, G., Benabid, A.L., and Pollak, P. (2002). Predictors of Effective Bilateral Subthalamic Nucleus Stimulation for PD. *Neurology*, *59* (6), 932-934.

Chen, C. C., Pogosyan, A., Zrinzo, L. U., Tisch, S., Limousin, P., Ashkan, K., Yousry,

T., Hariz, M.I. and Brown, P. (2006). Intra-Operative Recordings of Local Field Potentials Can Help Localize The Subthalamic Nucleus in Parkinson's Disease surgery. *Experimental Neurology*, *198* (1), 214–221. http://doi.org/10.1016/j.expneurol.2005.11.019

Chen, J., Vandewalle, J., Sansen, W., Vantrappen, G., & Janssens, J. (1990). Multichannel Adaptive Enhancement of the Electrogastrogram. *IEEE Transactions on Biomedical Engineering*, *37* (3), 285–294. http://doi.org/10.1109/10.52329

DeLong, M. R., and Wichmann, T. (2007). Circuits and Circuit Disorders of the Basal Ganglia. *Archives of Neurology*, *64* (1), 20–24. http://doi.org/10.1001/archneur.64.1.20

Desouza, R. M., Moro, E., Lang, A. E., and Schapira, A. H. V. (2013). Timing of Deep Brain Stimulation in Parkinson Disease: A Need for Reappraisal? *Annals of Neurology*, *73* (5), 565–575. http://doi.org/10.1002/ana.23890

Diamond, A., Shahed, J., and Jankovic, J. (2007). The effects of Subthalamic Nucleus Deep Brain Stimulation on Parkinsonian Tremor. *Journal of the neurological sciences*, *260* (1), 199-203.

Eggers, C., Kahraman, D., Fink, G. R., Schmidt, M., & Timmermann, L. (2011). Akinetic-Rigid and Tremor-Dominant Parkinson's Disease Patients Show Different Patterns of FP-CIT Single Photon Emission Computed Tomography. *Movement Disorders*, *26* (3), 416–423. http://doi.org/10.1002/mds.23468

Eusebio, A., Cagnan, H., and Brown, P. (2012). Does Suppression of Oscillatory Synchronisation Mediate Some of the Therapeutic Effects of DBS in Patients with

Parkinson's Disease? *Frontiers in Integrative Neuroscience*, *6* (July), 1–9. http://doi.org/10.3389/fnint.2012.00047

Eusebio, A., Thevathasan, W., Doyle Gaynor, L., Pogosyan, A., Bye, E., Foltynie, T., Zrinzo, L., Ashkan, K., Aziz, T., and Brown, P. (2011). Deep Brain Stimulation Can Suppress Pathological Synchronisation in Parkinsonian Patients. *Journal of Neurology, Neurosurgery & Psychiatry*, *82* (5), 569–573. http://doi.org/10.1136/jnnp.2010.217489

Fahn, S. (2003). Description of Parkinson's Disease as a Clinical Syndrome. *Ann. N.Y. Acad. Sci.*, *991*, 1–14.

Falkenberg, J. H., McNames, J., Favre, J., and Burchiel, K. J. (2006). Automatic Analysis and Visualization of Microelectrode Recording Trajectories to the Subthalamic Nucleus: Preliminary Results. *Stereotactic and Functional Neurosurgery*, *84* (1), 35–45. http://doi.org/10.1159/000093721

Fasano, A., Daniele, A., & Albanese, A. (2012). Treatment of Motor and Non-Motor Features of Parkinson's Disease with Deep Brain Stimulation. *The Lancet Neurology*, *11* (5), 429–442. http://doi.org/10.1016/S1474-4422(12)70049-2

Ferrara, E. R., and Widrow, B. (1982). Fetal Electrocardiogram Enhancement by Time-Sequenced Adaptive Filtering. *IEEE Transactions on Biomedical Engineering*, *BME-29* (6), 458–460. http://doi.org/10.1109/TBME.1982.324973

Foffani, G., and Priori, A. (2006). Deep Brain Stimulation in Parkinson's Disease Can Mimic the 300 Hz Subthalamic Rhythm. *Brain : A Journal of Neurology*, *129*, e59; author reply e60. http://doi.org/10.1093/brain/awl209

Foffani, G., Ardolino, G., Egidi, M., Caputo, E., Bossi, B., & Priori, a. (2006).

Subthalamic Oscillatory Activities at Beta or Higher Frequency Do Not Change After High-Frequency DBS in Parkinson's Disease. *Brain Research Bulletin, 69* (2), 123–130. http://doi.org/10.1016/j.brainresbull.2005.11.012

Foffani, G., Priori, A., Egidi, M., Rampini, P., Tamma, F., Caputo, E., Moxon, K.A., Cerutti, S., and Barbieri, S. (2003). 300-Hz Subthalamic Oscillations in Parkinson's Disease. *Brain, 126* (10), 2153–2163. http://doi.org/10.1093/brain/awg229

Foltynie, T., Zrinzo, L., Martinez-Torres, I., Tripoliti, E., Petersen, E., Holl, E., Aviles-Olmos, I., Jahanshahi, M., Hariz, M., and Limousin, P. (2011). MRI-Guided STN DBS in Parkinson's Disease without Microelectrode Recording: Efficacy and Safety. *Journal of Neurology, Neurosurgery, and Psychiatry*, *82* (4), 358–363. http://doi.org/10.1136/jnnp.2010.205542

Gelb, D. J., Oliver, E., and Gilman, S. (1999). Diagnostic Criteria for Parkinson Disease. *Archives of Neurology*, *56* (1), 33–9. http://doi.org/10.1001/archneur.56.1.33

Gerfen, C. R., and Bolam, J. P. (2010). *The Neuroanatomical Organization of the Basal Ganglia*. *Handbook of Basal Ganglia Structure and Function* (Vol. 20). Elsevier Inc. http://doi.org/10.1016/B978-0-12-374767-9.00001-9

Goetz, C. G. (2017). The History of Parkinson's Disease : Early Clinical Descriptions and Neurological Therapies. *Cold Spring Harbor perspectives in medicine, 1* (1), a008862.

Graham, J. M., and Sagar, H. J. (1999). A Data-Driven Approach to the Study of Heterogeneity in Idiopathic Parkinson's Disease: Identification of Three Distinct Subtypes. *Movement Disorders, 14* (1), 10–20. http://doi.org/10.1002/1531-

8257(199901)14:1<10::AID-MDS1005>3.0.CO;2-4

Groiss, S. J., Wojtecki, L., Sudmeyer, M., and Schnitzler, A. (2009). Review: Deep Brain Stimulation in Parkinson's Disease. *Therapeutic Advances in Neurological Disorders*, *2* (6), 379–391. http://doi.org/10.1177/1756285609339382

Gross, R. E., Krack, P., Rodriguez-Oroz, M. C., Rezai, A. R., and Benabid, A. L. (2006). Electrophysiological Mapping for the Implantation of Deep Brain Stimulators for Parkinson's Disease and Tremor. *Movement Disorders*, *21* (S14), S259–S283. http://doi.org/10.1002/mds.20960

Halliday, G. M., and McCann, H. (2010). The Progression of Pathology in Parkinson's Disease. *Annals of the New York Academy of Sciences*, *1184*, 188–195. http://doi.org/10.1111/j.1749-6632.2009.05118.x

Hamani, C. (2004). The Subthalamic Nucleus in the Context of Movement Disorders. *Brain*, *127*(1), 4–20. http://doi.org/10.1093/brain/awh029

Hariz, M. (2012). Twenty-Five Years of Deep Brain Stimulation: Celebrations and Apprehensions. *Movement Disorders*, *27* (7), 930–933. http://doi.org/10.1002/mds.25007

Hariz, M. I., Blomstedt, P., and Zrinzo, L. (2010). Deep Brain Stimulation Between 1947 and 1987: The Untold Story. *Neurosurgical Focus*, *29* (2), E1. http://doi.org/10.3171/2010.4.FOCUS10106

Helmich, R. C., Toni, I., Deuschl, G., and Bloem, B. R. (2013). The Pathophysiology of Essential Tremor and Parkinson's Tremor. *Current Neurology and Neuroscience Reports*, *13* (9), 378. http://doi.org/10.1007/s11910-013-0378-8

De Hemptinne, C., Swann, N. C. , Ostrem, J. L., Ryapolova-Webb, E. S., San Luciano,

M., Galifianakis, N. B., and Starr, P. A. (2015). Therapeutic Deep Brain Stimulation Reduces Cortical Phase-Amplitude Coupling in Parkinson's Disease. *Nature neuroscience*, 18, 779-786.

Herzog, J., Fietzek, U., Hamel, W., Morsnowski, A., Steigerwald, F., Schrader, B., Weinert, D., Pfister, G., Müller, D., Mehdorn, H.M., and Volkmann, J. (2004). Most Effective Stimulation Site in Subthalamic Deep Brain Stimulation for Parkinson's Disease. *Movement Disorders: 19* (9), 1050–4. http://doi.org/10.1002/mds.20056

Hoehn, M. M., Yahr, M. D., Hoehn, M. M., and Yahr, M. D. (1967). Parkinsonism : Onset , Progression , and Mortality. *Neurology, 17*.

Holdefer, R. N., Cohen, B. A., and Greene, K. A. (2010). Intraoperative Local Field Recording for Deep Brain Stimulation in Parkinson's Disease and Essential Tremor. *Movement Disorders*, *25* (13), 2067–2075. http://doi.org/10.1002/mds.23232

Hughes, A. J., Daniel, S. E., Kilford, L., and Lees, A. J. (1992). Accuracy of Clinical Diagnosis of Idiopathic Parkinson's Disease: A Clinico-Pathological Study of 100 Cases. *Journal of Neurology, Neurosurgery, and Psychiatry*, *55* (3), 181–4. http://doi.org/10.1136/jnnp.55.3.181

Hutchison, W. D., Allan, R. J., Opitz, H., Levy, R., Dostrovsky, J. O., Lang, A. E., and Lozano, A. M. (1998). Neurophysiological Identification of the Subthalamic Nucleus in Surgery for Parkinson's Disease. *Annals of Neurology, 44* (4), 622–628. http://doi.org/10.1002/ana.410440407

Ince, N. F., Goksu, F., Pellizzer, G., Tewfik, A., and Stephane, M. (2008). Selection of

Spectro-Temporal Patterns in Multichannel MEG with Support Vector Machines for Schizophrenia Classification. In *Engineering in Medicine and Biology Society, EMBS. 30th Annual International Conference of the IEEE*, 3554-3557.

Ince, N. F., Gupte, A., Wichmann, T., Ashe, J., Henry, T., Bebler, M., Eberly, L. and Abosch, A. (2010). Selection of Optimal Programming Contacts Based on Local Field Potential Recordings from Subthalamic Nucleus in Patients with Parkinson's Disease. *Neurosurgery*, *67* (2), 390–397. http://doi.org/10.1227/01.NEU.0000372091.64824.63

Jain S, Lo SE, L. E. (2006). Common Misdiagnosis of a Common Neurological Disorder. *Arch Neurol.*, *63*(8), 1100–1104. http://doi.org/10.1001/archneur.63.8.1100

Jankovic, J. (2008). Parkinson's Disease: Clinical Features and Diagnosis. *Journal of Neurology, Neurosurgery & Psychiatry*, *79* (4), 368–376. http://doi.org/10.1136/jnnp.2007.131045

Jankovic, J., and Kapadia, A. S. (2001). Functional Decline in Parkinson Disease. *Archives of Neurology*, *58* (10), 1611–1615. http://doi.org/10.1001/archneur.58.10.1611

Jankovic, J., McDermott, M., Carter, J., Gauthier, S., Goetz, C., Golbe, L., Huber, S., Koller, W., Olanow, C., Shoulson, I., and Stern, M. (1990). Variable Expression of Parkinsons Disease - A Base-Line Analysis of the Datatop Cohort. *Neurology*, *40* (10), 1529–1534.

Jellinger, K. A. (1999). Post Mortem Studies in Parkinson's Disease—Is It Possible to Detect Brain Areas for Specific Symptoms?. In *Diagnosis and Treatment of Parkinson's Disease—State of the Art* (pp. 1-29). Springer, Vienna.

Jenkinson, N., and Brown, P. (2011). New Insights into the Relationship between Dopamine, Beta Oscillations and Motor Function. *Trends in Neurosciences*, *34* (12), 611–618. http://doi.org/10.1016/j.tins.2011.09.003

Jenner, P. (2013). Wearing Off, Dyskinesia, and the Use of Continuous Drug Delivery in Parkinson's Disease. *Neurologic Clinics of NA*, *31* (3), S17–S35. http://doi.org/10.1016/j.ncl.2013.04.010

Kane, A., Hutchison, W. D., Hodaie, M., Lozano, A. M., and Dostrovsky, J. O. (2009a). Dopamine-Dependent High-Frequency Oscillatory Activity in Thalamus and Subthalamic Nucleus of Patients with Parkinson's Disease. *Neuroreport*, *20* (17), 1549–1553. http://doi.org/10.1097/WNR.0b013e32833282c8

Kane, A., Hutchison, W. D., Hodaie, M., Lozano, A. M., and Dostrovsky, J. O. (2009b). Enhanced Synchronization of Thalamic Theta Band Local Field Potentials in Patients with Essential Tremor. *Experimental Neurology*, *217* (1), 171–176. http://doi.org/10.1016/j.expneurol.2009.02.005

Klockgether, T. (2004). Parkinson's Disease : Clinical Aspects, *Cell and tissue research*, *318* (1), 115-120. http://doi.org/10.1007/s00441-004-0975-6

Kolb, R., Abosch, A., Felsen, G., and Thompson, J. A. (2017). Use of Intraoperative Local Field Potential Spectral Analysis to Differentiate Basal Ganglia Structures in Parkinson's Disease Patients,. *Physiological Reports*, *5* (12), p.e13322. http://doi.org/10.14814/phy2.13322

Krack, P., Hariz, M. I., Baunez, C., Guridi, J., and Obeso, J. A. (2010). Deep Brain Stimulation: From Neurology to Psychiatry?. *Trends in Neurosciences*, *33* (10), 474–484. http://doi.org/10.1016/j.tins.2010.07.002

Kühn, A. A., Kempf, F., Brücke, C., Gaynor Doyle, L., Martinez-Torres, I., Pogosyan, A., Trottenberg, T., Kupsch, A., Schneider, G.H., Hariz, M.I., and Brown, P. (2008). High-Frequency Stimulation of the Subthalamic Nucleus Suppresses Oscillatory Beta Activity in Patients with Parkinson's Disease in Parallel with Improvement in Motor Performance. *The Journal of Neuroscience : The Official Journal of the Society for Neuroscience, 28* (24), 6165–6173. http://doi.org/10.1523/JNEUROSCI.0282-08.2008

Kühn, A. A., Kupsch, A., Schneider, G.H., and Brown, P. (2006). Reduction in Subthalamic 8-35 Hz Oscillatory Activity Correlates with Clinical Improvement in Parkinson's Disease. *The European Journal of Neuroscience, 23* (7), 1956–60. http://doi.org/10.1111/j.1460-9568.2006.04717.x

Kühn, A. A., Tsui, A., Aziz, T., Ray, N., Brücke, C., Kupsch, A., Schneider, G.H., and Brown, P. (2009). Pathological Synchronisation in the Subthalamic Nucleus of Patients with Parkinson's Disease Relates to Both Bradykinesia and Rigidity. *Experimental Neurology*, *215* (2), 380–387. http://doi.org/10.1016/j.expneurol.2008.11.008

Lachaux, J., Rodriguez, E., Martinerie, J., and Varela, F. J. (1999). Measuring Phase Synchrony in Brain Signals. *Human brain mapping*, *8* (4), pp.194-208.

Lang, A. E., and Widner, H. (2002). Deep Brain Stimulation for Parkinson's Disease: Patient Selection and Evaluation. *Movement Disorders, 17* (S3).

Levy, R., Ashby, P., Hutchison, W. D., Lang, A. E., Lozano, A. M., and Dostrovsky, J. O. (2002). Dependence of Subthalamic Nucleus Oscillations on Movement and Dopamine in Parkinson's Disease. *Brain : A Journal of Neurology, 125* (Pt 6),

1196–1209. http://doi.org/10.1093/brain/awf128

Lewis, M. M., Du, G., Sen, S., Kawaguchi, A., Truong, Y., Lee, S., Mailman, R.B., and Huang, X. (2011). Differential Involvement of Striato- And Cerebello-Thalamo-Cortical Pathways in Tremor- and Akinetic/Rigid-Predominant Parkinson's Disease. *Neuroscience*, *177*, 230–239. http://doi.org/10.1016/j.neuroscience.2010.12.060

Lewis, S. J. G. (2005). Heterogeneity of Parkinson's Disease in the Early Clinical Stages Using A Data Driven Approach. *Journal of Neurology, Neurosurgery & Psychiatry*, *76* (3), 343–348. http://doi.org/10.1136/jnnp.2003.033530

Lopez-Azcarate, J., Tainta, M., Rodriguez-Oroz, M. C., Valencia, M., Gonzalez, R., Guridi, J., Iriarte, J., Obeso, J.A., Artieda, J., and Alegre, M. (2010). Coupling between Beta and High-Frequency Activity in the Human Subthalamic Nucleus May Be A Pathophysiological Mechanism in Parkinson's Disease. *J Neurosci*, *30* (19), 6667–6677. http://doi.org/10.1523/JNEUROSCI.5459-09.2010

Hayes, M. (1996). *Statistical digital signal processing and modeling* (2006th ed.). New York: John Wiley & Sons.

Machado, A., Rezai, A. R., Kopell, B. H., Gross, R. E., Sharan, A. D., and Benabid, A. L. (2006). Deep Brain Stimulation for Parkinson's Disease: Surgical Technique and Perioperative Management. *Movement Disorders*, *21* (14). http://doi.org/10.1002/mds.20959

Marras, C., and Lang, A. (2013). Parkinson's Disease Subtypes: Lost in Translation?. *Journal of Neurology, Neurosurgery & Psychiatry*, *84* (4), 409–415. http://doi.org/10.1136/jnnp-2012-303455

Marras, C., Rochon, P., and Lang, A. E. (2002). Predicting Motor Decline and Disability in Parkinson Disease: A Systematic Review. *Archives of neurology*, *59* (11), 1724-1728.

Maurer, C., Mergner, T., Xie, J., Faist, M., Pollak, P., & Lu, C. H. (2003). Effect of Chronic Bilateral Subthalamic Nucleus (STN) Stimulation on Postural Control in Parkinson's Disease, *Brain*, *126* (5), 1146-1163. http://doi.org/10.1093/brain/awg100

Meredith, G. E., and Kang, U. J. (2006). Behavioral Models of Parkinson's Disease in Rodents : A New Look at an Old Problem, *Movement disorders*, *21* (10), 1595-1606. http://doi.org/10.1002/mds.21010

Meyers, R. (1951). Surgical Experiments in the Therapy of Certain 'Extrapyramidal' Diseases: A Current Evaluation. *Acta psychiatrica et neurologica. Supplementum*, *67*, 1.

Michmizos, K. P., Tagaris, G. L., Sakas, D. E., and Nikita, K. S. (2008). Automatic Intra-Operative Localization of STN Using The Beta Band Frequencies Of Microelectrode Recordings. *2008 8th IEEE International Conference on BioInformatics and BioEngineering*, 1–6. http://doi.org/10.1109/BIBE.2008.4696820

Molnar, G. F., Pilliar, A., Lozano, A. M., and Dostrovsky, J. O. (2005). Differences in Neuronal Firing Rates in Pallidal and Cerebellar Receiving Areas of Thalamus in Patients with Parkinson's Disease, Essential Tremor, and Pain. *J Neurophysiol.*, *93* (0022–3077), 3094–3101. http://doi.org/10.1152/jn.00881.2004

Morrison, C. E., Borod, J. C., Perrine, K., Beric, A., Brin, M. F., Rezai, A., Kelly, P., Sterio, D., Germano, I., Weisz, D., and Olanow, C. W. (2004). Neuropsychological Functioning Following Bilateral Subthalamic Nucleus Stimulation in Parkinson's Disease. *Archives of Clinical Neuropsychology*, *19* (2), 165-181.

Murata, J. I., Kitagawa, M., Uesugi, H., Saito, H., Iwasaki, Y., Kikuchi, S., Tashiro, K., and Sawamura, Y. (2003). Electrical Stimulation of the Posterior Subthalamic Area for the Treatment of Intractable Proximal Tremor. *Journal of neurosurgery*, *99* (4), 708-715.

Nambu, A. (2011). Somatotopic Organization of the Primate Basal Ganglia. *Frontiers in Neuroanatomy*, *5* (April), 26. http://doi.org/10.3389/fnana.2011.00026

Newman, E. J., Breen, K., Patterson, J., Hadley, D. M., Grosset, K. A, and Grosset, D. G. (2009). Accuracy of Parkinson's Disease Diagnosis in 610 General Practice Patients in the West Of Scotland. *Movement Disorders : Official Journal of the Movement Disorder Society*, *24* (16), 2379–85. http://doi.org/10.1002/mds.22829

Novak, P., Przybyszewski, A. W., Barborica, A., Ravin, P., Margolin, L., and Pilitsis, J. G. (2011). Localization of the Subthalamic Nucleus in Parkinson Disease Using Multiunit Activity. *Journal of the Neurological Sciences*, *310* (1–2), 44–49. http://doi.org/10.1016/j.jns.2011.07.027

Nutt, J. G. (2016). Motor Subtype in Parkinson's Disease : Different Disorders or Different Stages of Disease? Importance of Subtypes Motor Subtypes in the Deprenyl and Tocopherol Antioxidant Therapy of Parkinsonism (DATATOP) Motor Subtypes Motor Subtypes in a Prospecti, *Movement Disorders*, *31* (7), 957-

961. http://doi.org/10.1002/mds.26657

Obeso, J. A., Marin, C., Rodriguez-Oroz, C., Blesa, J., Benitez-Temiño, B., Mena-Segovia, J., Rodríguez, M., and Olanow, C.W (2008). The Basal Ganglia in Parkinson's Disease: Current Concepts and Unexplained Observations. *Annals of Neurology*, *64* (SUPPL. 2), 30–46. http://doi.org/10.1002/ana.21481

Okun, M. S., and Foote, K. D. (2010). Parkinson's Disease DBS: What, When, Who and Why? The Time Has Come to Tailor DBS Targets. *Expert Review of Neurotherapeutics*, *10* (12), 1847–1857. http://doi.org/10.1586/ern.10.156

Okun, M. S., Fernandez, H. H., Rodriguez, R. L., & Foote, K. D. (2007). Identifying candidates for deep brain stimulation in Parkinson's disease. *Geriatrics*, *62* (5), 18-24.

Okun, M. S., Tagliati, M., Pourfar, M., Fernandez, H. H., Rodriguez, R. L., Alterman, R. L., and Foote, K. D. (2005). Management of Referred Deep Brain Stimulation Failures. *Archives of Neurology*, *62*, 1250–1255. http://doi.org/10.1001/archneur.62.8.noc40425

Oswal, A., Brown, P., and Litvak, V. (2013). Synchronized Neural Oscillations and the Pathophysiology of Parkinson's Disease. *Current Opinion in Neurology*, *26* (6), 662–70. http://doi.org/10.1097/WCO.0000000000000034

Özkurt, T. E., Butz, M., Homburger, M., Elben, S., Vesper, J., Wojtecki, L., and Schnitzler, A. (2011). High Frequency Oscillations in the Subthalamic Nucleus: A Neurophysiological Marker of The Motor State in Parkinson's Disease. *Experimental Neurology*, *229* (2), 324–31. http://doi.org/10.1016/j.expneurol.2011.02.015

Parent, A., and Hazrati, L. (1995). Functional Anatomy of the Basal Ganglia. I. The Corctico-Basal Ganglia-Thalamo-Cortical Loop, *Brain Research Reviews*, *20* (1), 91-127.

Patel, N. K., Khan, S., and Gill, S. S. (2008). Comparison of Atlas- and Magnetic-Resonance-Imaging-Based Stereotactic Targeting of the Subthalamic Nucleus in the Surgical Treatment of Parkinson's Disease. *Stereotactic and Functional Neurosurgery*, *86* (3), 153–61. http://doi.org/10.1159/000120427

Plaha, P., Ben-Shlomo, Y., Patel, N. K., and Gill, S. S. (2006). Stimulation of the Caudal Zona Incerta Is Superior to Stimulation of the Subthalamic Nucleus in Improving Contralateral Parkinsonism. *Brain*, *129* (7), 1732–1747. http://doi.org/10.1093/brain/awl127

Poewe, W., and Wenning, G. (2002). The Differential Diagnosis of Parkinson's Disease. *European Journal of Neurology*, *9* (s3), 23–30. http://doi.org/10.1046/j.1468-1331.9.s3.3.x

Priori, A., Foffani, G., Pesenti, A., Tamma, F., Bianchi, A., Pellegrini, M., Locatelli, M., Moxon, K.A., and Villani, R. (2004). Rhythm-Specific Pharmacological Modulation of Subthalamic Activity in Parkinson's Disease. *Experimental Neurology*, *189* (2), 369–379. http://doi.org/10.1016/j.expneurol.2004.06.001

Priori, A., Foffani, G., Rossi, L., and Marceglia, S. (2013). Adaptive Deep Brain Stimulation (aDBS) Controlled by Local Field Potential Oscillations. *Experimental Neurology*, *245*, 77–86. http://doi.org/10.1016/j.expneurol.2012.09.013

Priori, A., Giannicola, G., Rosa, M., Marceglia, S., Servello, D., Sassi, M., and Porta, M.

(2013). Deep Brain Electrophysiological Recordings Provide Clues to the Pathophysiology of Tourette Syndrome. *Neuroscience and Biobehavioral Reviews*, *37* (6), 1063–1068. http://doi.org/10.1016/j.neubiorev.2013.01.011

Przedborski, S. (2017). The Two-Century Journey of Parkinson Disease Research. *Nature Reviews Neuroscience*, *18* (4), 251-259.

Rajput, A. H., Voll, A., Rajput, M. L., Robinson, C. A., and Rajput, A. (2009). Course in Parkinson's Disease Subtypes: A 39-Year Clinicopathologic Study. *Neurology*, *73* (3), 206–212. http://doi.org/10.1212/WNL.0b013e3181ae7af1

Rajput, A. H., Rozdilsky, B., and Rajput, A. (1991). Accuracy of Clinical Diagnosis in Parkinsonism--A Prospective Study. *The Canadian Journal of Neurological Sciences. Le Journal Canadien Des Sciences Neurologiques*, *18* (3), 275–8. Retrieved from http://www.ncbi.nlm.nih.gov/pubmed/1913360

Reck, C., Florin, E., Wojtecki, L., Krause, H., Groiss, S., Voges, J., Maarouf, M., Sturm, V., Schnitzler, A., and Timmermann, L. (2009). Characterisation of Tremor-Associated Local Field Potentials in the Subthalamic Nucleus in Parkinson's Disease. *European journal of neuroscience*, 29, 599-612.

Rezai, A. R., Kopell, B. H., Gross, R. E., Vitek, J. L., Sharan, A. D., Limousin, P., and Benabid, A. (2006). Deep Brain Stimulation for Parkinson's Disease : Surgical Issues, *21*. http://doi.org/10.1002/mds.20956

Richardson, R. M., Ostrem, J. L., and Starr, P. A. (2009). Surgical Repositioning of Misplaced Subthalamic Electrodes in Parkinson's Disease: Location of Effective and Ineffective Leads. *Stereotactic and Functional Neurosurgery*, *87* (5), 297–303. http://doi.org/10.1159/000230692

Rizzo, G., Martino, D., Arcuti, S., Copetti, M., Fontana, A., and Logroscino, G. (2015). Accuracy of Clinical Diagnosis of Parkinson's Disease: A Systematic Review and Bayesian Meta-Analysis. *Movement Disorders*, *30*, S441. http://doi.org/10.1212/WNL.0000000000002350

Rodriguez-Oroz, M. C., Jahanshahi, M., Krack, P., Litvan, I., Macias, R., Bezard, E., and Obeso, J. a. (2009). Initial Clinical Manifestations of Parkinson's Disease: Features and Pathophysiological Mechanisms. *The Lancet Neurology*, *8* (12), 1128–1139. http://doi.org/10.1016/S1474-4422(09)70293-5

Rossi, C., Frosini, D., Volterrani, D., De Feo, P., Unti, E., Nicoletti, V., Kiferle, L., Bonuccelli, U., and Ceravolo, R. (2010). Differences in Nigro-Striatal Impairment in Clinical Variants of Early Parkinson's Disease: Evidence from A FP-CIT SPECT Study. *European Journal of Neurology*, *17* (4), 626–630. http://doi.org/10.1111/j.1468-1331.2009.02898.x

Rouse, A. G., Stanslaski, S. R., Cong, P., Jensen, R. M., Afshar, P., Ullestad, D., Gupta, R., Molnar, G.F., Moran, D.W., and Denison, T. J. (2011). A Chronic Generalized Bi-Directional Brain-Machine Interface. *Journal of Neural Engineering*, *8* (3), 36018. http://doi.org/10.1088/1741-2560/8/3/036018

Saint-Cyr, J. A., Trépanier, L. L., Kumar, R., Lozano, A. M., and Lang, A. E. (2000). Neuropsychological Consequences of Chronic Bilateral Stimulation of the Subthalamic Nucleus in Parkinson's Disease. *Brain*, *123* (10), 2091-2108.

Saint-Cyr, Jean A., et al. (2002). Localization of Clinically Effective Stimulating Electrodes in the Human Subthalamic Nucleus on Magnetic Resonance Imaging. *Journal of Neurosurgery*, *97.5*, 1152–1166.

Samii, A., Nutt, J. G., and Ransom, B. R. (2004). Parkinson's disease, *The Lancet*, *363*, 1783–1793.

Schiess, M. C., Zheng, H., Soukup, V. M., Bonnen, J. G., and Nauta, H. J. W. (2000). Parkinson's Disease Subtypes: Clinical Classification and Ventricular Cerebrospinal Fluid Analysis. *Parkinsonism and Related Disorders*, *6* (2), 69–76. http://doi.org/10.1016/S1353-8020(99)00051-6

Schneider, S. A., and Deuschl, G. (2015). Medical and Surgical Treatment of Tremors. *Neurologic Clinics*, *33* (1), 57–75. http://doi.org/10.1016/j.ncl.2014.09.005

Selikhova, M., Williams, D. R., Kempster, P. A., Holton, J. L., Revesz, T., and Lees, A. J. (2009). A Clinico-Pathological Study of Subtypes in Parkinson's Disease. *Brain*, *132* (11), 2947–2957. http://doi.org/10.1093/brain/awp234

Mathai, A., and Smith, Y. (2011). The Corticostriatal and Corticosubthalamic Pathways: Two Entries, One Target. So What?. *Frontiers in systems neuroscience*, *5*.

Spiegel, E. A., and Wycis, H. T. (1954). Ansotomy in Paralysis Agitans. *AMA Archives of Neurology & Psychiatry*, *71* (5), 598-614.

Spiegel, E. A., Wycis, H. T., Marks, M., and Lee, A. J. (1947). Stereotaxic Apparatus for Operations on the Human Brain. *Science*, *106* (2754), 349-350.

Spiegel, E. A., Wycis, H. T., Szekely, E. G., Adams, J., Flanagan, M., and Baird III, H. W. (1963). Campotomy in Various Extrapyramidal Disorders. *Journal of neurosurgery*, *20* (10), 871-884.

Starr, P. A., Markun, L. C., Larson, P. S., Volz, M. M., Martin, A. J., and Ostrem, J. L. (2014). Interventional MRI-Guided Deep Brain Stimulation in Pediatric Dystonia: First Experience with the Clearpoint System. *Journal of Neurosurgery.*

Pediatrics, *14* (4), 400–8. http://doi.org/10.3171/2014.6.PEDS13605

Stebbins, G. T., Goetz, C. G., Burn, D. J., Jankovic, J., Khoo, T. K., and Tilley, B. C. (2013). How to Identify Tremor Dominant and Postural Instability/Gait Difficulty Groups with the Movement Disorder Society Unified Parkinson's Disease Rating Scale: Comparison with the Unified Parkinson's Disease Rating Scale. *Movement Disorders*, *28* (5), 668–670. http://doi.org/10.1002/mds.25383

Strauss, I., Kalia, S. K., and Lozano, A. M. (2014). Where Are We with Surgical Therapies for Parkinson's Disease?. *Parkinsonism and Related Disorders*, *20*, S187–S191. http://doi.org/10.1016/S1353-8020(13)70044-0

Taghva. (2010). An Automated Navigation System for Deep Brain Stimulator Placement Using Hidden Markov Models. *Neurosurgery.*, *10.1227/01*, 108–17. Retrieved from http://medcontent.metapress.com/index/A65RM03P4874243N.pdf

Telkes, I., Ince, N. F., Onaran, I., and Abosch, A. (2014). Localization of Subthalamic Nucleus Borders Using Macroelectrode Local Field Potential Recordings. *36th Annual International Conference of the IEEE Engineering in Medicince and Biology Society*, 2621–2624. http://doi.org/10.0/Linux-x86_64

Telkes, I., Jimenez-Shahed, J., Viswanathan, A., Abosch, A., and Ince, N. F. (2016). Prediction of STN-DBS Electrode Implantation Track in Parkinson's Disease by Using Local Field Potentials. *Frontiers in Neuroscience*, *10* (May), 1–16. http://doi.org/10.3389/fnins.2016.00198

Thenganatt, M. A., and Jankovic, J. (2014). Parkinson Disease Subtypes. *JAMA Neurology*, *71* (4), 499–504. http://doi.org/10.1001/jamaneurol.2013.6233

Thompson, J. A., Lanctin, D., Ince, N. F., and Abosch, A. (2014). Clinical Implications

of Local Field Potentials for Understanding and Treating Movement Disorders. *Stereotactic and Functional Neurosurgery*, *92* (4), 251–263. http://doi.org/10.1159/000364913

Trottenberg, T., Fogelson, N., Kühn, A. A., Kivi, A., Kupsch, A., Schneider, G.-H., and Brown, P. (2006). Subthalamic Gamma Activity in Patients with Parkinson's Disease. *Experimental Neurology*, *200* (1), 56–65. http://doi.org/10.1016/j.expneurol.2006.01.012

Utter, A. A., and Basso, M. A. (2008). The Basal Ganglia: An Overview of Circuits and Function. *Neuroscience and Biobehavioral Reviews*, *32* (3), 333–342. http://doi.org/10.1016/j.neubiorev.2006.11.003

Voges, J., Volkmann, J., Allert, N., Lehrke, R., Koulousakis, A., Freund, H. J., and Sturm, V. (2002). Bilateral High-Frequency Stimulation in the Subthalamic Nucleus for the Treatment of Parkinson Disease: Correlation of Therapeutic Effect with Anatomical Electrode Position. *Journal of neurosurgery*, *96* (2), 269-279.

Wang, J., Hirschmann, J., Elben, S., Hartmann, C. J., Vesper, J., Wojtecki, L., and Schnitzler, A. (2014). High-Frequency Oscillations in Parkinson's Disease: Spatial Distribution and Clinical Relevance. *Movement Disorders : Official Journal of the Movement Disorder Society*, *0* (0), 1–8. http://doi.org/10.1002/mds.25962

Weinberger, M., Mahant, N., Hutchison, W. D., Lozano, A. M., Moro, E., Hodaie, M., Lang, A.E., and Dostrovsky, J. O. (2006). Beta Oscillatory Activity in the Subthalamic Nucleus and Its Relation to Dopaminergic Response in Parkinson's

Disease. *Journal of Neurophysiology*, *96* (6), 3248–56. http://doi.org/10.1152/jn.00697.2006

Widrow, B., Williams, C. S., Glover, J. R., McCool, J. M., Hearn, R. H., Zeidler, J. R., Dong, J.E., and Goodlin, R. C. (1975). Adaptive Noise Cancelling: Principles and Applications. *Proceedings of the IEEE*, *63* (12), 1692–1716. http://doi.org/10.1109/PROC.1975.10036

Williams, N. R., Foote, K. D., and Okun, M. S. (2014). Subthalamic Nucleus Versus Globus Pallidus Internus Deep Brain Stimulation: Translating the Rematch Into Clinical Practice. *Movement Disorders Clinical Practice*, *1* (January), 24–35. http://doi.org/10.1002/mdc3.12004

Wong, S., Baltuch, G. H., Jaggi, J. L., and Danish, S. F. (2009). Functional Localization and Visualization of the Subthalamic Nucleus from Microelectrode Recordings Acquired During DBS Surgery with Unsupervised Machine Learning. *Journal of Neural Engineering*, *6* (2), 26006. http://doi.org/10.1088/1741-2560/6/2/026006

Xiaowu, H., Xiufeng, J., Xiaoping, Z., Bin, H., Laixing, W., Yiqun, C., Jinchuan, L., Aiguo, J., and Jianmin, L. (2010). Risks of Intracranial Hemorrhage in Patients with Parkinson's Disease Receiving Deep Brain Stimulation and Ablation. *Parkinsonism & Related Disorders*, *16* (2), 96–100. http://doi.org/10.1016/j.parkreldis.2009.07.013

Yelnik, J., Damier, P., Demeret, S., Gervais, D., Bardinet, E., Bejjani, B. P., François, C., Houeto, J.L., Arnulf, I., Dormont, D., and Galanaud, D. (2003). Localization of Stimulating Electrodes in Patients with Parkinson Disease by Using A Three-

Dimensional Atlas—Magnetic Resonance Imaging Coregistration Method. *Journal of neurosurgery*, *99* (1), 89-99.

Zaidel, A., Spivak, A., Shpigelman, L., Bergman, H., and Israel, Z. (2009). Delimiting Subterritories of the Human Subthalamic Nucleus by Means of Microelectrode Recordings and A Hidden Markov Model. *Movement Disorders*, *24* (12), 1785–1793. http://doi.org/10.1002/mds.22674

Zonenshayn, M., Rezai, A.R., Mogilner, A.Y., Beric, A, Sterio, D., and Kelly, P. J. (2000). Comparison of Anatomic and Neurophysiological Methods for Subthalamic Nucleus Targeting. *Neurosurgery*, *47* (2), 282-92–4. Retrieved from http://www.ncbi.nlm.nih.gov/pubmed/10942001